Report No. UMTA-NC-0010-81-2

OPTIMUM DESIGN METHODOLOGY FOR ELEVATED TRANSIT STRUCTURES

James F. Wilson
Department of Civil Engineering
Duke University
Durham, NC 27706

October, 1981

Final Report

Document is available to the U.S. public through the National Technical Information Service, Springfield, Virginia 22161.

PREPARED FOR

U.S. DEPARTMENT OF TRANSPORTATION
URBAN MASS TRANSPORTATION ADMINISTRATION
OFFICE OF POLICY RESEARCH
UNIVERSITY RESEARCH AND TRAINING PROGRAM
WASHINGTON DC 20590

Technical Report Documentation Page

1. Report No.	2. Government Accession No.	3. Recipient's Catalog No.
UMTA-NC-0010-81-2		

4. Title and Subtitle	5. Report Date
Optimum Design Methodology for Elevated Transit Structures	October, 1981
	6. Performing Organization Code
	8. Performing Organization Report No.

7. Author(s)	
James F. Wilson	

9. Performing Organization Name and Address	10. Work Unit No. (TRAIS)
Department of Civil Engineering Duke University Durham, NC 27706	11. Contract or Grant No. NC-11-0010
	13. Type of Report and Period Covered
12. Sponsoring Agency Name and Address Urban Mass Transportation Administration 400 Seventh Street, SW Washington, DC 20590	June, 1980 to October, 1981
	14. Sponsoring Agency Code

15. Supplementary Notes
Mr. George Izumi (UMTA) was technical monitor
Mr. Nathanial Jasper was the grant manager (202-426-0080)

16. Abstract

Methodologies are investigated for designing high efficiency, elevated, urban guideways. The most efficient spans are continuous where the pier supports, bending stiffness and unit mass are optimally distributed. Calculations lead to spans of least overall weight, balanced peak stresses under all loading, and minimum rms vertical deflection for the vehicle trajectories.

The study is in four parts. In Chapter 1, optimal pier spacings for uniform spans are predicted, where span inertia effects are included. Calculated optimal span responses to constant loads at constant speed, verified experimentally, show a peak stress reduction of up to 30 percent, compared to simple spans end-to-end. In Chapter 2, similar results are found for uniform, continuous, inertialess, spans where the transit mass is much larger than the span mass. In Chapter 3, the effects on span efficiency of the nonuniform stiffness and unit mass parameters are investigated, where extensive use is made of computer graphics to illustrate the design methodology. In Chapter Four, the Duke University transit system is the reference case used for alternative design studies, where up to 40 percent reductions in concrete weight are possible.

These methodologies can be successively employed to minimize urban guideway costs through weight reduction. The optimal spans are slim, aesthetic structures, affording high degrees of passenger ride comfort.

17. Key Words	18. Distribution Statement
guideways, beam dynamics, bridges, optimum design, transit structures	This document is available to the U.S. public through the National Technical Information Service, Springfield, Virginia, 22161.

19. Security Classif. (of this report)	20. Security Classif. (of this page)	21. No. of Pages	22. Price
Unclassified	Unclassified		

PREFACE

The principal investigator wishes to acknowledge the interest of the Urban Mass Transportation Administration in the conceptual development of methods to achieve efficient, minimum cost urban transit structures. The pertinent technical comments and other information offered by George Izumi, the technical monitor, were greatly appreciated, as was the patience of Nathanial Jasper, the grant manager, in dealing with budget matters.

Several students in the School of Engineering at Duke University contributed to this research. As a Master's degree candidate, Serghios T. Barbas helped to formulate the dynamic theory and wrote the several computer programs needed in Chapter 1. David M. Wilson, an undergraduate student at Duke assisted in the extensive experimental program of Chapter 1; and wrote the computer program for Chapter 2. As a Ph.D. candidate, Peter Carrato generated most of the technical results for Chapters 3 and 4. Mohamed Essawi, also a Ph.D. candidate, was an occasional consultant on computer programming.

Several people were involved in report preparation. The expert typing was done by Linda Hayes, Bonnie Farrell and Jo Ann Scott; and the graphics were well done by Fred Avent.

James F. Wilson
Professor and
Principal Investigator
Duke University
September, 1981

TABLE OF CONTENTS

CHAPTER 4. ALTERNATIVE, HIGH EFFICIENCY DESIGNS FOR THE DUKE UNIVERSITY GUIDEWAYS

EXECUTIVE SUMMARY

There is a continuing need to design more efficient, minimum cost supporting structures for guideway transit systems. Since such guideway structures typically represent about 35 percent of the total design life cost of urban mass transit systems, there are great potential dollar savings if optimal structural design methodologies are employed. Such methodologies are investigated here. Calculations lead to continuous, elevated spans of least overall weight, which also implies lower costs for materials if standard construction practices are followed. Calculations also lead to balanced peak stress in these spans, subjected to both dead weight loading and live or transit vehicle loading. In addition, the spans' rms vertical deflection response under the transit vehicle is kept to a minimum, and in this way high degrees of passenger ride comfort are achieved. The highlights of this four-part study are summarized.

1. DYNAMICS OF NEAR-OPTIMAL SPANS WITH MOVING LOADS

In this Chapter, optimal pier spacings are predicted for uniform, continuous spans based on equal peak moments (stresses) at midspan. Under a range of vehicle speeds, these spans are near-optimal. The loading is a constant point force, representing a relatively light-weight, short vehicle (4 to 7 m long) on a long, clear span (25 to 35 m long). Continuous spans with up to 11 supports, or N = 10 segments, are investigated. Some results are summarized in Figure 1. This shows that the choice of a continuous span configuration instead of a series of simple spans of the same total length and stiffness, can lead to a 20 to 30 percent reduction in peak moment, depending on whether the piers are evenly spaced or optimally spaced, respectively.

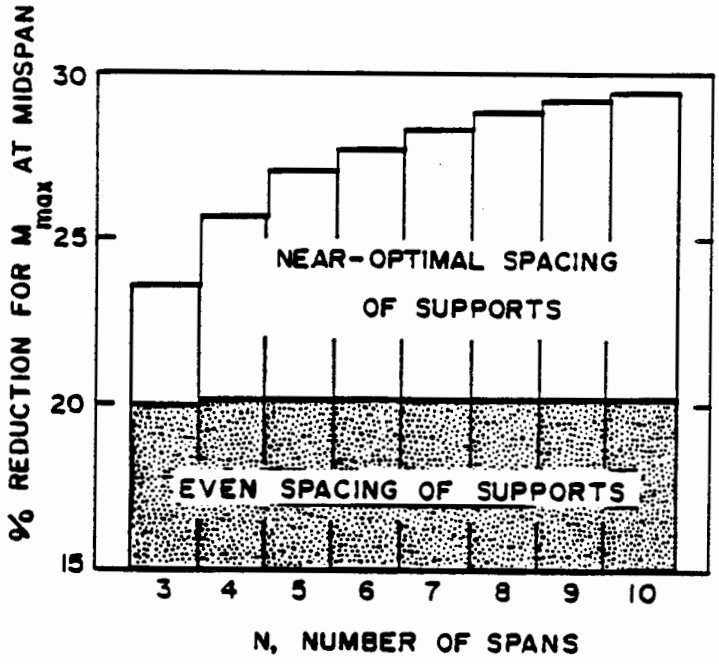

Figure 1 Moment reduction of continuous spans compared to simple spans

The general dynamic response analysis and the laboratory experimental validations of these results for optimal, uniform guideways comprise the main part of this chapter. For instance the peak moment responses for the four-span configuration as a function of nondimensional vehicle speed are shown in Figure 2. Results clearly show an excellent agreement between theory and experiment, as well as an increased efficiency (lower moment) for the spans with optimal or near-optimal pier spacing. A last conclusion is that the rms deflections under both point loads and split or tandem loads can result in lower rms vertical deflections for the vehicle, thus indicating improved ride quality.

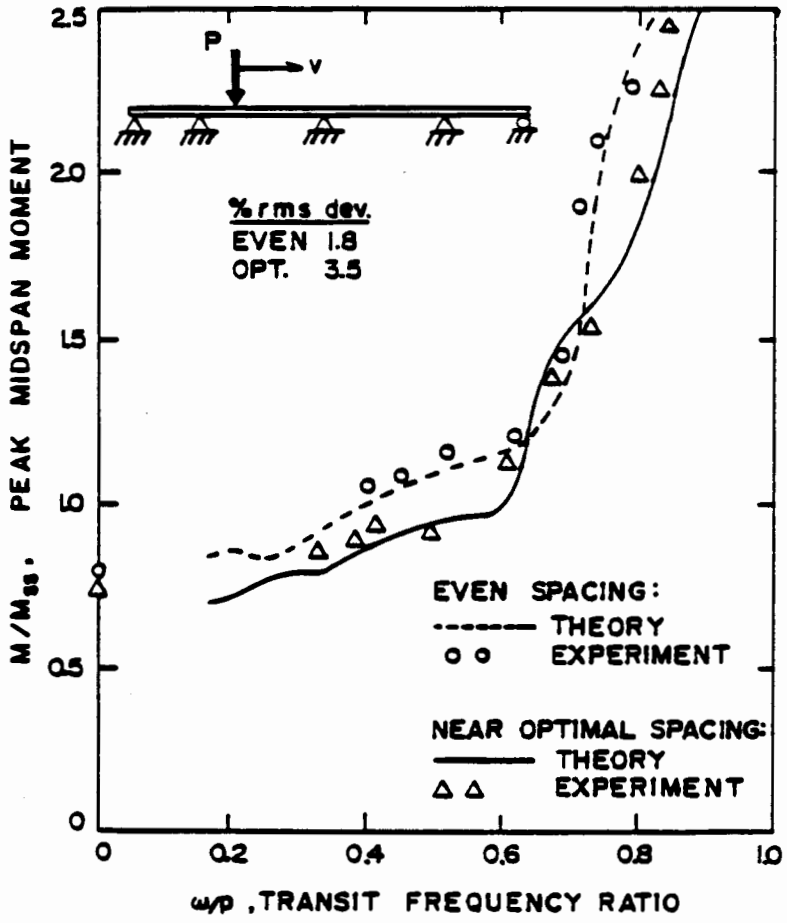

Figure 2 Peak four-span moments with a point load

2. NEAR-OPTIMAL INERTIALESS SPANS

In this Chapter, the results are similar to those found in Chapter 1; but the mathematical span model is different. Here, the transit mass is always much larger than the segment mass of a uniform, continuous, inertialess span. Physically, of course, this corresponds to a short but relatively heavy transit vehicle on a long, light-weight span. Critical span responses (peak deflections and moments are evaluated numerically as a function of a dimensionless velocity parameter, V, for spans of order N from one to six. A comparison of peak moments for several span configurations is shown in Figure 3. The continuous spans with optimal pier spacing clearly exhibit superior performance or smaller moments, when compared to those with even support spacing; and all continuous spans are superior in this respect to the simple span.

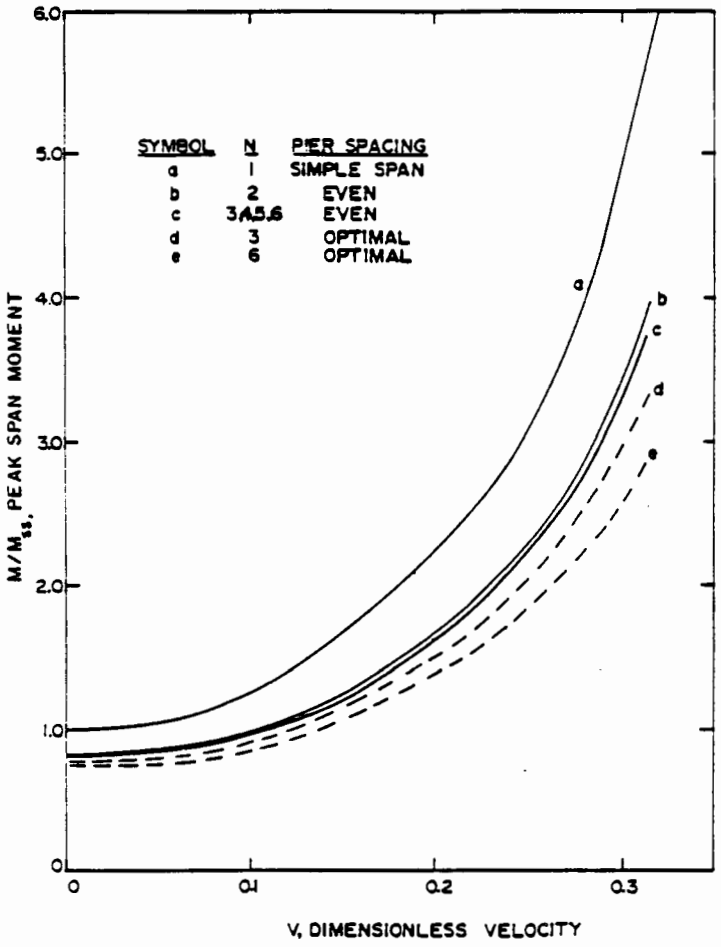

Figure 3

Comparisons of peak moments for several span configurations

3. OPTIMAL RESPONSE FOR GUIDEWAYS WITH MULTIPLE DISTRIBUTED PARAMETERS

In this Chapter, systematic studies are made of the three-parameter problem: the spans' pier spacing, bending stiffness and unit mass are all allowed to vary from segment to segment; but are held constant in any one span segment. The dynamic problem is completely reformulated and solved numerically, where all span inertia effects are included for constant speed transit loads of constant intensity. A new measure of span efficiency, ϕ , is defined as a linear combination of four weighted, dimensionless span characteristics: the peak dynamic stress; the peak live load stress difference between span segments; the rms vertical deflection under the transit load; and the total span mass. For a fixed set of distributed parameters, for a vehicle at constant design speed,

a minimum ϕ is sought, subjected to practical constraints such as stress, deflection and construction techniques. A continuous, three-span configuration is chosen to illustrate the direct-search methodology for evaluating relative efficiencies of alternative designs. Results are presented as three-dimensional, computer graphic isometric displays. For instance, Figure 4 shows that the ϕ surface does have a well-defined minimum for a particular set of (X,Y) coordinate parameters corresponding to bending stiffness and support spacing distributions for a three-span "I" beam guideway. From such studies it is concluded that structural efficiencies can be increased up to 33 percent compared to simple span counterparts. Finally, these efficiencies are most sensitive to the pier spacing parameters and the least sensitive to the stiffness distribution parameters.

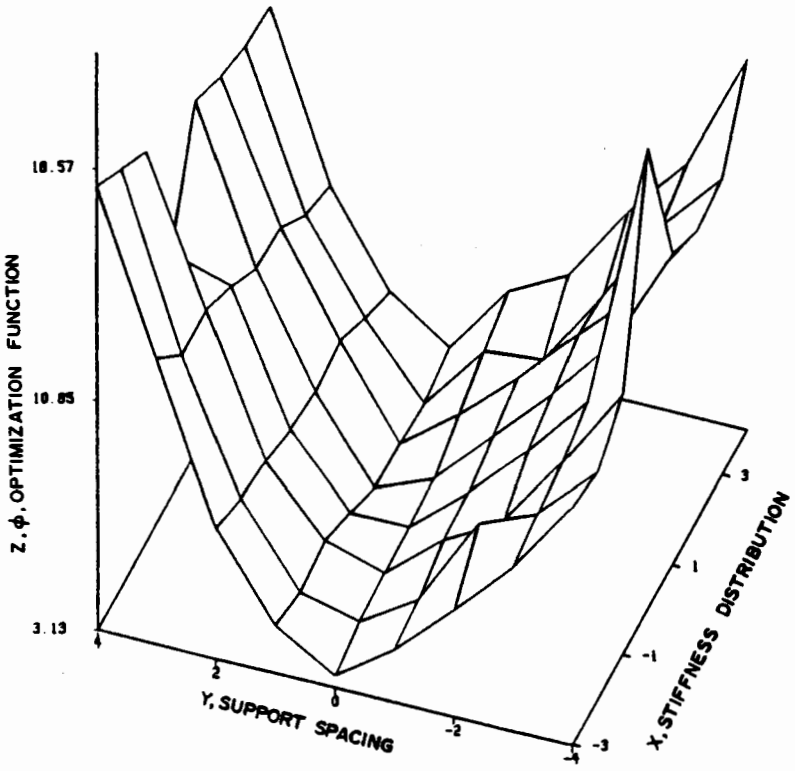

Figure 4

Optimization function surface for an "I"-beam configuration

4. ALTERNATIVE, HIGH EFFICIENCY DESIGNS FOR THE DUKE UNIVERSITY GUIDEWAYS

To illustrate the design methodologies, precast, concrete, elevated guideways with "H"-shaped cross sections are proposed as practical alternatives to a successful state-of-the-art reference design: the transit system at Duke University. Typical alternative configurations are shown in Table below, where weight reductions of 30 to 40 percent are shown to be possible.

Weight reductions for alternative "H" guideways, compared to the Duke University system

	Design		WT. 10^3lb	WT. 10^3N	TOTAL WT. CHANGE percent	LIFT WT. CHANGE percent
Ia AASHTO load	Normal Strength	simple support	57.7	257	-30.1	42.5
		shored	53.2	237	-35.6	31.4
	High Strength	simple support	53.2	237	-35.6	31.4
		shored	50.9	226	-38.4	25.7
	Prestressed (both simple supports)	no transfer rebar	59.5	265	-28.0	46.9
		transfer rebar	51.6	230	-37.5	27.4
Ib modified load	Normal Strength	simple support	55.4	246	-32.9	36.8
		shored	49.0	218	-40.7	21.0
	High Strength	simple support	49.0	218	-40.7	21.0
		shored	47.3	210	-42.7	16.8
	Prestressed	simple support	47.4	211	-42.3	17.8

It is concluded that the most efficient designs are continuous span configurations with a minimum number of pier supports, properly spaced so that balanced stresses are achieved. The proper balance of span length, stiffness and unit mass distribution is ultimately up to the individual designer whose judgement must be tempered by specific and sometimes subtle constraints. The methodologies presented herein should greatly aid the designer in producing advanced-concept, minimum cost, urban transit structures with high strength to weight ratios, which also have aesthetic appeal and afford a high degree of ride comfort.

1. DYNAMICS OF NEAR-OPTIMAL SPANS WITH MOVING LOADS

INTRODUCTION

There is a continuing need to design efficient supporting structures with minimal vibration response for use in modern transit vehicle systems. Related literature published in the last ten years emphasizes the dynamic interactions of beam-type guideways with captive vehicles [1.4], [1.7], [1.8], with an added emphasis on the optimization of transit vehicle parameters to keep vehicle vibrations within bounds of ride comfort [1.1], [1.9]. The thrust herein is different. It focuses on continuous beam-type guideway configurations designed for balanced static stresses and for minimal vibration amplitudes imparted to the transit vehicles.

Consider a series of uniform, simple beams, each of length ℓ and stiffness EI, placed end-to-end and subjected to a vertical static load distribution. It is well known that the peak bending moments (and stresses) can be reduced in this guideway configuration by requiring span continuity across the interior supports. For instance, for a three-span continuous beam (N=3), simply supported at its extreme ends, and with evenly spaced supports, the peak midspan moments for a single point force P (located consecutively in spans one, two and three) are given by $0.80M_{ss}$, $0.7M_{ss}$ and $0.80M_{ss}$, respectively. Here, $M_{ss}(=P\ell/4)$ is the peak reference moment for the simple span. Similar fractional reductions in peak, midspan moments for up to N=10 are listed in Table 1.1 for a point load (Type A); and in Table 1.2 for two loads, each of intensity P/2 and

TABLE 1.1 Peak static midspan values of M/M_{ss} for N continuous spans with supports equally spaced, with a single point load.

N, SPAN TYPE	n=1,N	n=2,N-1	n=3,N-2	n=4,N-3	n=5,N-4
1	1	----	----	----	----
3	0.800	0.700	0.800	----	----
4	0.798	0.692	0.692	0.798	----
5	0.798	0.692	0.684	0.692	0.798
6	0.798	0.692	0.684	0.684	0.692
7	0.798	0.692	0.684	0.682	0.684
8	0.798	0.692	0.684	0.682	0.682
9	0.798	0.692	0.684	0.682	0.682
10	0.798	0.692	0.684	0.682	0.682

TABLE 1.2 Peak static midspan values of M/M_{ss} for N continuous spans with supports equally spaced, with two loads P/2 spaced at $\ell/4$

N, SPAN TYPE	n=1,N	n=2,N-1	n=3,N-2	n=4,N-3	n=5,N-4
1	0.750	----	----	----	----
3	0.587	0.487	0.587	----	----
4	0.587	0.481	0.481	0.587	----
5	0.587	0.481	0.474	0.481	0.587
6	0.587	0.481	0.473	0.473	0.481
7	0.587	0.481	0.473	0.473	0.473
8	0.587	0.481	0.473	0.473	0.473
9	0.587	0.481	0.473	0.473	0.473
10	0.587	0.481	0.473	0.473	0.473

separated by $\ell/4$ (Type B). As one would expect, peak static moments are further reduced by splitting the load. Calculations were based on a finite element computer program [1.6].

These results suggest the use of even more "efficient" continuous spans, or ones which would equalize and further reduce the peak moments and deflections under moving loads. Such a reduction in bending moment due to "live" load could lead to a span configuration with less material as compared to a common configuration: simple spans placed end-to-end. Higher efficiency spans involve a fine tuning of the support spacings and ultimately a non-constant stiffness and mass distribution. The dynamics of near-optimal spans based on static loading are analyzed herein to determine continuous span behavior, such as critical moments and rms deflection under transit loads. Finally, these analytical results are validated in certain cases by laboratory-scale experiments. Since the presentation of all data is in nondimensional form, the results are directly useful in design.

NEAR-OPTIMAL SPANS FOR STATIC LOADING

The continuous span reference configurations chosen for dynamic analysis are defined as follows. See Figure 1.1.

(1) The extreme ends rest on simple supports.

(2) Vertical displacements are zero at all supports.

(3) Continuity of slope and moment are maintained at all interior supports.

(4) Each N-span configuration has a fixed total length $L=N\ell$ where ℓ is the mean span length between consecutive supports.

(5) The support spacings are defined by the multipliers f_n, normally in the range $0.85 \leq f_n \leq 1.15$, where

$$L = N\ell = \sum_{n=1}^{N} f_n \ell$$

(6) The multipliers for each n span are calculated from classical (static) beam theory, based on the requirement that the peak midspan moments are all equal, for a single, vertical point load traversing at crawl speed.

As a consequence of this definition, each reference guideway is symmetric about its midlength so that the multipliers are related by $f_n = f_{N+1-n}$ $(n = 1,2,\ldots,N)$.

Calculations of multiplier sets $(f_1, f_2, \ldots f_N)$ for N=3 through 10 were made using a finite elements program [1.6] and a direct search, trial and error procedure. For each N, the multipliers were adjusted until the peak midspan moments in all spans were equal within a tolerance of 0.1 per cent. The multiplier sets for eight span configurations N=3 through 10, are listed in Table 1.3. It is observed that for all N, the extreme end spans are shorter by 19 to 20% compared to the longest interior spans.

Table 1.4 shows the peak midspan moments calculated for these near-optimum spans subjected to Types A and B load configurations at crawl speed. Although the multipliers f_n were based on the single load, the partitioning of this load as noted yielded peak midspan moments which were equal within a tolerance of 0.3 percent. Again, the effect of dividing the load was to reduce the magnitude of this peak moment (from $0.764M_{ss}$ to $0.548M_{ss}$ for N=3, for in-

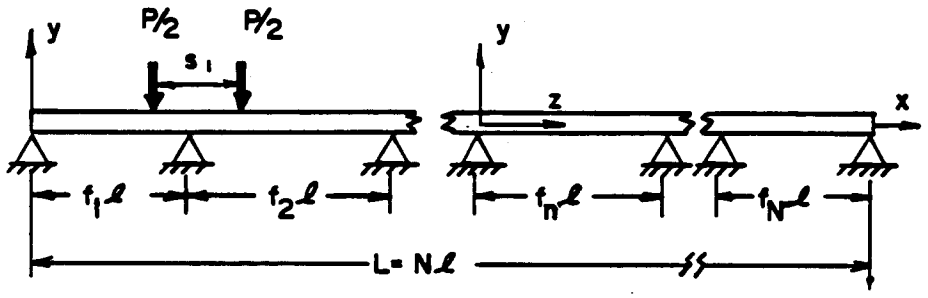

Figure 1.1 Nonperiodic, continuous beam model

TABLE 1.3 Span length multipliers f_n for near-optimal configurations

N, SPAN TYPE	n=1,N	n=2,N-1	n=3,N-2	n=4,N-3	n=5,N-4
3	0.937	1.126	0.937	----	----
4	0.910	1.090	1.090	0.910	----
5	0.896	1.070	1.068	1.070	0.896
6	0.885	1.059	1.056	1.056	1.059
7	0.876	1.051	1.049	1.048	1.049
8	0.870	1.046	1.043	1.041	1.043
9	0.867	1.0415	1.0375	1.036	1.036
10	0.864	1.037	1.033	1.033	1.033

TABLE 1.4 Peak static midspan values of M/M_{ss} for near-optimal configurations, with a point load P (row A) and a split load P/2 spaced at ℓ/4 (row B)

LOAD TYPE	N, SPAN TYPE 3	4	5	6	7	8	9	10
A	.764	.743	.729	.722	.716	.711	.708	.705
B	.548	.528	.517	.515	.503	.499	.496	.493

stance). For both load configurations, as N approaches 10, the reduction in peak moment becomes less and less significant.

Figure 1.2 summarizes these trends. Note that as much as a 20 percent moment reduction, compared with simple spans, can be achieved by employing continuous spans with equal spacings; but for the near optimal spacings of Table 1.2, the reduction may be as high as 30%.

It should be emphasized that the continuous spans labeled "near-optimal", based on the equalization of peak midspan moments are meant for comparison purposes only. For design, one must proceed with caution. For instance, these midspan data give the absolute peak moments in all but the two extreme end spans. In these latter spans, the peak moments never exceed by more than 4 percent those at midspan; and occur under the load, located between 0.4ℓ and 0.5ℓ, measured from the extreme end of the support. Table 1.5 shows such data from which absolute peak moments can be calculated using the corresponding data of the previous tables. As the speed of the load increases above the crawl speed, dynamic span effects cause the peak moments to move closer to and even beyond the midspan location [1.7]. The midspan is thus the common and convenient reference point chosen here for study of both static and dynamic efficiency of continuous spans.

DYNAMIC MODEL AND SYSTEM PARAMETERS

The well-known Bernoulli-Euler equation of motion,

$$EI \frac{\partial^4 y}{\partial x^4} + \bar{m} \frac{\partial^2 y}{\partial t^2} = F(x,t) \qquad (1.1)$$

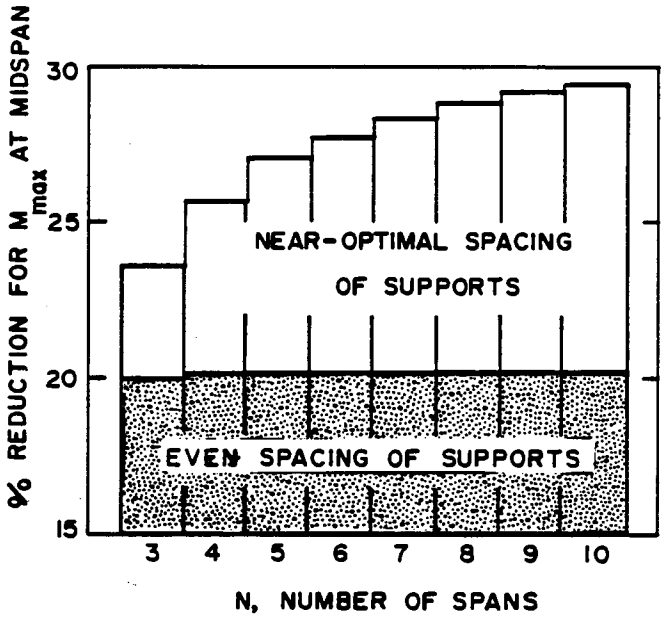

Figure 1.2 Moment reduction of continuous spans compared to simple spans

TABLE 1.5 Percent increase of peak, static M/M_{ss} values over the midspan values in Tables 1.1, 1.2, and 1.4

SUPPORT LOAD SPACING TYPE	N, SPAN TYPE 3	4	5	6	7	8	9	10
EVEN A	2.5	2.6	2.6	2.6	2.6	2.6	2.6	2.6
EVEN B	3.8	3.8	3.8	3.8	3.8	3.8	3.8	3.6
OPTIMAL A	2.1	1.9	2.2	2.1	1.8	1.8	2.0	2.0
OPTIMAL B	4.0	4.0	3.9	2.5	3.8	3.6	3.8	3.9

is used to model the vertical deflection $y = y(x,t)$ of a uniform, undamped, elastic beam guideway with nonperiodic supports shown in Figure 1.1. The mass per unit length is $\bar{m}$.

Consider first a special case. For a simply supported beam, initially flat and at rest, and subjected suddenly to a constant vertical point force P, traveling at constant speed, the solution to equation (1.I) is derived elsewhere [1.5]. Cast in nondimensional form for reference purposes the dynamic deflection y, and bending moment, $M(=EI\ \partial^2 y/\partial x^2)$, can be written as

$$\frac{y}{y_{ss}} = \frac{96}{\pi^2}\sum_{m=1}^{\infty} G_m(X,Z) \tag{1.2a}$$

$$\frac{M}{M_{ss}} = \frac{8}{\pi^2}\sum_{m=1}^{\infty} m^2 G_m(X,Z) \tag{1.2b}$$

$$G_m(X,Z) = \left\{\frac{\sin\ (m\pi Z) - \frac{\omega}{mp}\sin(m^2 p\pi Z/\omega)}{m^4\left[1 - \omega^2/\left(p^2m^2\right)\right]}\right\}.\sin\ (m\pi X) \tag{1.2c}$$

where $y_{ss}=P\ell^3/48EI$, where EI is the stiffness and where $0 \leq Z \leq 1$. The free vibration bending frequencies are written as

$$p_m = (\lambda_m \ell)^2 \left(\frac{EI}{\bar{m}\ \ell^4}\right)^{\frac{1}{2}} \tag{1.3}$$

where the frequency parameter is

$$\lambda_m \ell = m\pi \quad , m=1,2,3,.... \tag{1.4}$$

and where the reference (fundamental) frequency p is given by equations (1.3) and (1.4) when m=1.

These results show that the responses at material point $X=x/\ell$ for a point load at position $Z = vt/\ell$ depend only on the nondimen-

sional frequency parameter ω/p, where $\omega=\pi\ v/\ell$ defines the transit frequency. For K tandem point forces at constant speed, the solutions to equation (1.1) can be superimposed [1.7]. Thus, the additional system parameters are the (K-1) spacing ratios (s_k/ℓ), where $s_1, s_2, \ldots s_{k-1}$ are spaces between equal consecutive loads of magnitude P/K.

For N uniform, continuous, nonperiodic spans modeled by equation (1.1), subject to the same boundary conditions defined for the near-optimal static spans, and subject to the loadings just described, there are only two additional nondimensional parameters: N and the corresponding set of span length multipliers ($f_1, f_2, \ldots f_N$). The four sets of nondimensional system parameters needed for dynamic response studies of near optimal spans are thus summarized.

ω/p = transit frequency ratio

s_k/ℓ = the (K-1) spacing ratios for K tandem loads, P/K.

N = number of spans in guideway of total length L

$f_1, f_2, \ldots, f_N$ = span length multipliers, Table 1.3.

Before proceeding to the dynamic analysis of nonperiodic spans, it is important to point out that two basic assumptions are invoked to model transit vehicles as point loads. The first is that the sum of all vehicle mass on any guideway section between supports, at any time, should always be much less than the mass of that span. It was found experimentally for periodic spans [1.8] that if this peak mass ratio is less than 0.1 and also if $\omega/p<0.7$ (the second assumption) then one is justified in modeling sprung, wheeled vehicles as constant point forces to accurately predict beam guideway dynamic responses.

The purpose of the analysis which follows is to show the extent to which critical dynamic moments for both the evenly-spaced and for near optimal continuous spans can be reduced below those of the simple span counterpart. The latter reference responses, based on equations (1.2b) and (1.2c) show both the peak midspan moment response (X=1/2) and the peak moment response under the point load (X=Z), Figure 1.3. Note that the latter responses are equal to or greater than those at midspan for $\omega/p \leq 0.72$. Finally, although $\omega/p \leq 0.3$ for current guideways limited to 80 km/hr vehicles, values of ω/p approaching 0.7 may soon be a reality for future rapid transit vehicles approaching 450 km/hr.

FREE VIBRATIONS OF NON-PERIODIC SPANS

The free vibration frequencies and mode shapes needed to calculate the response of the near optimum static designs are discussed elsewhere [1.2]. Briefly, the method involves transforming the governing homogeneous form of equation (1.1) into a local coordinate system z such that

$$\left.\begin{array}{lll} z = x & \text{for} & 0 \leq x \leq f_1 \ell \\ z = x - \sum_{j=1}^{n-1} f_j \ell & \text{for} & n = 2,3,\ldots N \end{array}\right\} \qquad (1.5)$$

where N is the number of spans in the continuous guideway of length $L-N\ell$, with the set of multipliers $(f_1, f_2, \ldots, f_N)$ applied to the average span length ℓ. For free, harmonic vibrations, $F(x,t)=0$ in equation (1.1), which, with equations (1.5), reduces to

$$\frac{d^4 y_{m,n}(z)}{dz^4} - \lambda_m^4 y_{m,n}(z) = 0 \qquad (1.6)$$

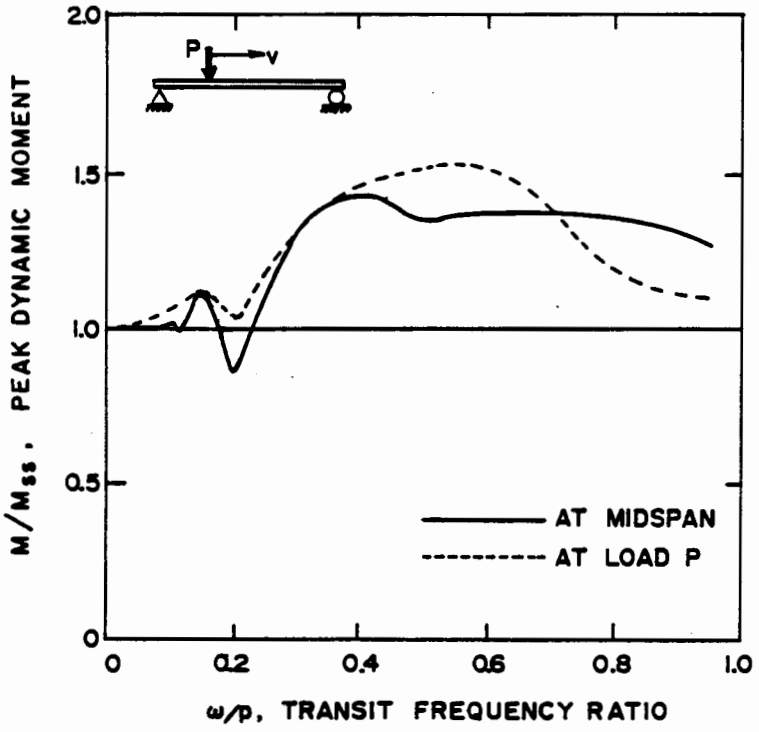

Figure 1.3 Peak simple span moments with a constant speed point load

TABLE 1.6 Typical values for $\lambda_m \ell$

SIMPLE SPAN	N=3 EQUAL SPANS	N=3, OPTIMAL SPANS
π	3.14159	3.08833
	3.56562	3.74124
	4.28836	4.19443
2π	6.28319	6.07527
	6.70722	7.04105
	7.42995	7.37685
3π	9.42478	9.00790
	9.84881	10.32241
	10.5715	10.62833
4π	12.5664	11.92428
	12.9904	13.57136
	13.7131	13.91087
5π	15.7080	14.85856
	16.1320	16.75506
	16.8547	17.20711
6π	18.8496	17.85148
	19.2736	19.83728
	19.9963	20.50701
7π	21.9911	20.94409
	22.4152	22.82260

where n=1,2,...N designates the span segment and m=1,2,3,... designates the mode number. The free vibration frequencies are defined by equation (1.3), where the frequency parameters, $\lambda_m \ell$, are not given by equation (1.4); but are calculated as follows. For a particular set (m,n) in an N span system, the general solution to equation (1.5) describing the mode shapes is given by

$$y_{m,n}(z) = A(m,n) \cosh \lambda_m z + B(m,n) \sinh \lambda_m z + C(m,n) \cos \lambda_m z + D(m,n) \sin \lambda_m z \tag{1.7}$$

By applying the boundary and continuity conditions defined previously for the near-optimal spans, to equation (1.7), the relationships between the constants on any two consecutive spans becomes

$$A(m,n) = -C(m,n) \tag{1.8a}$$

$$B(m,n) = \frac{C(m,n) \cosh (\lambda_m f_n \ell) - C(m,n+1)}{\sinh (\lambda_m f_n \ell)} \tag{1.8b}$$

$$D(m,n) = \frac{C(m,n+1) - C(m,n) \cos (\lambda_m f_n \ell)}{\sin (\lambda_m f_n \ell)} \tag{1.8c}$$

$$C(m,n) \cdot \psi(m,n) - C(m,n+1) \cdot [\theta(m,n) + \theta(m,n+1)] + C(m,n+2) \cdot \psi(m,n+1) = 0 \tag{1.8d}$$

where

$$\theta(m,n) = \coth (\lambda_m f_n \ell) - \cot(\lambda_m f_n \ell) \tag{1.8e}$$

$$\psi(m,n) = \operatorname{csch}(\lambda_m f_n \ell) - \csc(\lambda_m f_n \ell) \tag{1.8f}$$

Thus, for a fixed N and a known set of multipliers $(f_1, f_2, \ldots f_N)$, equation (1.8d) with equations (1.8e) and (1.8f), form a set of (N-1) homogeneous algebraic equations in C(m,2), C(m,3),...C(m,N)

The consecutive roots $\lambda_m \ell$ of the determinant of order (N-1), formed from the coefficients of these unknown C(m,n) coefficients, yield the consecutive system frequencies through equation (1.3). With these roots and equations (1.8), the free vibration modes found from equation (1.7) within an arbitrary constant, which is set equal to unity.

A numerical procedure utilizing an IBM 370/165 digital computer was developed to calculate the frequency parameters and mode shapes. Table 1.6 shows typical results for N=3, both for equally spaced supports and for the near-optimum case defined by Table 1.3. The latter spans show a depressed fundamental frequency since $\lambda_1 \ell = 3.0883 < \pi$; and both show a cluster of two frequencies between each consecutive frequency of the simple span. For N spans, there are (N-1) frequencies in such a cluster. Such frequency parameters and mode shapes are utilized in the forced vibration analysis which follows.

FORCED VIBRATION RESPONSE

The theory of normal mode analysis for a specified force distribution F(x,t) applied to a linear structure is well-known [1.3]. In this problem, a mode shape $Y_m(x)$, valid for all modes at every point on the N-span beam guideway is constructed from the sum of individual span mode shapes, or

$$Y_m(x) = \sum_{n=1}^{N} y_{m,n}(z) \qquad (1.9)$$

For a vertical point force of constant magnitude P, starting at x=0 at t=0 and traveling at a constant horizontal speed v over the

guideway, the loading term is given by

$$F(x,t) = P\ (x - vt) \tag{1.10}$$

where the total load on the system is

$$F(x,t) = \int_0^L P\delta(x - vt)dx = \begin{cases} P\ , & 0 \leq vt \leq L \\ 0\ , & \text{otherwise} \end{cases} \tag{1.11}$$

Both the loading and the deflection are expanded in a series of normal modes $Y_m(x)$:

$$F(x,t) = \sum_{m=1}^{\infty} P_m(t)\ Y_m(x) \tag{1.12a}$$

$$y(x,t) = \sum_{m=1}^{\infty} Q_m(t)\ Y_m(x) \tag{1.12b}$$

Equations (1.12) are substituted into equation (1.1); the resulting equation is multiplied by $Y_j(x)$; each term is integrated over the interval $0 \leq x \leq L$; use is made of the orthogonality of the modes:

$$\int_0^L Y_m(x)\ Y_j(x)dx = \begin{cases} 0 & \text{for } m \neq j \\ I_m & \text{for } m = j \end{cases} \tag{1.13}$$

With equations (1.9), (1.11) and (1.13) it follows

$$\ddot{Q}_m(t) + p_m^2\ Q_m(t) = \frac{1}{\bar{m}} P_m(t) \tag{1.14}$$

$$P_m(t) = \frac{1}{I_m} \int_0^L P\ \delta(x - vt) Y_m(x)dx = \frac{P}{I_m}\ Y_m(vt) \tag{1.15}$$

$$I_m = \int_0^L Y_m^2(x)dx = \sum_{n=1}^{N} \int_0^{f_n \ell} \left[y_{m,n}(z) \right]^2 dz \tag{1.16}$$

Based on the free vibration frequency parameters, $\lambda_m \ell$, and the

corresponding mode shapes, $y_{m,n}(z)$, the normalizing factor, I_m, of equation (1.16), the overall mode shape of equation (1.9), and the loading term of equation (1.15) were all calculated; then the ordinary differential equation (1.14) was solved for zero initial conditions corresponding to an initially flat, motionless system, and the deflection response was calculated from equation (1.12b). The moment response was calculated from

$$M(x,t) = EI \sum_{m=1}^{\infty} Q_m(t)\, Y_m''(x) \tag{1.17}$$

For a string of r constant tandem loads, F_i, at constant speed, the only change from the above procedure is that $Q_m(t)$ is now calculated from

$$\ddot{Q}_m(t) + p_m^2 Q_m(t) = \frac{1}{mI_m} \sum_{i=1}^{r} F_i Y_m(x_i) \tag{1.18}$$

where $Y_m(x_i)$ is the amplitude of the m-th mode under load F_i.

THEORETICAL AND EXPERIMENTAL RESULTS

The above results for the free vibration mode shapes, the frequency parameters and the forced span vibration responses were formulated into a Fortran IV algorithm. An IBM 370/165 digital computer was utilized to calculate time histories of bending moments and vertical deflections, both at selected span locations and also under each load. The midspan moment time histories were selected as the critical points for this study since such results could be compared most easily to experimental measurements.

Typical numerical results for Type A loading are shown in Figures 1.4 through 1.9, which depict envelopes of the peak midspan

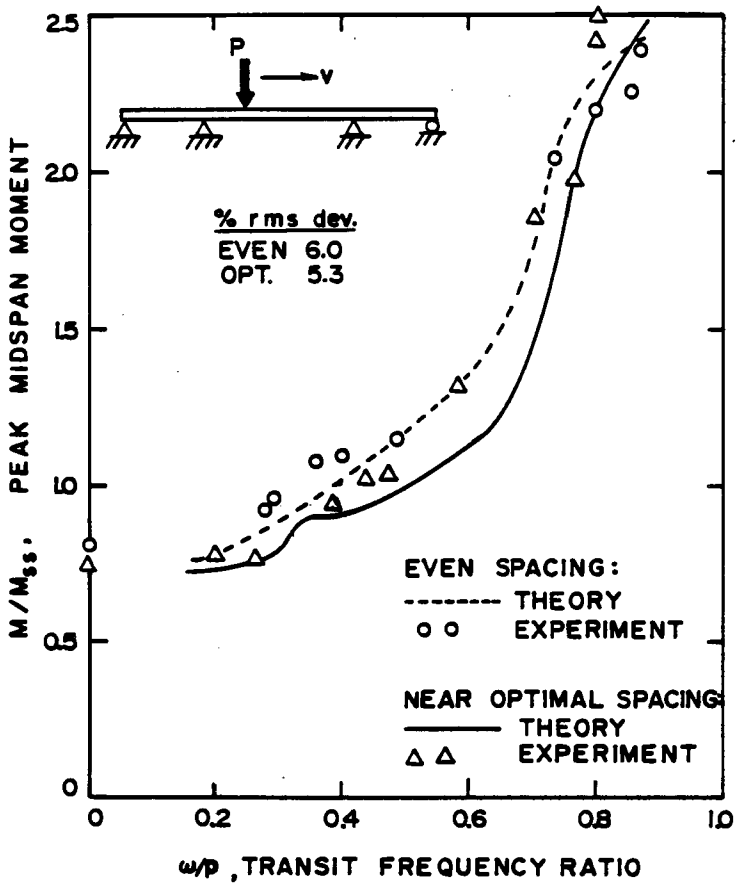

Figure 1.4 Peak three-span moments with a point load

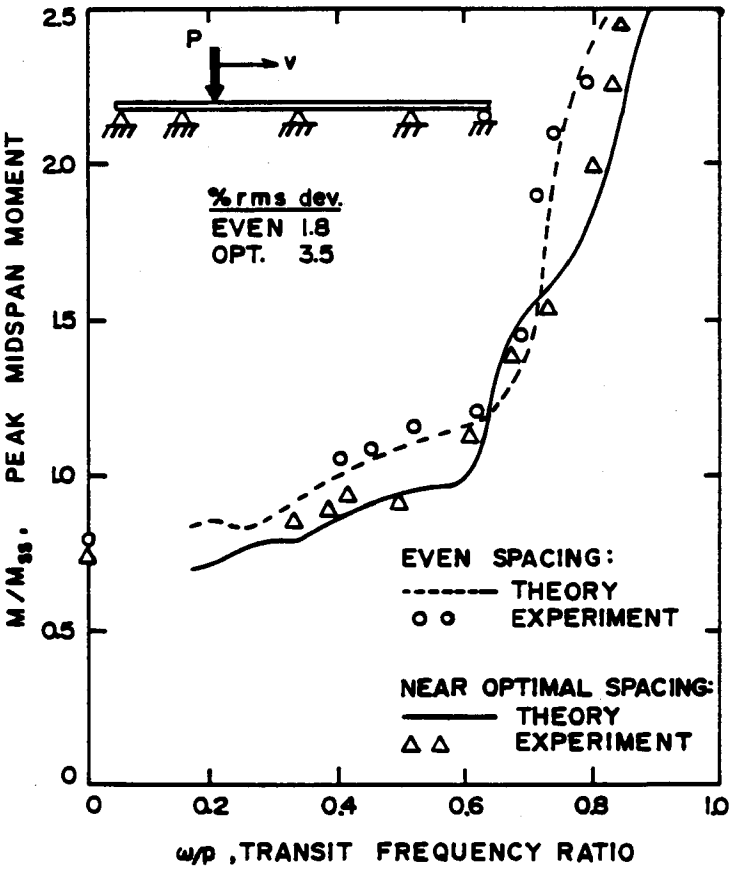

Figure 1.5 Peak four-span moments with a point load

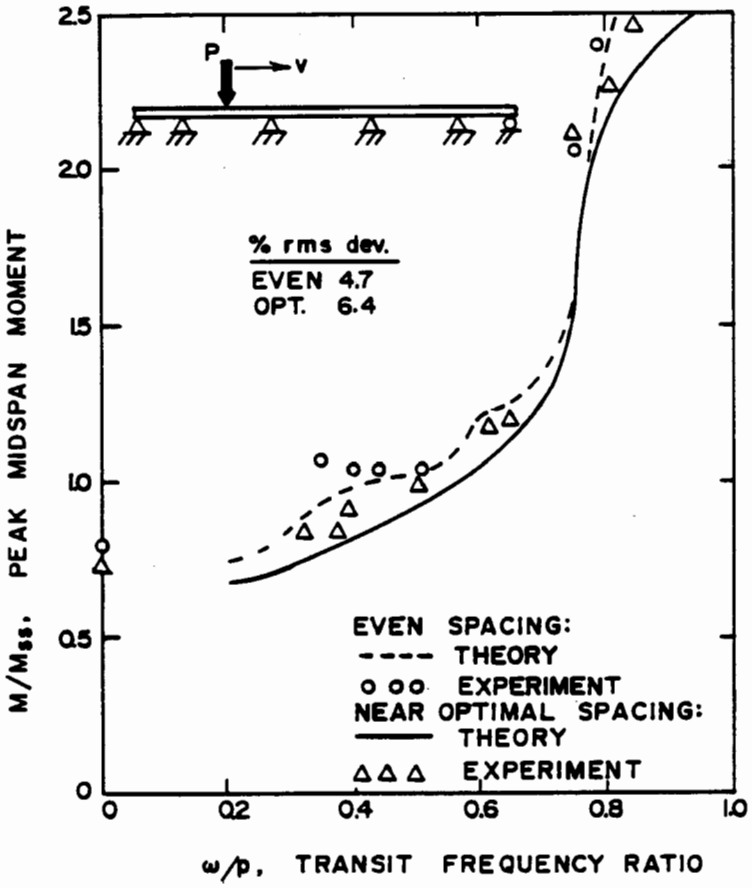

Figure 1.6 Peak five-span moments with a point load

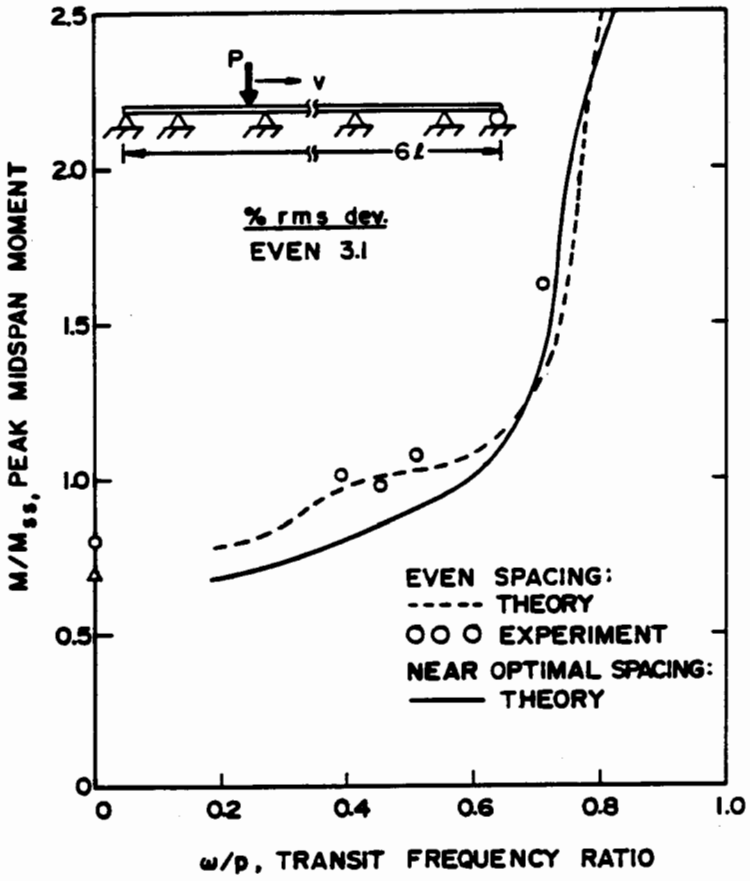

Figure 1.7 Peak six-span moments with a point load

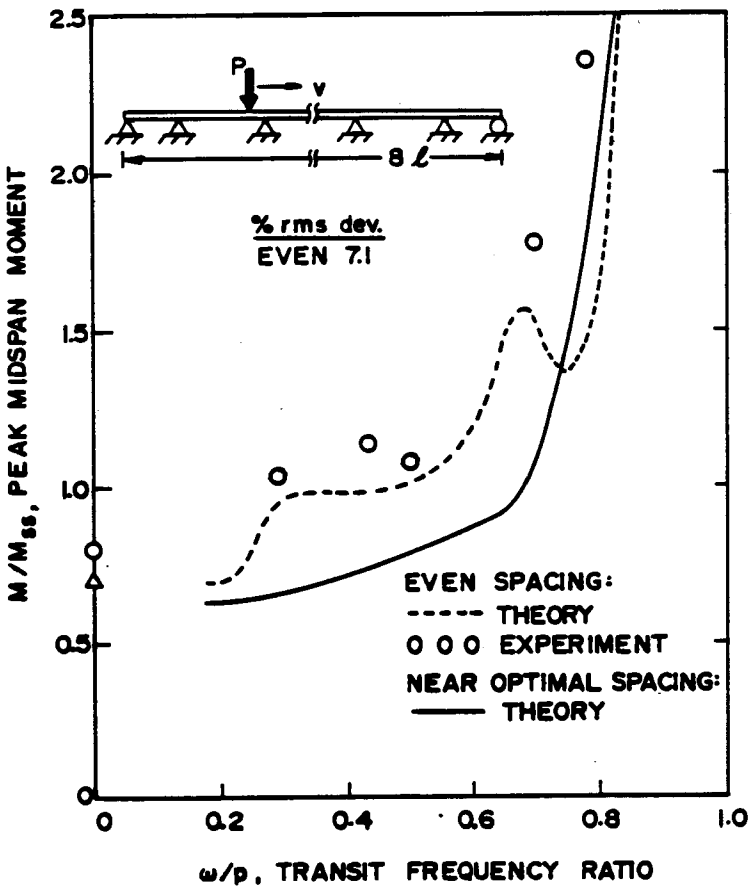

Figure 1.8 Peak eight-span moments with a point load

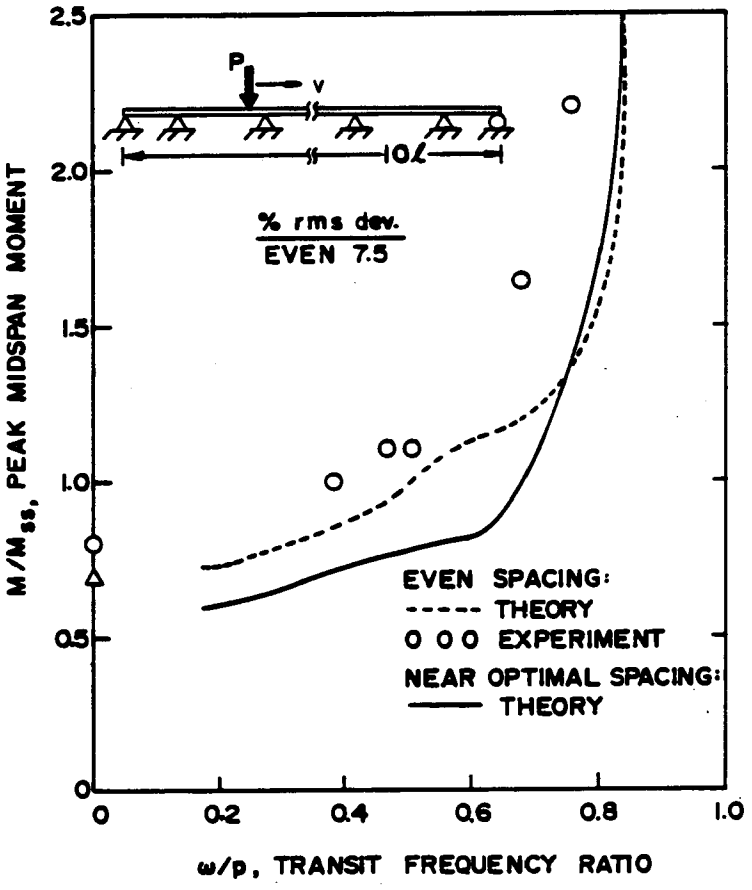

Figure 1.9 Peak ten-span moments with a point load

moments for N=3 through 6, 8 and 10 respectively. Similar data for Type B loading are shown in Figures 1.10 through 1.15 for the same N values. It was found that for NM=20 modes, suitable convergence was obtained. For the near-optimal spans (the solid lines), the span length multipliers are given by Table 1.3; and for even pier spacings (the broken lines), these multipliers are all unity. For a fixed N and ω/p, the ordinate M (normalized to the simple span moment) corresponds to the highest dynamic moment, comparing moments among midspans. This peak either occurred during the time $0<t<L/v$, when the load was traversing length L; or during free vibration, $t>L/v$.

These Figures do <u>not</u> show several facts. First, in the limit of zero transit speed ($\omega/p \to 0$), the midspan moments are all equal for the near optimal configurations; but in all configurations, these peak dynamic moments vary and shift from those near the entrance span to the exit span as ω/p approaches 0.7. Second, these peak moments do not always represent the absolute peak moments in the system. These latter moments occur within a range of ± 10 percent of midspan depending upon n, N and ω/p; but the absolute peak moments were calculated and were found to never exceed by more than 8 percent those depicted in Figures 1.4 through 1.15.

These Figures <u>do</u> show, by comparison with Figure 1.3, that at least a 20 percent reduction in peak midspan moments may be achieved by utilizing continuous rather than simple spans in the range $0 \leq \omega/p \leq 0.3$; that an even higher reduction is achieved near $\omega/p=0.5$; and that continuous span moments approach and then exceed

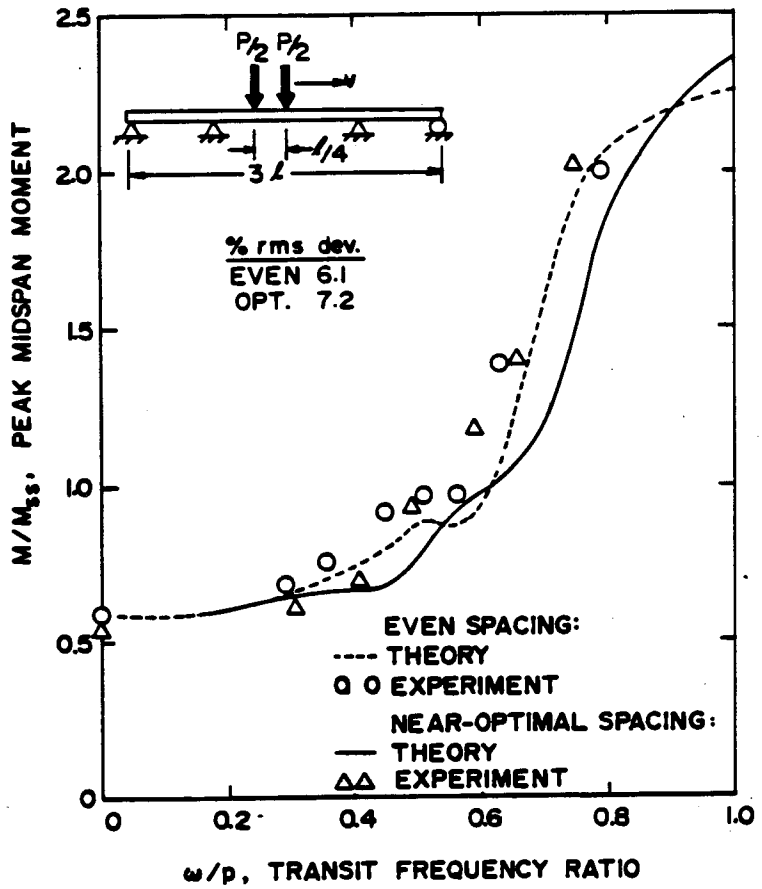

Figure 1.10 Peak three-span moments with a two-point tandem load

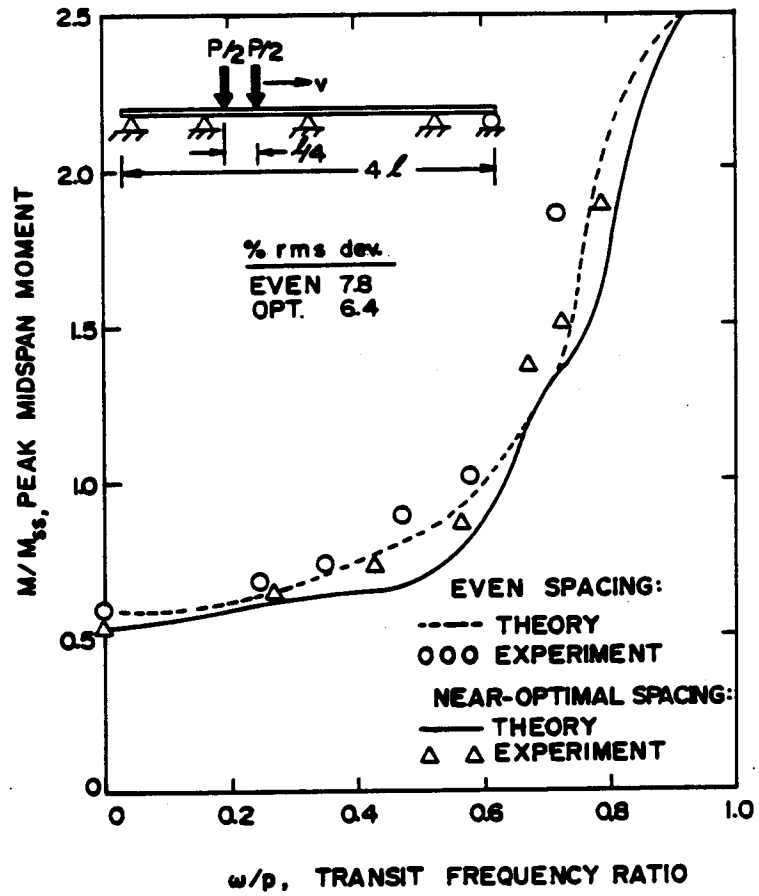

Figure 1.11 Peak four-span moments with a two-point tandem load

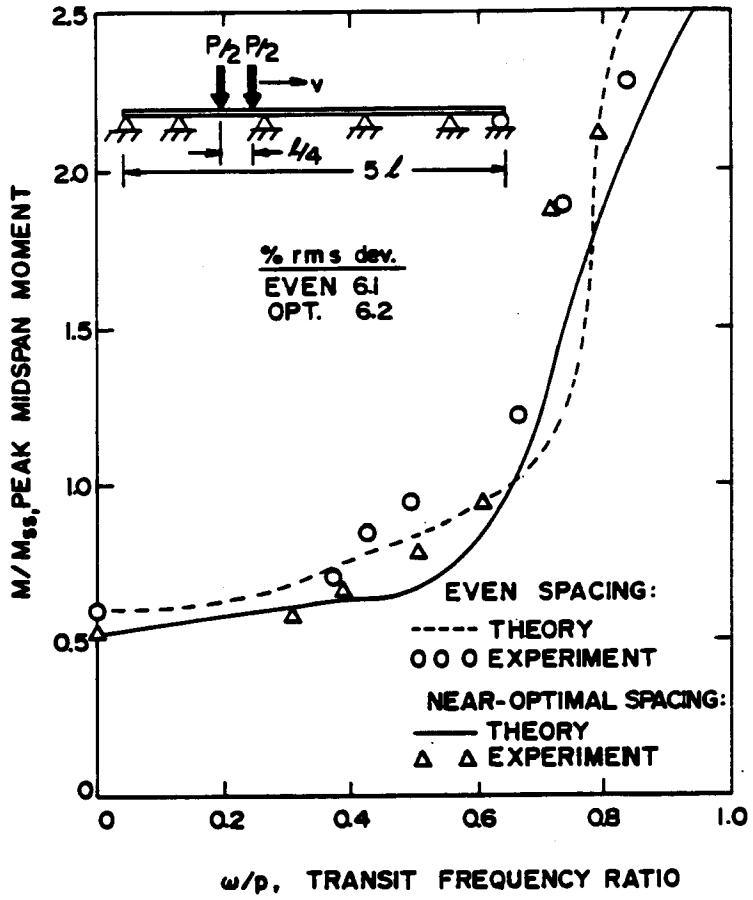

Figure 1.12 Peak five-span moments with a two-point tandem load

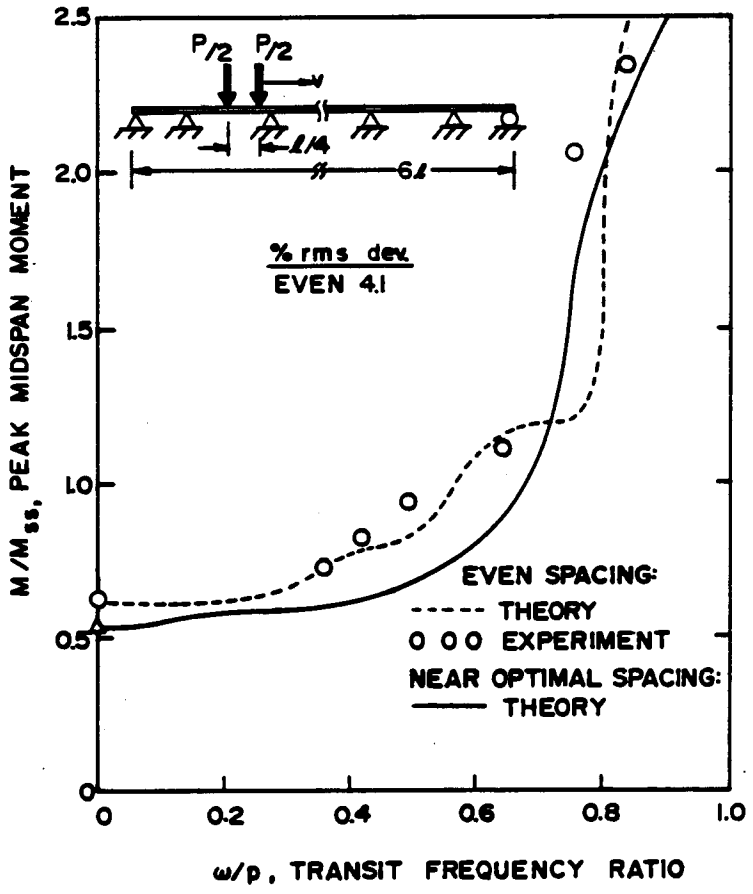

Figure 1.13 Peak six-span moments with a two-point tandem load

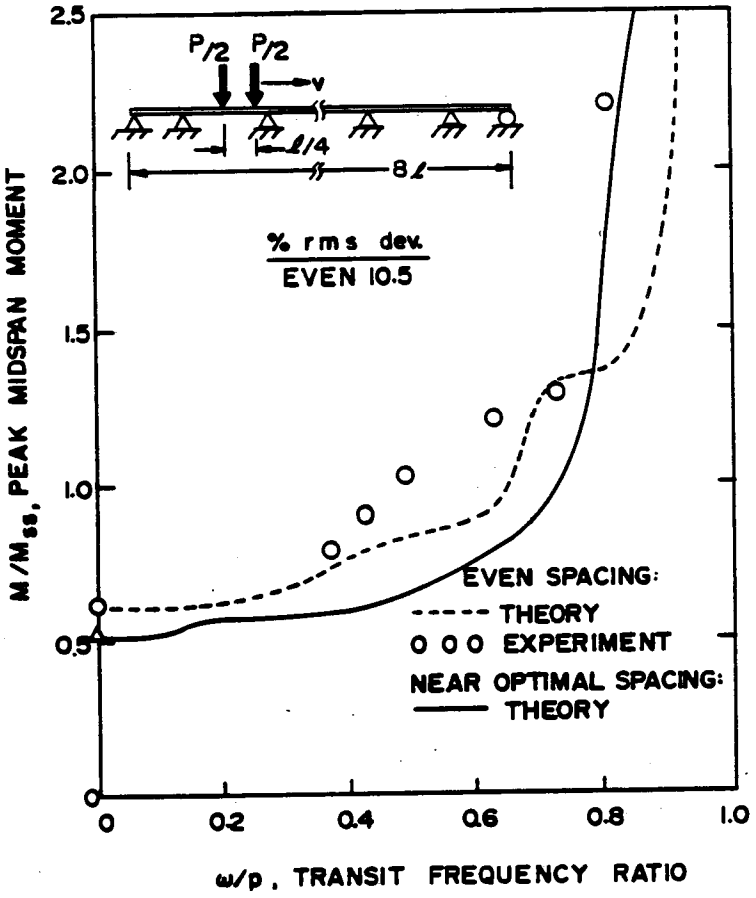

Figure 1.14 Peak eight-span moments with a two-point tandem load

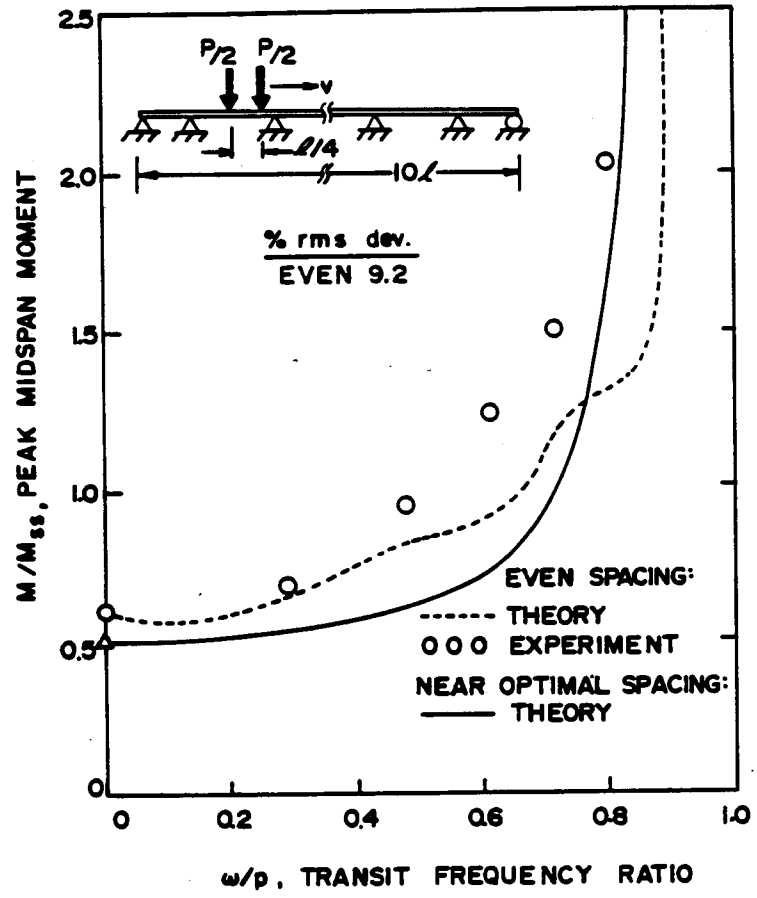

Figure 1.15 Peak ten-span moments with a two-point tandem load

the absolute peak simple span ratio of 1.55 as ω/p approaches and then exceeds 0.7. However, for $\omega/p<0.6$, the near-optimal spans always give dynamic moment reductions.

To validate the above analysis, an experimental program was undertaken. Details of the experimental system in which laboratory-scale multiple spans, instrumented with midspan strain gages to give a measure of midspan moment during the passage of a point load, are documented elsewhere [1.8]. In Figures 1.4 through 1.15, the experimental values (triangles for the near-optimal and circles for the evenly spaced configurations) usually lie a little above their respective theoretical curves; but none-the-less follow the predicted dynamics quite closely. In each of these Figures, the percent rms deviation of a set of experimental values from its counterpart predicted curve, is noted. To arrive at these deviations, it was assumed that the possible error in measuring load speed (or the abscissa, ω/p) was the same as the possible error in measuring midspan strain (or the ordinate, M/M_{ss}). Thus, the deviation was based on the least distance of a data point from its predicted curve. The deviations for Type A loadings were generally lower (1.8 to 7.5 percent) than for those for Type B loadings (4.1 to 10.5 percent). This was probably because the Type A loading more closely approximated a constant point force, where the ratio of transit mass to span mass between consecutive supports was about 0.15. For Type B loading, this ratio, including both transit loads, was about 0.2, which accentuated the vertical inertia effects of this transit load, making the effective span loading deviate somewhat more from its "dead

load" value. Nevertheless, with the cluster of deviations about 5 percent, these experiments do serve to validate the theoretical results quite satisfactorily.

SPAN DESIGN FOR RIDE COMFORT

An important consideration in span configuration design is the effect of span vibrations on the passing vehicle. It is well known, for instance, that a comfortable ride means that the vertical acceleration felt by the passenger should not exceed 0.05g's, on the average, for harmonic vibrations in the range of 5 hz [1.1]. To calculate such heave accelerations, one must specify both the span and vehicle suspension configuration [1.9]. Without becoming vehicle-specific, however, it is proposed herein to define the rms vertical span deflection, y_{rms}, under the single load P (Type A) or under the leading load P/2 (Type B) as an approximate measure of input vehicle excitation and relative ride comfort when comparing alternative span configurations. The idea seems reasonable: that minimizing y_{rms} for fixed values of L, EI, $\bar{m}$ and ω/p, would produce lower amplitudes of excitation and thus higher ride comfort for a particular vehicle. Also, as y_{rms} approaches zero, the ride becomes ever more smooth.

With these ideas in mind, one can use the calculated values of y_{rms} (normalized to y_{ss}) shown in Figures 1.16 and 1.17 as relative guides in choosing span configurations. For instance, compared to a series of five simple spans each of length ℓ and stiffness EI, its counterpart continuous configurations all give a higher ride quality in the range of $0<\omega/p<0.5$, since y_{rms} is

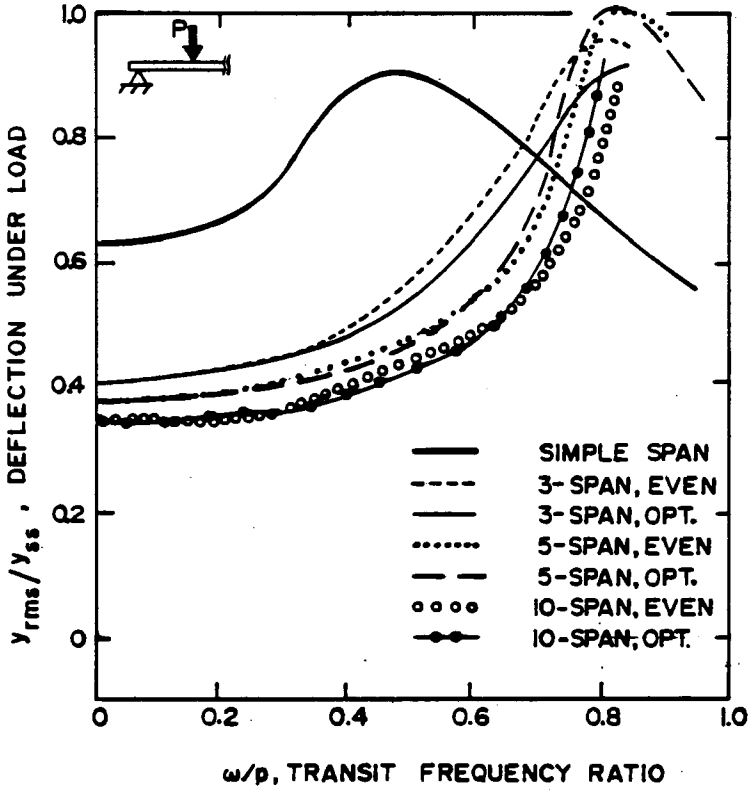

Figure 1.16 RMS deflection under a constant speed point load

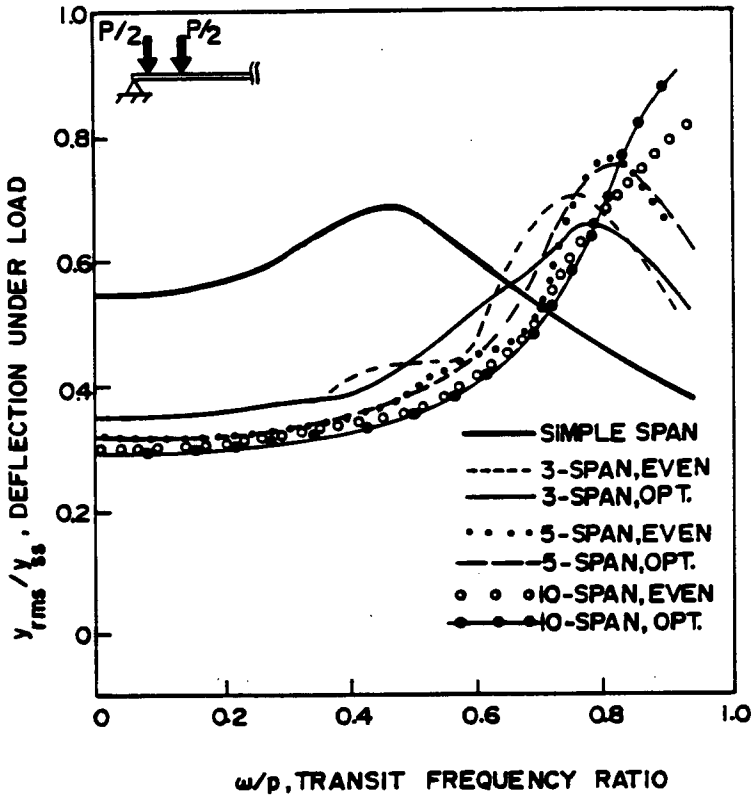

Figure 1.17 RMS deflection under the leading load for a two-point tandem load.

from 30 to 40% lower. Also, the near-optimal spans yield slightly lower values of y_{rms} than their evenly spaced counterparts if $\omega/p<0.6$. It is noted that y_{rms} decreases as N increases at constant ω/p; and decreases when the load is split. The curves for N=4 and 6 through 9 are not shown (for clarity) but these do lie between the sets shown. Finally, consistent with the moment response studies, deflection responses exceed those of the simple span for ω/p above about 0.7.

CONCLUSIONS

In conclusion, the choice of a continuous span configuration instead of a series of simple spans of the same total length and stiffness, can lead to a 20 to 30 percent reduction in peak dynamic moment, depending on whether the span piers are evenly spaced or optimally spaced respectively, as long as $\omega/p<0.6$. In this range of transit frequency ratio, the values of y_{rms} under the point load and the split load are considerably reduced by employing continuous rather than simple span configurations. The reduction in dynamic moment and y_{rms} achieved by employing the optimal spans can lead to span weight reduction, increased ride comfort and more aesthetic structures for modern transit systems.

REFERENCES FOR CHAPTER 1

1.1 "A Guide to Evaluation of Human Exposure to Whole Body Vibration," Draft Standard ISO/DIS 2361, International Organization for Standardization, Geneva, Switzerland, 1972.

1.2 Fertis, Demeter G., Dynamics and Vibration of Structures, John Wiley and Sons, N.Y., 1973, pp. 127-132.

1.3 Kolousek, Vladimir, Dynamics in Engineering Structures, Halsted Press, N.Y., 1973, pp. 132-135.

1.4 Richardson, H. H. and Wormley, D. N., "Transportation Vehicle/Beam Elevated Guideway Dynamic Interactions: A State-of-the-Art Review," Journal of Dynamic Systems, Measurement and Control, Transactions, American Society of Mechanical Engineers, Vol. 96, June, 1974, pp. 169-179.

1.5 Timoshenko, S. and Young, D. H., Vibration Problems in Engineering, D. Van Nostrand Co., Princeton, N.J., 1955, pp. 351-355.

1.6 Utku, S., "ELAS Computer Program for the Analysis of Structures using the IBM 360 Computer," Structural Mechanics Series No. 8, Dept. of Civil Engineering, Duke University, Durham, N.C., August, 1971.

1.7 Wilson, J. F. and Biggers, S. B., "Dynamic Interactions of High Speed Tracked Air Cushion Vehicles with their Guideways," Journal of Dynamic Systems, Measurement and Control, Transactions, American Society of Mechanical Engineers, Vol. 95, March 1973, pp. 76-85.

1.8 Wilson, J. F., "Model Experiments for Span-Vehicle Dynamics," Journal of the Engineering Mechanics Division, ASCE, Vol.

103, No. EM4, Proc. Paper 13160, August, 1977, pp. 701-715.

1.9 Young, J. W. and Wormley, D. N., "Optimization of Linear Vehicle Suspensions Subjected to Simultaneous Guideway and External Force Disturbances," Journal of Dynamic Systems, Measurement and Control, Transactions, American Society of Mechanical Engineers, Vol. 95, June, 1973, pp. 213-219.

2. NEAR-OPTIMAL, INERTIALESS SPANS

INTRODUCTION

For the near-optimal beam-type elevated guideway configurations of Chapter 1, the transit mass m_o was assumed to be small compared to the span mass m_1 between two adjacent supports, or $m_o/m_1 << 1$. The purpose of this Chapter is to investigate the responses for these same near-optimal spans under another extreme assumption: that the span has negligible inertia. That is, the transit mass is much larger than the span mass, or $m_o/m_1 >> 1$. It is noted that in both extreme cases, the same set of optimal span multipliers $(f_1, f_2, \ldots f_n)$, by definition, produce equal midspan moments for m_o at crawl speed [2.1].

The first solutions to the moving mass on an inertialess, simple beam was reported by Stokes in 1849 [2.2]. In the present study, this problem is generalized to include an N-span continuous beam with simple supports at the extreme ends and with arbitrary pier spacing. The problem is reduced to a pseudostatic one where the trajectories of the transit mass are described by an ordinary differential equation with variable coefficients and with prescribed initial conditions for each span segment. The curvatures of these trajectories determine the dynamic moments, set up essentially by the "centrifugal" forces of m_o. For a given guideway configuration, it is shown that the dynamic loading can be described by a single nondimensional load-speed parameter, V. Within the practical limitations of design, the results show that improved guideway efficiency is achieved by employing the same span length multipliers to both classes of moving load problems: $m_o/m_1 << 1$ and $m_o/m_1 >> 1$.

MATHEMATICAL FORMULATION

The general, continuous span configuration is defined in Figure 2.1, with the usual assumptions of deflection, slope and moment continuity across the fixed, interior supports. Also shown in this Figure is the free body sketch of the transit mass, located at distance z from the left end and moving with a constant horizontal speed v. At any given instant of time t, the deflection curve of the beam is y(x,z) and the load trajectory is described by y(z) where x = z.

Newton's second law applied to m_o is

$$Q - m_o g = m_o \frac{d^2y}{dt^2} \tag{2.1}$$

where Q is the vertical load on the beam. Since v = dz/dt, it follows that

$$\frac{dx}{dt} = \frac{dy}{dz}\frac{dz}{dt} = v\frac{dy}{dz} \tag{2.2}$$

$$\frac{d^2y}{dt^2} = \frac{d}{dt}(v\frac{dy}{dz}) = v\frac{d}{dz}(\frac{dy}{dt}) = v^2\frac{d^2y}{dz^2} \tag{2.3}$$

With Eq. (2.3), the equation governing the motion of m_o becomes:

$$Q = m_o g + m_o v^2 \frac{d^2y}{dz^2} \tag{2.4}$$

where d^2y/dz^2 is the curvature of the mass trajectory.

The beam responses are derived from elementary theory using Macauley's notation [2.3]. For an N-span beam of uniform stiffness EI, with reaction forces at the supports, left to right, defined as $R_o, R_1, \ldots R_N$, the equations for moment and deflection are given respectively by

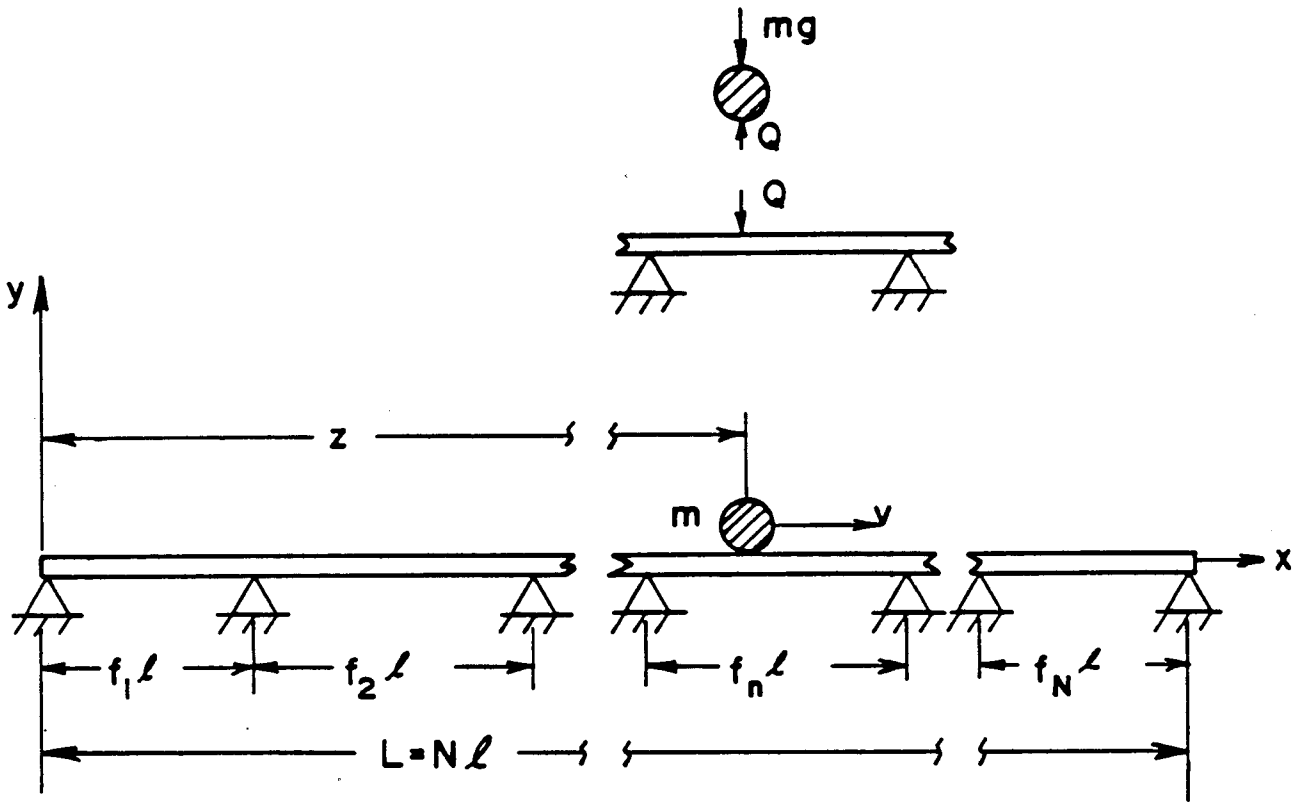

Figure 2.1 Continuous, inertialess beam with a constant speed point mass load

$$M(x,z) = R_o x - Q\langle x - z\rangle^1 + \sum_{n=1}^{N-1} R_n \left\langle x - \sum_{m=1}^{n} f_m \ell \right\rangle^1 \tag{2.5}$$

$$6EI \cdot y(x,z) = R_o x^3 - Q\langle x - z\rangle^3 + \sum_{n=1}^{N-1} R_n \left\langle x - \sum_{m=1}^{n} f_m \ell \right\rangle^3 + c_o \ell^2 x \tag{2.6}$$

Here, the moment and deflection at x = o are zero, corresponding to a simple end support; c_o is a constant; and $(f_1, f_2, \ldots f_N)$ are the span length multipliers. The Macauley bracket convention is defined as follows, where α is a real number and m is a positive integer.

$$\begin{aligned} \langle \alpha \rangle^m &= 0 \quad \text{if } \alpha \leq 0 \\ \langle \alpha \rangle^m &= \alpha^m \text{ if } \alpha > 0 \end{aligned} \tag{2.7}$$

There are N deflection boundary conditions yet to be satisfied, or

$$\begin{aligned} y(f_1 \ell) = y(f_1 \ell + f_2 \ell) = \ldots \\ = y(f_1 \ell + f_2 \ell + \ldots f_{N-1} \ell) = y(L) = 0 \end{aligned} \tag{2.8}$$

There are two equations of static equilibrium, or

$$\sum_{n=0}^{N} R_n - Q = 0 \tag{2.9a}$$

$$\sum_{n=1}^{N} \ell R_n \cdot \left(\sum_{m=1}^{n} f_m \right) - zQ = 0 \tag{2.9b}$$

When the (N + 2) equations given by Eqs. (2.8) and (2.9) are applied to Eq. (2.6), the (N + 2) unknowns $(R_o, R_1, \ldots R_N; c_o)$ can be found in terms of the location z of load Q.

From these results, the trajectory equations are obtained. To do this, first define the nondimensional coefficients which are independent of Q:

$$\left.\begin{aligned} C &= c_o/Q \\ S_{m=1} &= R_m/Q, \; m = 1,2,\ldots N \end{aligned}\right\} \tag{2.10}$$

The moment under Q and the load trajectory are then evaluated from Eq. (2.5) and (2.6), respectively, where x = z. Using Eqs. (2.10), these results are

$$M(z) = Q\left[S_1 z + \sum_{n=1}^{N-1} S_{n+1} \left\langle z - \sum_{m=1}^{n} f_m \ell \right\rangle^1\right] \tag{2.11}$$

$$6EI \cdot y(z) = Q\left[S_1 z^3 + \sum_{n=1}^{N-1} S_{n+1} \left\langle z - \sum_{m=1}^{n} f_m \ell \right\rangle^3\right] \tag{2.12}$$

Now, eliminate the unknown load Q in Eq. (2.12) by substitution, using Eq. (2.4). The resulting differential equation is written in nondimensional form based on the following reference parameters for a simple span with load $m_o g$ at the middle.

$$\left.\begin{aligned} y_s &= \frac{m_o g \ell^3}{48EI}, \text{ peak midspan deflection} \\ M_{ss} &= \frac{m_o g \ell}{4}, \text{ peak midspan moment} \end{aligned}\right\} \tag{2.13}$$

The nondimensional system parameters are defined.

$$\left.\begin{aligned} V &= \left(\frac{v^2}{g\ell^2} y_s\right)^{1/2}, \text{ dimensionless velocity} \\ Y(Z) &= y(Z)/y_s, \text{ dimensionless trajectory} \\ Z &= z/\ell, \text{ dimensionless load coordinate} \end{aligned}\right\} \tag{2.14}$$

The result is

$$\frac{d^2Y(Z)}{dZ^2} = \frac{Y(Z)}{8V^2F(Z)} - \frac{1}{V^2} \tag{2.15}$$

where

$$F(Z) = CZ + S_1 Z^3 + \sum_{n=1}^{N-1} S_{n+1} \left\langle Z - \sum_{m=1}^{n} f_m \right\rangle^3 \tag{2.16}$$

To obtain unique solutions to the governing differential equation (2.15), two initial conditions need to be prescribed at the beginning of each span segment. If the whole span is initially flat and horizontal when Z = 0, it will be so for Z = f_1, $f_1 + f_2$,...L, as well, since the beam is inertialess. The initial conditions at the beginning of each span segment n are:

$$Y(Z_o) = 0; \quad \frac{dY(Z_o)}{dZ} = 0 \tag{2.17}$$

where, for n = 1,2,3,...N, respectively:

$$Z_o = 0, \; f_1, (f_1 + f_2), \ldots \sum_{m=1}^{N-1} f_m \tag{2.18}$$

As mentioned previously, the coefficients (S_1,S_2,...S_{N+1};C) depend only on Z, N and the prescribed set of span multipliers. These are calculated as follows. Apply each of the N conditions of Eq. (2.8) to Eq. (2.6). Then eliminate R_N between Eqs. (2.9a) and (2.9b). The result is (N + 1) algebraic equations which, with the definitions of Eqs. (2.10), involve the (N + 1) unknowns (S_1,S_2,... S_N;C). One of these equations is

$$C = \frac{1}{f_1} < f_1 - Z>^3 - f_1^2 S_1 \tag{2.19}$$

When Eq. (2.19) is substituted into the remaining N equations, the result in matrix form is

$$\underset{\sim}{A} \; \underset{\sim}{S} = \underset{\sim}{F} \tag{2.20}$$

Here, the column vector of the unknowns is

$$\underset{\sim}{S} = [S_1 \; S_2 \; S_3 \; \ldots \; S_N]^T \tag{2.21}$$

where (T) denotes transpose. The nonzero elements of the (NxN) coefficient matrix $\underset{\sim}{A}$ are given by

$$
\begin{aligned}
a_{11} &= N \\
a_{1j} &= N - \sum_{m=1}^{j-1} f_m \qquad && j = 2,3,\ldots N \\
a_{ii} &= f_i^{\,3} && i = 2,3,\ldots N \\
a_{i1} &= \left(\sum_{m=1}^{i} f_m\right)^3 - f_1^{\,2} \sum_{m=1}^{i} f_m && i = 2,3,\ldots N \\
a_{ij} &= \left(\sum_{m=j}^{i} f_m\right)^3 && i = 3,4,5,\ldots N \\
& && j = (i-1)
\end{aligned}
\tag{2.22}
$$

The loading vector is given by

$$
\underset{\sim}{F} = [F_1, F_2, \ldots F_N]^T \tag{2.23}
$$

where

$$
\left.
\begin{aligned}
F_1 &= N - Z \\
F_i &= \left\langle \left(\sum_{m=1}^{i} f_m\right) - Z \right\rangle^3 - \frac{1}{f_1}\left(\sum_{m=1}^{i} f_m\right) \left\langle f_1 - Z \right\rangle^3 \\
& \qquad i = 2,3,\ldots N
\end{aligned}
\right\} \tag{2.24}
$$

The results obtained so far are summarized. For an N-span continuous beam with a fixed set of span multipliers $(f_1, f_2, \ldots f_N)$ and a fixed velocity parameter V, the deflection response to the moving point mass is given by solving Eq. (2.15) with Eq. (2.16) and initial conditions of Eqs. (2.17) and (2.18). For each location Z of the transit mass, the variable coefficients $(S_1, S_2, \ldots S_N; C)$ are found from solutions of Eqs. (2.20) - (2.24). With the solution Y(Z), the beam load Q is calculated from the dimensionless form of Eq. (2.4) together with Eqs. (2.15) and (2.16), or

$$\frac{Q}{m_o g} = \frac{Y(Z)}{8F(Z)} \tag{2.25}$$

With this last result, along with Eqs. (2.11), (2.13) and (2.14), the nondimensional span moment under the transit mass (the peak span moment) is found, or

$$\frac{M}{M_{ss}} = \frac{Y(Z)}{2F(Z)}\left[S_1 Z + \sum_{n=1}^{N-1} S_{n+1}\ \ Z - \sum_{m=1}^{n} f_m\ \ 1\right] \tag{2.26}$$

SIMPLE SPAN RESPONSES

For the special case of the simple span, $N = f_1 = 1$ and $0 \leq Z \leq 1$. The trajectory equation (2.15) is solved where Eqs. (2.16) - (2.26) become:

$$\left.\begin{aligned} F(Z) &= (1 - Z)Z^3 + Z(1 - Z)[(1 - Z)^2 - 1] \\ Y(0) &= 0;\ \frac{d\ Y(0)}{dZ} = 0 \\ C &= (1 - Z)^3 - (1 - Z) \\ a_{11} &= 1 \\ F_1 &= S_1 = 1 - Z \\ \frac{M}{M_{ss}} &= \frac{Y(Z)}{2F(Z)} Z(1 - Z) \end{aligned}\right\} \tag{2.27}$$

Numerical results for the trajectories were obtained using the integration package EPISODE [2.4] and an IBM 370/165 digital computer. Figure 2.2 shows trajectories for several values of the speed parameter ranging from the crawl speed (V = 0) to a critical value (V = 0.316). The reason for considering the latter value "critical" will be discussed presently. These results agree with those obtained

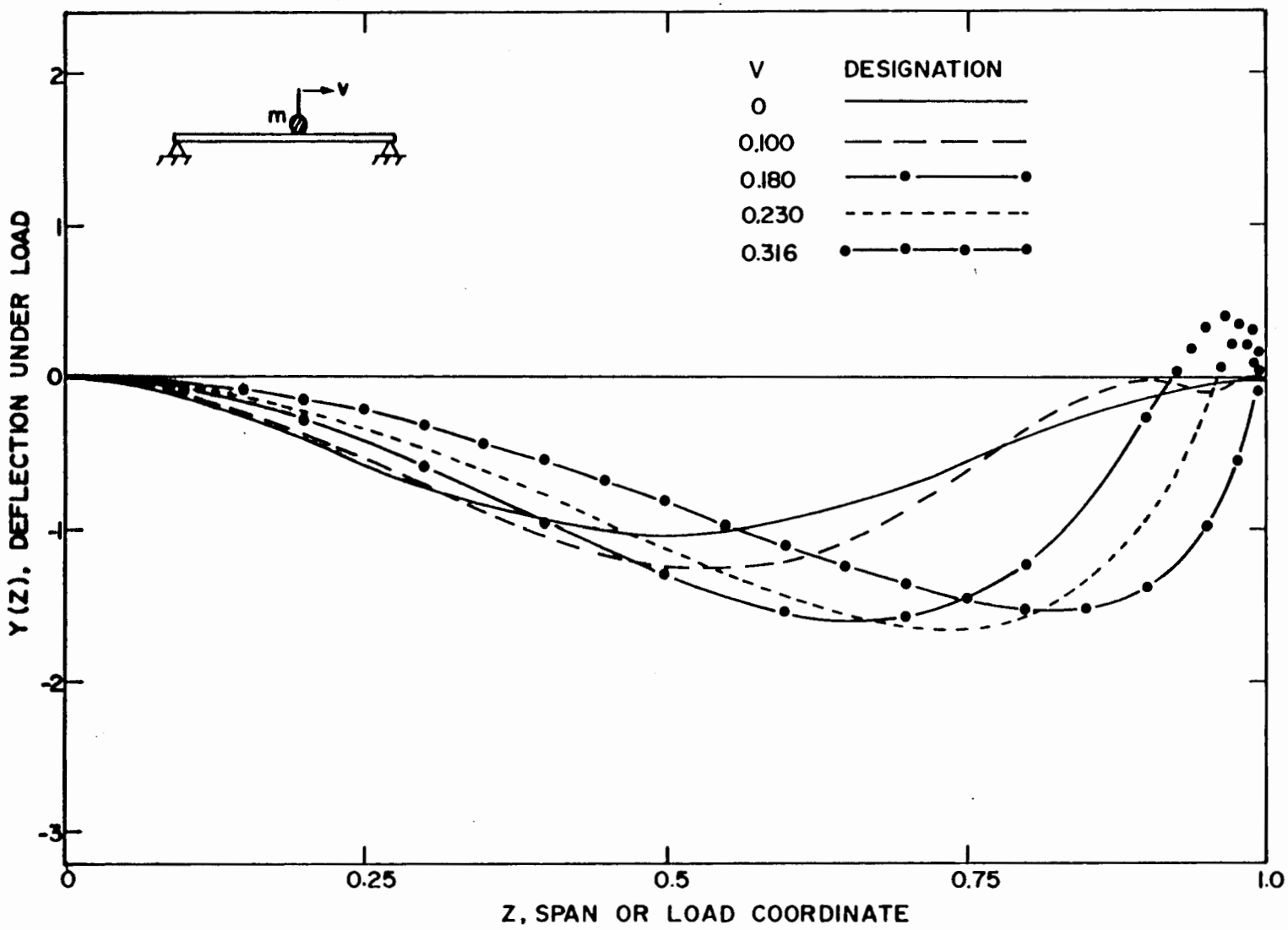

Figure 2.2 Simple span trajectories for a point mass load at several constant speeds

by Stokes [2.2], who correctly interpreted the regions of positive deflections (the dots for Y > 0) as unreal, since this implies a negative or upward Q load in this region. This phenomenon is a consequence of the inertialess beam assumption, which breaks down as m_o comes close to the right support. The peak (negative) deflections are considered accurate, however, for $0 \leq Z \leq 0.9$ where $m_o/m_1 >> 1$.

Figure 2.3 shows the peak deflection at midspan as a function of V. The comparison of the present results with those of Stokes [2.2] is excellent. However, the approximate solution suggested by Timoshenko for design purposes is not very accurate and not necessarily conservative, since Fig. 2.2 shows that the peak deflections do not occur at midspan. Timoshenko's approximate formula for midspan deflections is

$$Y(\tfrac{1}{2}) = 1 + 16V^2 \tag{2.28}$$

Further numerical results showing the absolute peak deflection and moment variations with V in simple spans are discussed in the following section.

RESPONSES OF EVEN AND NEAR-OPTIMAL SPANS

A general computer program was written to calculate the response trejectories for continuous spans up to N = 10, with arbitrary pier spacings. At each increment of Z, usually 0.01, the coefficients $(S_1, S_2, \ldots S_N; C)$ were calculated from Eqs. (2.19) and (2.20); and the EPISODE subroutine [2.4] was employed to solve Eqs. (2.15) and (2.16), with boundary conditions of Eqs. (2.17) and (2.18). For a given N, the span multipliers were all chosen as unity for evenly spaced supports; or as the near optimal values for spans symmetric

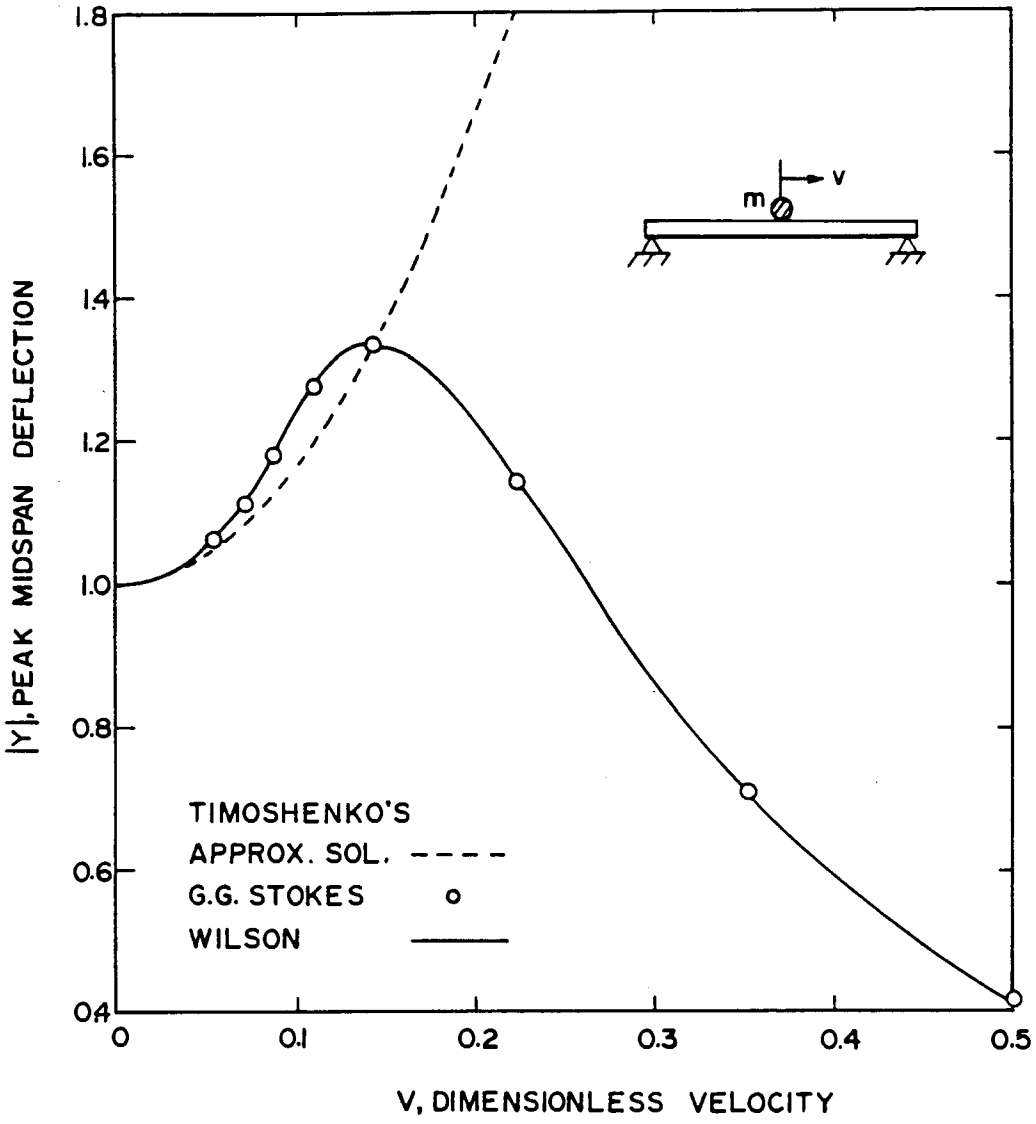

Figure 2.3 Comparison of theories for peak midspan deflections of a simple span

about the middle (x = L/2), as listed in Table 1.3.

Several deflection trajectories for span segment five of a six-span, near-optimal beam are shown in Fig. 2.4. Span segment five is depicted because this one produced the highest values of deflection of any segment. Note its similarity to Fig. 2.2. Again, the dots for positive Y(Z) should not be considered since negative Q values are disallowed. The significant result here is that the peak values of Y(Z), by comparison with those of the simple span, are drastically reduced: from about 1.7 to 1.0 over the range of V shown.

The summary of results useful for design are presented in Figs. 2.5 and 2.6. Figure 2.5 shows the absolute peak value for the deflection trajectories in the range $0 \leq Z \leq N$, corresponding to N values of 1 through 6, and plotted as a function of the dimensionless velocity parameter. The peak of each of the five trajectories of Fig. 2.2 for the simple span are represented, for instance, in curve (a); and the peaks of Fig. 2.4 are represented in curve (g). In curves (b) and (c), the pier supports are evenly spaced, so all the span multipliers are unity. The broken curves, (d) - (g), are based on the near-optimal spacings. Except for curve (d), the three-span optimal configuration curves (e), (f) and (g) show a uniform improvement (less peak deflection) than their counterparts, curve (c). Obviously, any of the multiple spans is a vast improvement over the simple span.

Figure 2.6, calculated from Eq. (2.26), shows the uniform reductions in the peak span moments as one proceeds from the simple span, curve (a); to the multiple spans with even supports, N = 2 through 6; and to the near-optimal configurations, curves (d) and (e). The curves for the near-optimal, N = 4 and N = 5 configurations are not

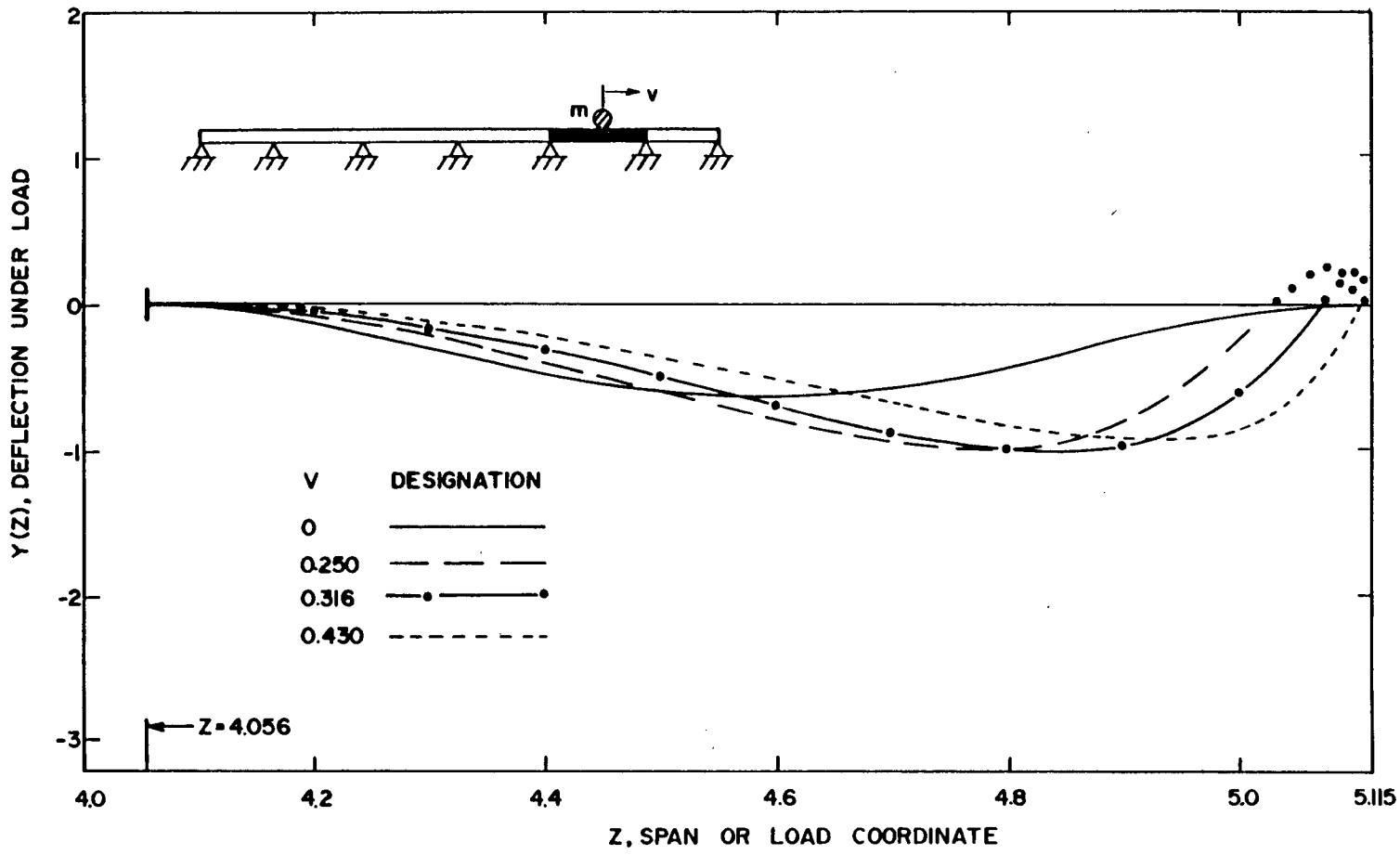

Figure 2.4 Trajectories in span five of a six-span beam with optimal pier spacing

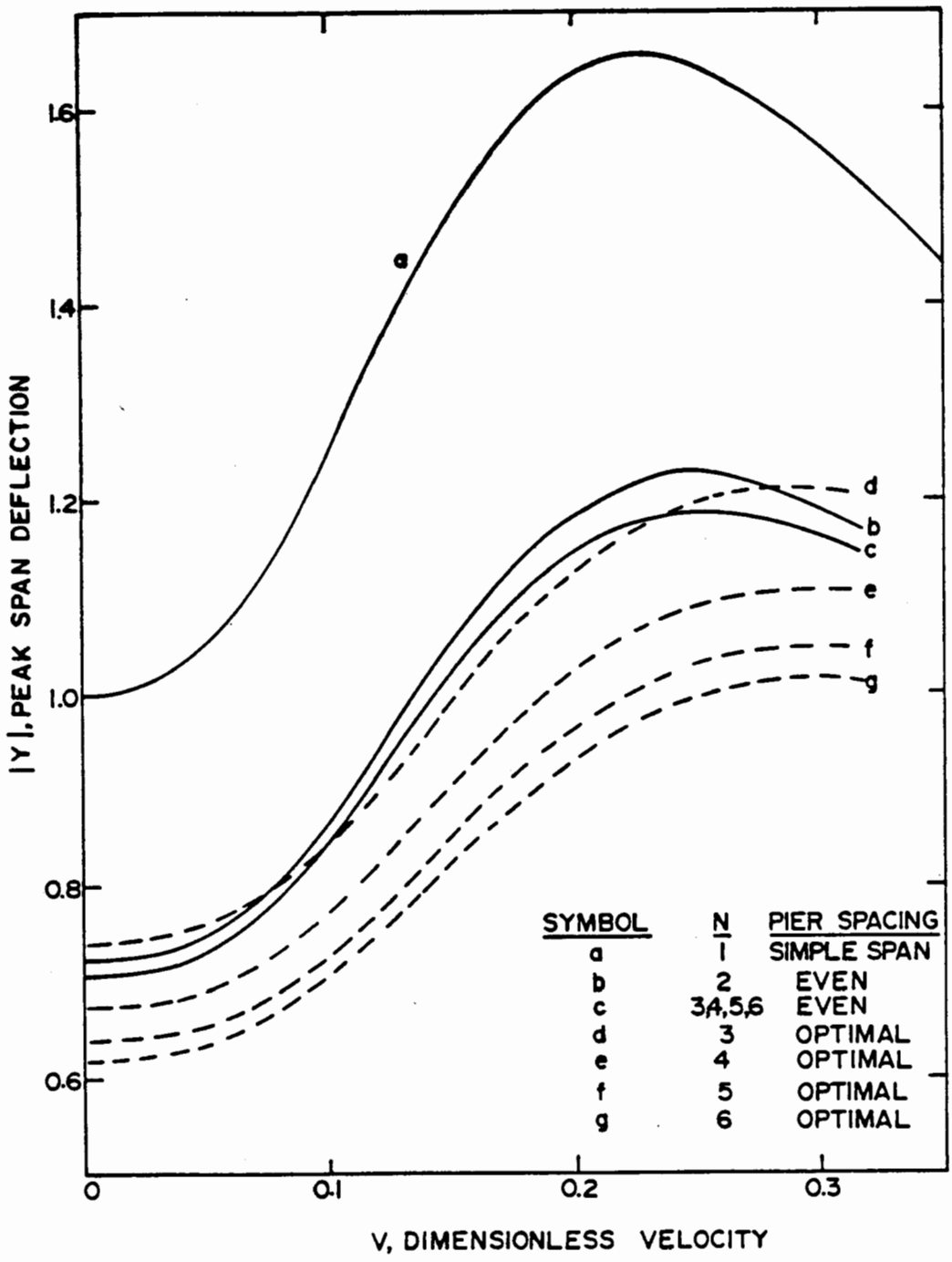

Figure 2.5 Comparison of peak deflections for several span configurations

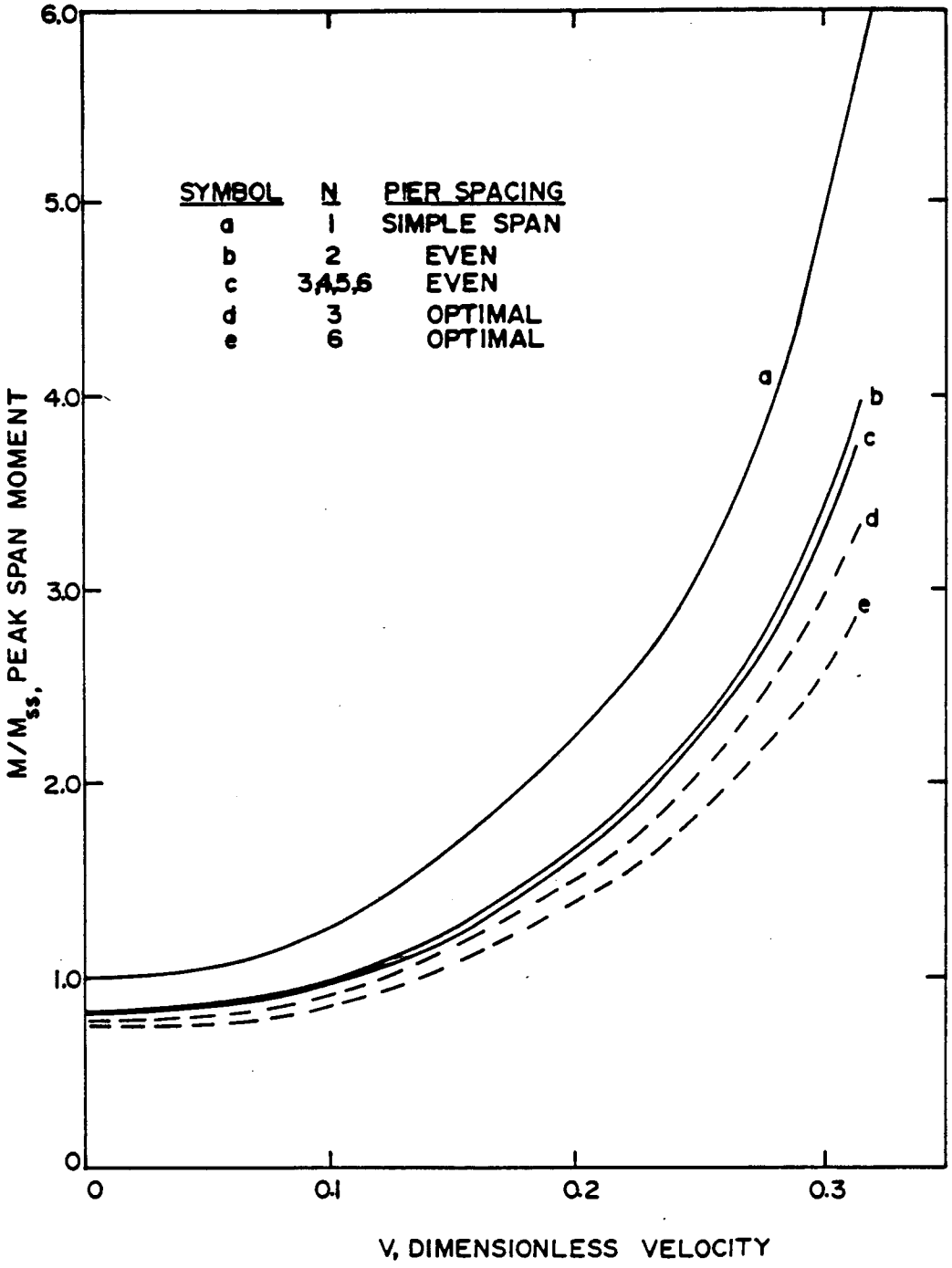

Figure 2.6 Comparison of peak moments for several span configurations

shown for clarity; but do lie between the curves (d) and (e). As V is increased to the critical value of 0.316, the peak moment occurs closer and closer to one of the pier supports lying just ahead of the transit mass, regardless of the span segment. As indicated by the sample deflection trajectories of Figs. 2.2 and 2.4, the curvatures become tighter and tighter near this pier support. For $V > 0.316$, the trajectories near the supports become positive, the bending moments approach unboundedness and the mathematical model with the inherent assumption of an inertialess beam, completely breaks down. The inclusion of beam inertia in the multiple spans would undoubtedly obliterate this erratic and unbounded behavior for $V > 0.316$; but for values of $V < 0.316$ the results are conservative from the design point of view, just as Stokes pointed out for simple spans [2.2].

CONCLUSIONS

The limitations of the mathematical model consisting of an inertialess beam with a relatively massive transit point load are well recognized. However, the calculated results for peak span deflection and moment responses are valid and conservative from the design viewpoint if the velocity parameter is less than about 0.3. Finally, compared to a simple span, significant reductions in these responses are achieved in continuous spans with $N > 3$, using the near-optimal pier spacings of previous studies.

REFERENCES FOR CHAPTER 2

2.1 Wilson, J. F. and Barbas, S. T., "Dynamics of Near-Optimal Spans with Moving Loads," ASCE Proc. Paper No. 80-654, 1980.

2.2 Stokes, G. G., "Discussion of a Differential Equation Relating to the Breaking of Railway Bridges (1849)," Mathematical and Physical Papers, Vol. 2, Cambridge Press, 1883, pp. 178-220.

2.3 Lardner, T. J., editor, An Introduction to the Mechanics of Solids, McGraw-Hill Book Co., 1978, Chapter 8.

2.4 Hindmarsh, A. C. and Byrne, G. D., "EPISODE: An Experimental Package for the Integration of Systems of Ordinary Differential Equations," UCID-30112, Lawrence Livermore Laboratory, Calif., May, 1975.

2.5 Timoshenko, S. and Young, D. H., Vibration Problems in Engineering, D. Van Nostrand Co., N.J., 1968, pp. 358-360.

3. OPTIMAL RESPONSE FOR GUIDEWAYS WITH MULTIPLE DISTRIBUTED PARAMETERS

INTRODUCTION

In the design of multiple span, continuous, beam-type guideways with transit loading, the choice of the most efficient sets of distributed parameters: pier spacing, bending stiffness and unit mass, can be difficult and time consuming. As shown in Chapters 1. and 2., even the choice of efficient structural configurations allowing for the variation of just one set of distributed parameters, the pier spacing, can be a formidable task. To systematically study this three-parameter problem, both a new dynamic span analysis and a new definition of span efficiency are needed. As in Chapter 1, this reformulated dynamic analysis includes the effects of a single or multiple point forces of constant intensity to simulate a vehicle or vehicles in tandem, at constant speed. The new measure of span efficiency is ϕ, defined as a linear combination of four weighted, dimensionless span characteristics: the peak dynamic stress; the peak live load stress difference between span segments; the rms vertical deflection under the transit point load; and the total span mass. For a fixed set of distributed parameters, for a vehicle at a fixed design speed, a minimum ϕ is sought, subjected to practical constraints such as stress, deflection and construction techniques. A continuous, three span-configuration is chosen to illustrate the direct-search methodology for evaluating relative

efficiencies of alternative designs. Results are presented as three-dimensional, computer-drawn isometric plots showing the effects of the three sets of distributed parameters as well as vehicle speed on span efficiency.

DYNAMIC ANALYSIS

Figure 3.1 illustrates a three-span continuous, beam-type guideway with the three design parameters defined for each of its span segments. In general, n designates the span segment number where $n = 1,2,\ldots,N$ and where N is the total number of spans. The span segment length is $f_n\ell$, where ℓ is the mean segment length and $L = N\ell$ is the overall length. The stiffness, EI_n, and mass per unit length, $\bar{m}_n$, are constant over each span segment, but do vary among segments. Here, x is the global longitudinal coordinate and z_n is the local or segment coordinate.

The mathematical model for these studies is the Bernoulli-Euler equation, applicable to each span segment, describing the transverse displacement, $\bar{v} = \bar{v}(x,t)$, [3.1]. That is

$$EI_n \cdot \frac{\partial^4 \bar{v}}{\partial x^4} + \bar{m}_n \frac{\partial^2 \bar{v}}{\partial t^2} = q \qquad (3.1)$$

where $q = q(x,t)$ is the transverse load per unit length. The local coordinates are related to x by

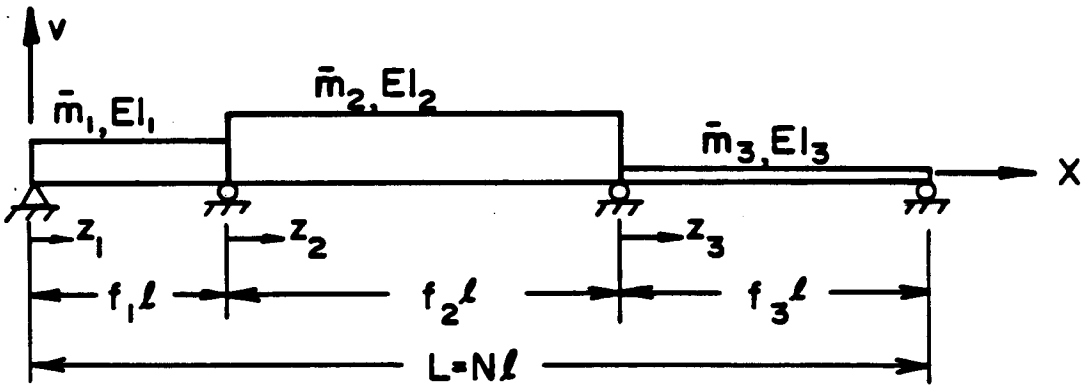

Figure 3.1 A typical continuous, 3-span beam with distributed parameters

$$z_n = x - \sum_{j=1}^{n-1} f_j \ell \ , \quad n = 1,2,...N \tag{3.2}$$

For free, harmonic vibrations, assume

$$\bar{v}(x,t) = y(x) \sin pt \tag{3.3}$$

where p is a frequency parameter. When Equation (3.3) is substituted into the homogeneous form of Equation (3.1) corresponding to $q = 0$, the result is

$$\frac{d^4y}{dx^4} - \lambda^4 y = 0 \tag{3.4}$$

where

$$\lambda^4 = \frac{\bar{m}_n p^2}{EI_n} \tag{3.5}$$

The general solution to Equation (3.4) is

$$y = A \cosh \lambda x + B \sinh \lambda x + C \cos \lambda x + D \sin \lambda x \tag{3.6}$$

where the constants (A, B, C, D, λ) are determined for each span segment by applying the appropriate boundary and continuity conditions at the segment junctions (the pier supports). These conditions are summarized in terms of the local coordinates, z_n, defined by Equation (3.2).

rigid pier supports:

$$y_n = 0 \quad \text{at} \quad z_n = 0, \quad f_1\ell, \ldots . f_N\ell \tag{3.7a}$$

slope continuity at interior supports:

$$\left.\frac{dy_n}{dz_n}\right|_{z_n = f_n\ell} = \left.\frac{dy_{n+1}}{dz_{n+1}}\right|_{z_{n+1} = 0} \tag{3.7b}$$

moment continuity at interior supports:

$$EI_n \left.\frac{d^2y_n}{dz_n^2}\right|_{z_n = f_n\ell} = EI_{n+1} \left.\frac{d^2y_{n+1}}{dz_{n+1}^2}\right|_{z_{n+1} = 0} \tag{3.7c}$$

simply supported extreme ends:

$$\left.\frac{d^2y_1}{dz_1^2}\right|_{z_1 = 0} = \left.\frac{d^2y_N}{dz_N}\right|_{z_N = f_N\ell} = 0 \tag{3.7d}$$

For mode number m and span segment n, Equation (3.6) is re-written as

$$\begin{aligned} y(m,n) = {} & A(m,n) \cdot \cosh \lambda(m,n) z_n + B(m,n) \cdot \sinh \lambda(m,n) z_n \\ & + C(m,n) \cdot \cos \lambda(m,n) z_n + D(m,n) \cdot \sin \lambda(m,n) z_n \end{aligned} \tag{3.8}$$

When Equations (3.7) are applied to Equation (3.8), the relationships among the constants are derived, or

$$A(m,n) = -C(m,n) \tag{3.9a}$$

$$B(m,n) = \frac{1}{G(m,n)} \left[-C(m,n+1)\ \lambda^2(m,n+1) EI_{n+1} + C(m,n) \lambda^2(m,n) EI_n \cosh \lambda(m,n) f_n \ell\right] \tag{3.9b}$$

$$D(m,n) = \frac{1}{H(m,n)} \left[C(m,n+1) \lambda^2(m,n+1) EI_{n+1} - C(m,n) \lambda^2(m,n) EI_n \cos \lambda(m,n) f_n \ell\right] \tag{3.9c}$$

$$C(m,n)\psi(m,n) - C(m,n+1)\left[\frac{\lambda^2(m,n+1)}{\lambda^2(m,n)} \frac{EI_{n+1}}{EI_n} \theta(m,n) + \frac{\lambda(m,n+1)}{\lambda(m,n)} \theta(m,n+1)\right] + C(m,n+2) \frac{\lambda^2(m,n+2)}{\lambda(m,n)\ (m,n+1)} \cdot \cdot \frac{EI_{n+2}}{EI_{n+1}} \psi(m,n+1) = 0 \tag{3.9d}$$

where

$$G(m,n) = \lambda^2(m,n) EI_n \sinh \lambda(m,n) f_n \ell \tag{3.10a}$$

$$H(m,n) = \lambda^2(m,n) EI_n \sin \lambda(m,n) f_n \ell \tag{3.10b}$$

$$\theta(m,n) = \coth \lambda(m,n) f_n \ell - \cot \lambda(m,n) f_n \ell \tag{3.11a}$$

$$\psi(m,n) = \operatorname{csch} \lambda(m,n) f_n \ell - \csc \lambda(m,n) f_n \ell \tag{3.11b}$$

The assumption of simple supports for the extreme end spans is a practical boundary condition that allows for thermal expansions. This condition leads to

$$C(m,1) = C(m,N+1) = 0 \tag{3.12}$$

The span frequencies and mode shapes can now be calculated for a given set of system parameters: N, $\bar{m}_n$, EI_n, f_n, and L, where $n = 1,2,...N$. The recursion formula Equation (3.9d), with Equations (3.11) and (3.12), form a set of (N-1) homogeneous, algebraic equations in the constants C(m,2) through C(m,N). By setting the determinant of these coefficients equal to zero, the consecutive positive roots corresponding to $m = 1,2,3,...$ yield the frequency parameters $\lambda(m,1),\lambda(m,2),...\lambda(m,N)$. The m characteristic system frequencies are then expressed by Equation (3.5), or

$$p_m = \left[\frac{EI_n \lambda^4(m,n)}{\bar{m}_n}\right]^{\frac{1}{2}} \tag{3.13}$$

Then the mode shapes y(m,n) of Equation (3.8) are calculated as follows: set C(m,2) = 1 arbitrarily; calculate the remaining (N-1) coefficients C(m,n) from Equations (3.9d) and (3.12); then calculate A(m,n), B(m,n) and D(m,n) from Equations (3.9a), (3.9b) and (3.9c), respectively.

With these results it is now possible to solve Equation (3.1) subject to a point force, F_0, moving at constant speed, v.

The normal mode method is used [3.2]. It is summarized as follows. Express the mode shape $Y_m(x)$ for the total system of length L as the sum of the individual span segment mode shapes, or

$$Y_m(x) = \sum_{n=1}^{N} y(m,n) \tag{3.14}$$

Expand the solution and the applied load, respectively, in the following series:

$$v(x,t) = \sum_{m=1}^{\infty} Q_m(t) Y_m(x) \tag{3.15}$$

$$\frac{1}{\bar{m}_n(x)} q(x,t) = \sum_{m=1}^{\infty} P_m(t)\ Y_m(x) \tag{3.16}$$

From Equation (3.4), using Equation (3.13), the relationship

$$\frac{d^4 Y_m(x)}{dx^4} = \lambda^4(m,n)\ Y_m(x)$$

is valid for all mode shapes associated with the defined boundary conditions. When Equations (3.15) and (3.16) are substituted into Equation (3.1), and Equation (3.13) is used again, it follows that

$$\ddot{Q}_m(t) + p_m^2\, Q_m(t) = P_m(t) \tag{3.17}$$

where $(\cdot)$ is the operator d/dt. The right hand side of

Equation (3.17) is found by multiplying Equation (3.16) by $\bar{m}_n(x)$ and the mode shape function, $Y_k(x)$, and integrating the result over the whole beam length, $0 \leq x \leq L$. Then the orthogonality condition is used, or

$$\int_0^L \bar{m}_n(x)\ Y_m(x)\ Y_k(x)\,dx = \begin{cases} 0 & \text{if } k \neq m \\ E(m,n) & \text{if } k = m \end{cases} \tag{3.18}$$

The result, valid for all loadings, is

$$P_m(t) = \frac{1}{E(m,n)} \int_0^L q(x,t)\ Y_m(x)\,dx \tag{3.19}$$

where

$$E(m,n) = \sum_{n=1}^{N} \bar{m}_n \int_0^{f_n \ell} y^2(m,n)\,dz \tag{3.20}$$

In the special case of a vertical point force of constant magnitude F_0, starting at $x = 0$ at $t = 0$, and traveling at a constant horizontal speed v, the loading is expressed as

$$q(x,t) = F_0 \cdot \delta(x - vt) \tag{3.21}$$

where the total load on the beam is given by

$$\int_0^L F_0 \cdot \delta(x - vt)\,dx = \begin{cases} F_0 & , \quad 0 \leq vt \leq L \\ 0 & , \quad \text{otherwise} \end{cases} \tag{3.22}$$

With Equations (3.21) and (3.22), Equation (3.19) is evaluated, or

$$P_m(t) = \frac{F_0 \, Y_m(vt)}{E(m,n)} \tag{3.23}$$

These results are summarized. The vertical span deflection $v(x,t)$ is found from numerical solutions of Equation (3.17) for $Q_m(t)$, with $P_m(t)$ given through Equations (3.20), (3.23); with $Y_m(x)$ given by Equation (3.14); and with the mode shapes $y(m,n)$ and corresponding frequencies, p_m. In calculating numerical solutions of Equation (3.17), zero initial conditions are assumed, compatible with a span system initially flat and at rest. That is, $v(x,0) = \partial v(x,0)/\partial t = 0$, or $Q_m(0) = \dot{Q}_m(0) = 0$. The associated bending moments in each span segment n can then be calculated from

$$M_n(x,t) = EI_n \sum_{m=1}^{\infty} Q_m(t) \frac{d^2 Y_m(x)}{dx^2} \tag{3.24}$$

with which bending stresses are found using elementary theory.

In the more general case of several tandem point forces of constant magnitude and constant speed, superposition holds and Equation (3.17) becomes

$$\ddot{Q}_m(t) + p_m^2 \, Q_m(t) = \sum_{i=1}^{a} F_i \cdot Y_m(x_i) \tag{3.25}$$

where $Y_m(x_i)$ is the amplitude of the m-th mode under force F_i

and "a" is the number of point forces on the guideway. The rest of the analysis in which the deflection and moment responses are calculated then proceeds as in the case of the single point force outlined above. For multiple transit loads, care must be taken to impose the compatible initial conditions to each span, each time a new load enters. Indexing schemes to account for these details in computer-aided calculations are well documented [3.3].

It should be noted that mode shapes for a special class of beam configurations can not be obtained from the above formulation. Excluded are beams defined by either of the two following configurations.

(1) $f_1 = f_2 = \ldots f_N$; $\bar{m}_1 = \bar{m}_2 = \ldots \bar{m}_N$ and $EI_1 = EI_2 = \ldots EI_N$

(2) all odd $N \geq 3$ configurations with a symmetric distribution of f_n, $\bar{m}_n$ and EI_n about the beam centerpoint, $x = L/2$.

If either of these conditions are met, then

$$\lambda(m,n) \cdot f_n \ell = \pi, \ 2\pi, \ 3\pi, \ \ldots \ .$$

This leads to $H(m,n) = 0$ in Equation (3.10b), undefined values for $D(m,n)$ in Equation (3.9c) and undefined mode shapes, $y(m,n)$. Special cases of uniform beams with symmetric distributions of f_n about $x = L/2$ where $\bar{m}_1 = \bar{m}_2 = \ldots \bar{m}_6$ and $EI_1 = EI_2 = \ldots EI_6$ are considered elsewhere [3.4]. However, for

the design of equal span segment structures, the present analysis and computer code can still be used to obtain approximate answers if the segment lengths are allowed to vary from equality by just two or three percent. This computer program is described in the Appendix.

EXPERIMENTAL VALIDATIONS OF THE ANALYSIS

The above analysis and corresponding computer program were validated experimentally for a special case. The overall laboratory experimental system used has been described elsewhere [3.5]. For the test case, the three-span steel beam configuration shown in Figure 3.2 was chosen: a design whose center span had a mass and stiffness each 80 percent of the equal end spans. As in the analysis, the extreme ends were simply supported. With a straightforward static calculation, it can be shown that this test beam has a near-optimal or balanced stress design. That is, the peak bending stresses at the midspans, corresponding to a transit point force at crawl speed, are all equal, or very nearly so.

In a series of experiments, the test beam was subjected to an approximately constant point force at constant speed v; and simultaneously the time history of each midspan strain was measured. This strain was converted to a bending moment, M, using the appropriate value of stiffness, EI_n; and this moment was normalized by the peak moment M_{ss} of a simple span of the same segment length ℓ, where $M_{ss} = F_0\ell/4$.

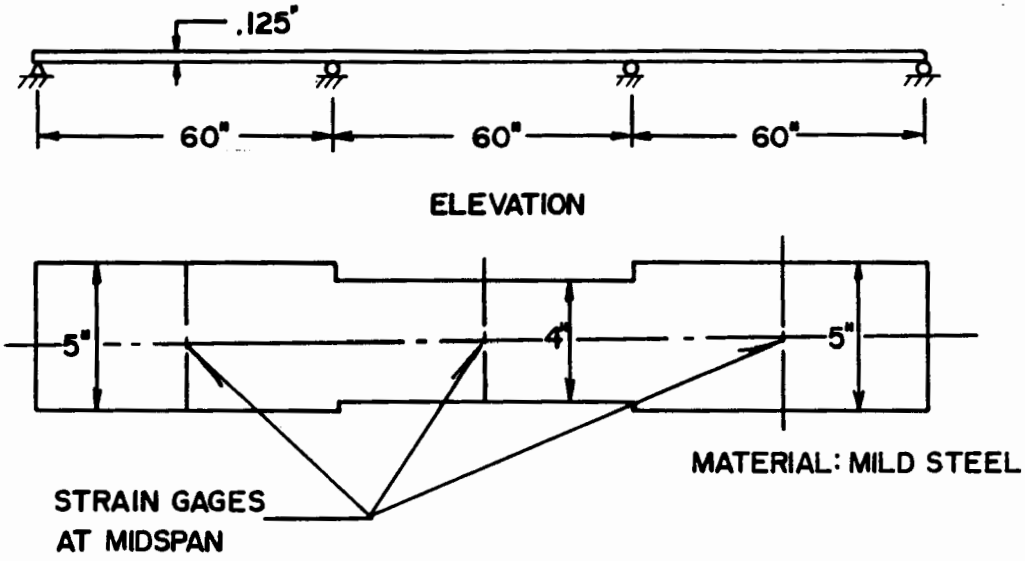

Figure 3.2 Continuous beam selected for laboratory-scale experiments

Figure 3.3 shows a typical time history of M at the middle of span one. It is observed that the measured points (circles) agree well with the behavior predicted by the analysis based on a 20 mode solution. The transit frequency ratio for Figure 3.3, corresponding to $v = 26.0$ ft/sec. is $\omega/p = 0.82$, where ω is the transit frequency:

$$\omega = \frac{\pi v}{\ell} \tag{3.26}$$

and p is the simple span reference frequency:

$$p = \frac{\pi^2}{\ell^2} \frac{EI_1}{\bar{m}_1} = 19.92 \text{ rad/sec} \tag{3.27}$$

As discussed previously [3.5], the peaks of the moments obtained from such curves as Figure 3.3, plotted as a function of the system parameter ω/p, are useful for design purposes. Such curves are shown in Figures 3.4 through 3.6, corresponding to spans one through three. The model test data is again in good agreement with the computer calculations, which serves to validate the mathematical analysis.

OPTIMIZATION FUNCTIONS AND REFERENCE CONFIGURATIONS

A rational definition of a optimal guideway with three sets of distributed parameters: $(f_1, f_2, \ldots f_N)$, $(EI_1, EI_2, \ldots EI_n)$ and $(\bar{m}_1, \bar{m}_2, \ldots \bar{m}_N)$ is needed for efficient computer-aided studies of alternative configurations. This leads to an optimization

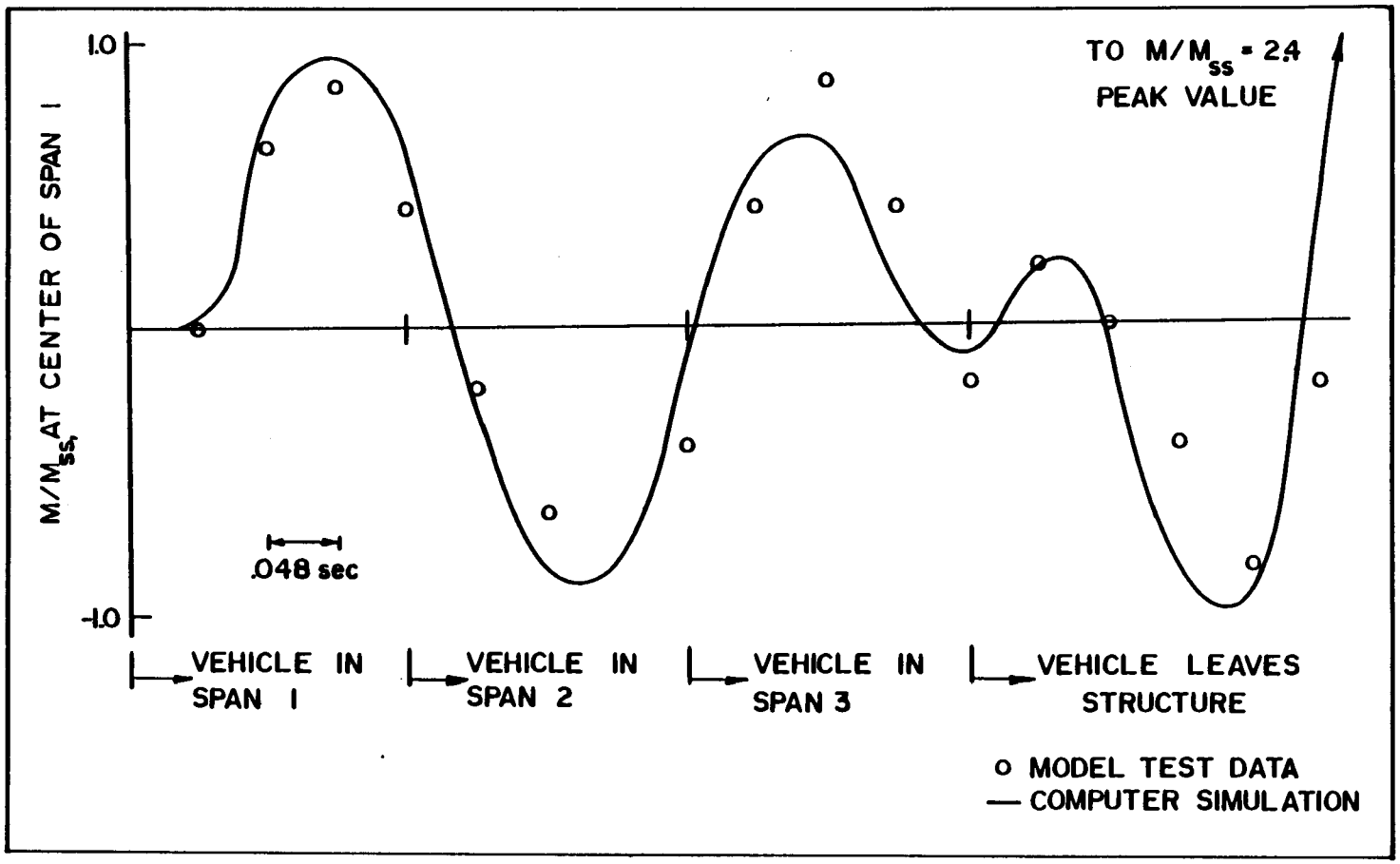

Figure 3.3 A comparison of measured and predicted moment histories for $\omega/p = 0.82$

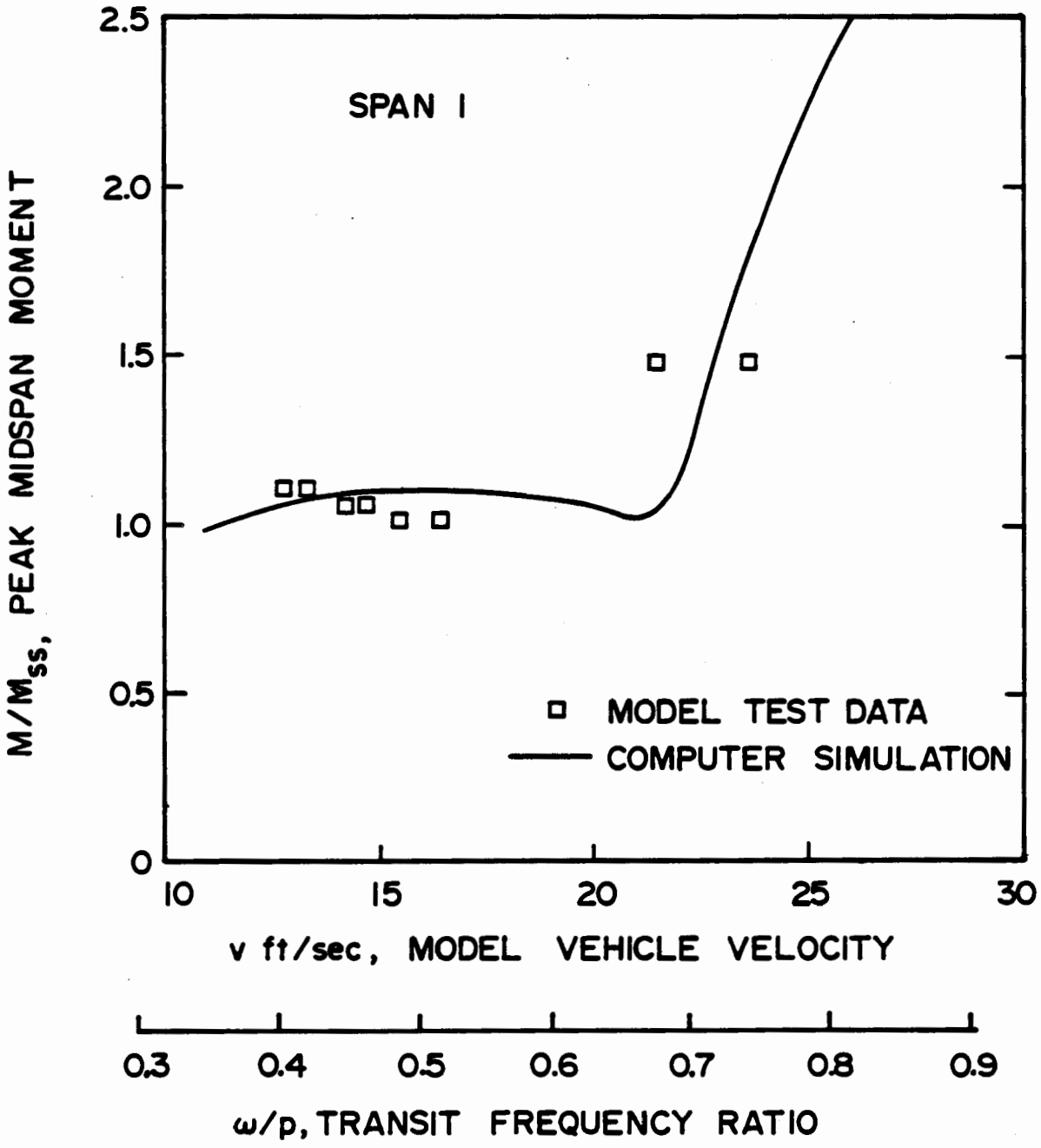

Figure 3.4 Peak midspan moments in span 1

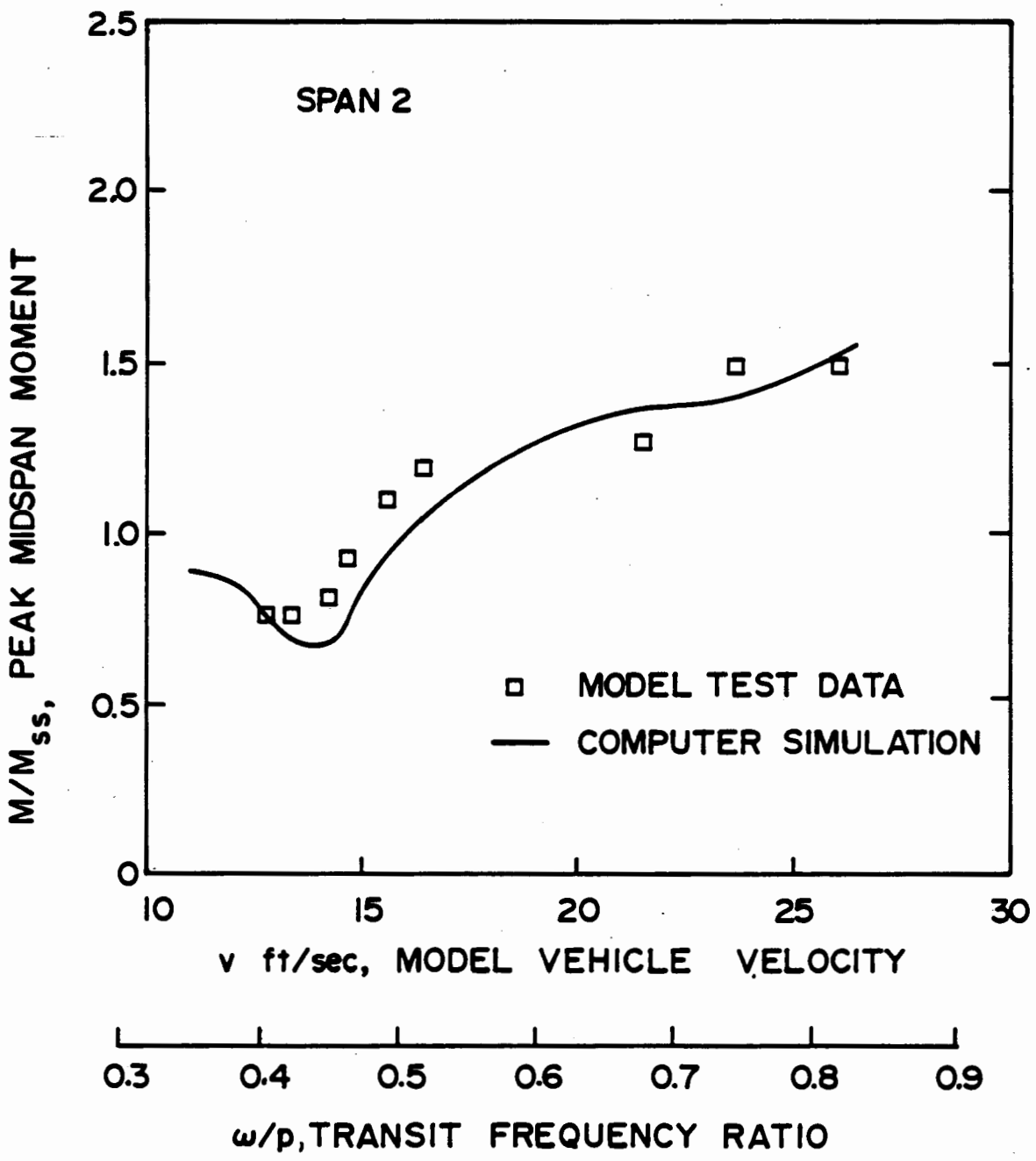

Figure 3.5 Peak midspan moments in span 2

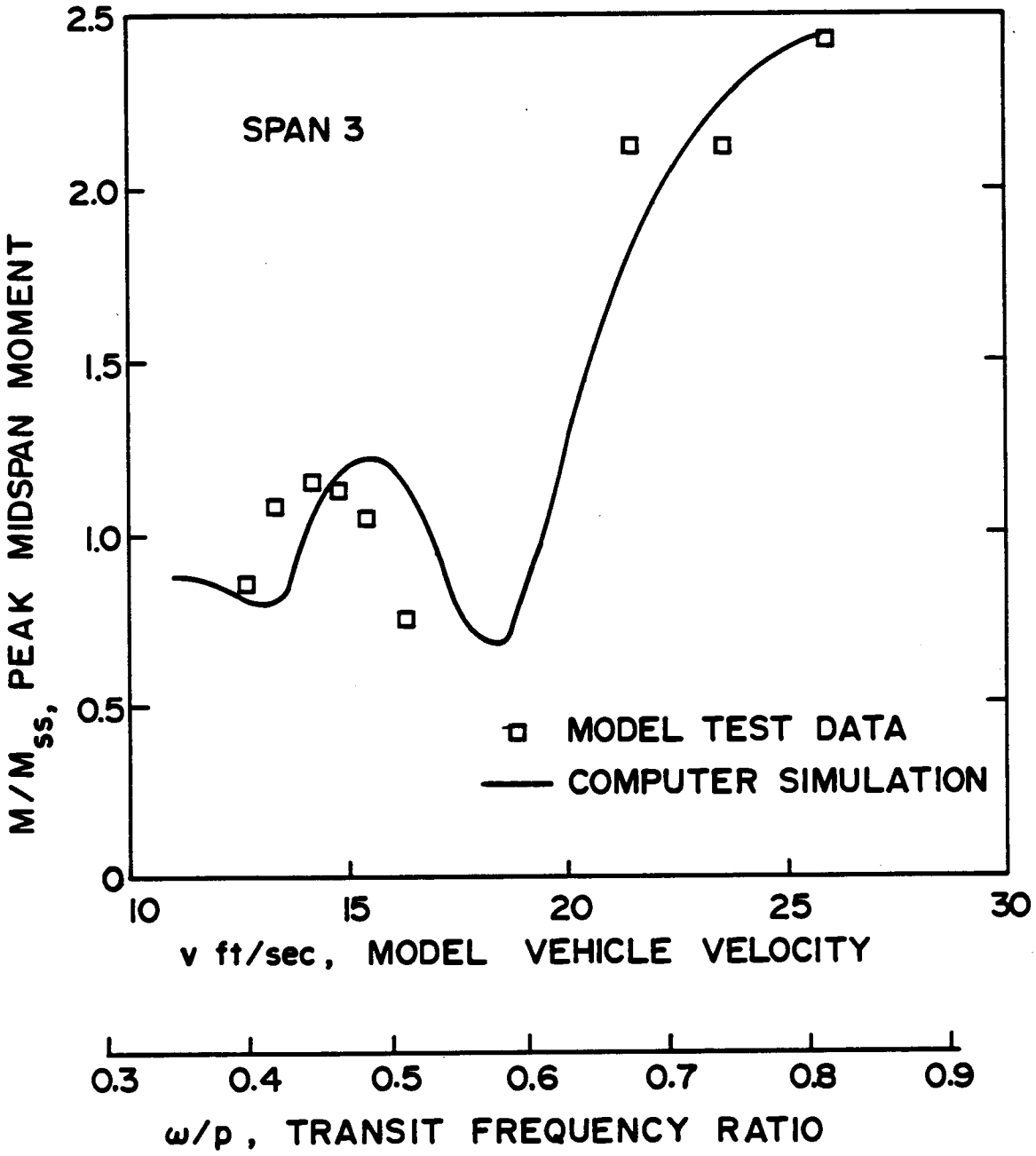

Figure 3.6 Peak midspan moments in span 3

function, ϕ, defined as a linear combination of four of the most important system characteristic ratios, or

$$\phi = c_1 \frac{\sigma_m}{\sigma_r} + c_2 \frac{\Delta\sigma_m}{\Delta\sigma_r} + c_3 \frac{\bar{y}}{\bar{y}_r} + c_4 \frac{M}{M_r} \tag{3.28}$$

where the weighting coefficients c_k $(k = 1,2,3,4)$ are arbitrarily chosen subjected to the restraint that $\sum_{4} c_k = 4$. In the first ratio, σ_m is the calculated peak midspan stress response considering all span segments. In the second ratio, $\Delta\sigma_m$ is the calculated difference between σ_m and the peak midspan stress occurring in the least stressed span segment. In the third ratio, $\bar{y}$ is the calculated rms vertical deflection under the transit point load. In the fourth ratio, M is the total mass of the whole beam, given by

$$M = \sum_{n=1}^{N} \bar{m}_n \cdot f_n \ell \tag{3.29}$$

In each term of Equation (3.28), the normalizing factor, subscripted r, is the counterpart quantity for an arbitrary, non-optimal reference guideway configuration. If $c_1 = c_2 = c_3 = c_4 = 1$, then $\phi = 4$ for the reference configuration and a ϕ less than 4 indicates a superior or more efficient structure than the reference case. It is observed that the σ_m, $\Delta\sigma_m$ and M terms of ϕ are measures of the efficient use of the structural material. That is, σ_m indicates the strength required of the

material; $\Delta\sigma_m$ is a measure of the live load stress distribution; and M is the total dead load of the structure. The remaining term, the rms deflection, is a measure of structural performance as it affects the transit vehicle. That is, low values of $\bar{y}$ imply that low amplitude levels of vertical excitation are imparted to the vehicle. For a constant ω/p_r ratio, this implies a high level of passenger ride comfort [3.4].

In a typical optimization study, N, L and v (remain fixed). Then the terms of ϕ are calculated and configurations producing minimum ϕ values are sought, consistent with material stress limits, deflection constraints and construction practice. Of course, the optimal configuration is tempered by the distribution of c_k, which reflects a designer's perception of the relative importance of the four terms to overall structural performance.

In the numerical studies which follow, the arbitrary reference configuration, subscripted r in the ϕ function, was based on the laboratory model test facility at Duke University. In this three-span test configuration, all of the spans are of equal length, ℓ, and the unit mass, $\bar{m}_r$, and stiffness, EI_n, are constant throughout. These and other pertinent reference parameters are summarized in Table 3.1. All sets of the three distributed system parameters (pier spacing,

Table 3.1 Reference configuration

N = 3, number of span segments

ℓ = 60 in, span segment length

EI_r = 2.44×10^4, lb-in^2, span stiffness

F_0 = 2.63 lb, transit point load

$\bar{m}_r$ = 4.58×10^{-4} lb sec^2/in^2, span mass per unit length

p_r = 20 rad/sec, fundamental span frequency

v = 1.0 ft/sec; 9.54 ft/sec; 15.9 ft/sec, vehicle speeds

ω/p_r = 0.03 ; 0.3 ; 0.5, crossing ratio

stiffness and unit mass) used to define alternative span configurations in later studies, are defined as multiples of these reference configuration parameters. Also, all system responses, including the ϕ surfaces, are presented as nondimensional quantities based on the laws of similitude [3.6]. For these reasons, all calculated results based on this reference configuration are applicable to full-scale designs as well. For instance, the reference point load "vehicle" speeds of 1.0, 9.54 and 15.9 ft/sec correspond, respectively, to ω/p_r values of 0.03 (crawl speed), 0.3 and 0.5. These transit frequency ratios cover the range of practical, full-scale designs. Thus, in a prototype span where $\ell = 70$ ft and $p = 20$ rad/sec, the prototype vehicle speed for $\omega/p = 0.3$ would be 133 ft/sec or 90.7 mph.

SELECTED CLASSES OF SPAN CONFIGURATIONS

Three general classes of three-span configurations were selected for the optimization studies. In all three classes, symmetry about the midlength $x = L/2$ is imposed for the support spacing, bending stiffness and unit mass. Thus, $f_1 = f_3$ and $f_2 = 3 - 2f_1$; $EI_1 = EI_3$; and $\bar{m}_1 = \bar{m}_3$.

For a Class A configurations, a solid, rectangular span cross section is assumed and the span depth, h, is taken as constant throughout its entire length, L. The experimental span of Figure 3.2 is a Class A configuration, for instance. In these spans, the ratios of unit mass, stiffness and section modulus, $S_n = 2\ I_n/h$, between adjacent segments are all equal, or

$$\frac{\bar{m}_2}{\bar{m}_1} = \frac{\bar{m}_2}{\bar{m}_3} = \frac{EI_2}{EI_1} = \frac{EI_2}{EI_3} = \frac{S_2}{S_1} = \frac{S_2}{S_3} = \alpha$$

where α is a constant. In Class A, 72 sets of parameters distributions were investigated, corresponding to 9 different support spacings, each applied to 8 different constants α, all for a fixed value of ω/p_r. These configurations are summarized in Table 3.2 where the coordinates (X,Y) designate the parameter set used in the later presentations of results.

For Class B configurations, the span cross section is assumed to be an "I" beam, or a series of "I" beams side by side, each with negligible web thickness. In these spans, the unit mass remains fixed, or $\bar{m}_1 = \bar{m}_2 = \bar{m}_3$; and the flange area and shape remain constant over the entire length, L. However, the beam depths between adjacent span segments are h and βh, respectively, where β is a constant. For these cross sections, the stiffnesses vary approximately as the square of the beam depth, or

$$\frac{EI_2}{EI_1} = \frac{EI_2}{EI_3} = \beta^2$$

and the section moduli vary linearly with beam depth, or

$$\frac{S_2}{S_1} = \frac{S_2}{S_3} = \beta$$

Table 3.2 shows the matrix of the 72 sets of parameters studied for Class B configurations, with their (X,Y) coordinate designations.

Table 3.2 Matrix of distributed parameters used in optimization studies of three-span continuous beams

CLASS	X COORD.	MASS DISTRIBUTION $\frac{\bar{m}_1}{\bar{m}_r}$	$\frac{\bar{m}_2}{\bar{m}_r}$	$\frac{\bar{m}_3}{\bar{m}_r}$	STIFFNESS DISTRIBUTION $\frac{EI_1}{EI_r}$	$\frac{EI_2}{EI_r}$	$\frac{EI_3}{EI_r}$	f_n, SUPPORT SPACINGS
A	4	.6	1	.6	.6	1	.6	$f_1 = f_2 = f_3 = 1$
	3	.7	1	.7	.7	1	.7	
	2	.8	1	.8	.8	1	.8	
	1	.9	1	.9	.9	1	.9	
	0	1	1	1	1	1	1	REF. SPAN
	-1	1	.9	1	1	.9	1	
	-2	1	.8	1	1	.8	1	
	-3	1	.7	1	1	.7	1	
B	4	1	1	1	.6	1	.6	
	3	1	1	1	.7	1	.7	
	2	1	1	1	.8	1	.8	
	1	1	1	1	.9	1	.9	
	0	1	1	1	1	1	1	REF. SPAN
	-1	1	1	1	1	.9	1	
	-2	1	1	1	1	.8	1	
	-3	1	1	1	1	.7	1	
C	4	.6	1	.6	1	1	1	
	3	.7	1	.7	1	1	1	
	2	.8	1	.8	1	1	1	
	1	.9	1	.9	1	1	1	
	0	1	1	1	1	1	1	REF. SPAN
	-1	1	.9	1	1	1	1	
	-2	1	.8	1	1	1	1	
	-3	1	.7	1	1	1	1	

Y, SPACING PARAMETER COORDINATE:	-4	-3	-2	-1	0	1	2	3	4
	$f_1 = 1.2$ $f_2 = .6$ $f_3 = 1.2$	$f_1 = 1.15$ $f_2 = .7$ $f_3 = 1.15$	$f_1 = 1.1$ $f_2 = .8$ $f_3 = 1.1$	$f_1 = 1.05$ $f_2 = .9$ $f_3 = 1.05$		$f_1 = .9$ $f_2 = 1.2$ $f_3 = .9$	$f_1 = .8$ $f_2 = 1.4$ $f_3 = .8$	$f_1 = .7$ $f_2 = 1.6$ $f_3 = .7$	$f_1 = .6$ $f_2 = 1.8$ $f_3 = .6$

For Class C configurations, the cross sections were chosen so that both the bending stiffness and the section modulus are uniform through the entire length, L. There, the unit mass in adjacent span segments is allowed to change, or

$$\bar{m}_1 = \bar{m}_3 = \gamma \bar{m}_2$$

where γ is a constant. As for Class A and B configurations, Table 3.1 shows the same 9 sets of spacing parameters, each applied to 8 configurations of different unit mass distributions. It is recognized that Class C designs may be, for the most part, the least practical of the three classes considered. However, there may be merit in Class C designs in particular instances. If adverse resonances are predicted in a certain, continuous span design, these resonance amplitudes could be reduced or eliminated by the addition of dead weight in selected span segments without changing the bending stiffnesses.

The guideways selected for study and the reasons for their selection are summarized. The general guideway type is $N = 3$. Investigated are 216 distinct configurations (Table 3.1), with 72 configurations in each of Class A, B and C. In each class, the reference configuration is the same, defined by the parameter coordinate $(X,Y) = (0,0)$ in Table 3.1. To include the effects of the transit speed of the point load, three values of ω/p_r, are selected for each configuration: 0.03 (crawl speed), 0.3 and 0.5. This raises the total number of computer simulations to 648. In each simulation, the total mass, the critical span responses

and ϕ are calculated. The justification for limiting the numerical studies to this range of parameters is simply one of computational economy. Nonetheless, the results which follow illustrate the methodology and should indicate trends applicable to future optimization studies of higher N guideways, with intermediate values of ω/p_r. For instance, such trends were very clear in previous studies [3.4] for a single distributed parameter where the optimum pier spacings changed very little from $N = 3$ to $N = 10$; and where the peak span responses were not only continuous in the range $0 < \omega/p < 0.5$, but were reduced with the use of optimum pier spacings.

NUMERICAL RESULTS AND CONCLUSIONS

To obtain numerical results, use was made of the facilities at the Triangle University Computation Center located in Research Triangle Park, N. C. The digital system consisted of two IBM 370/165 computers coupled with an AMDAHL 470/V8 computer. The isometric surfaces describing the components of ϕ were generated on a Complot DP-7 plotter using SAS/GRAPH software [3.7]. Calculated for each of the 648 simulations was the time history of each midspan deflection and bending moment; each peak midspan response; and each normalized component of the optimization function ϕ, Equation (3.28). In all cases, 600 integration steps were used to solve Equation (3.17) numerically; and the truncation of the series of Equation (3.15) and Equation (3.24) at $m = 20$ modes was found to give adequate convergence for the responses.

The results are presented as computer generated surfaces, $Z = Z(X,Y)$, shown in Figures 3.7 through 3.26. For each class of problems (A, B or C), the coordinates (X,Y) representing the distribution of system parameters, is given in Table 3.1. The coordinates $(X,Y) = (0,0)$ always represent the reference span; and Y always represents support spacing parameter. The calculated ordinate Z represents one of five quantities: a term of the ϕ function (σ_m/σ_r, $\Delta\sigma_m/\Delta\sigma_r$, $\bar{y}/\bar{y}_r$, M/M_r); or the ϕ function itself, where $c_1 = c_2 = c_3 = c_4 = 1$. For each numbered Figure, there are two perspectives of the same $Z(X,Y)$ surface, (a) and (b), representing a rotation difference about the vertical axis of 25 degrees and a tilt above the Y-axis of 10 degrees.

The calculated surfaces for Class A configurations (solid, rectangular cross sections with varying segment widths) are shown in Figures 3.7 through 3.11, based on $\omega/p_r = 0.03$. The total span mass surface, Figure 3.7 is calculated directly from Equation 3.29 using the preselected values of Table 3.1, where $Z = M/M_r \leq 1$. The computed surfaces for σ_m/σ_r , $\Delta\sigma_m/\Delta\sigma_r$, $\bar{y}/\bar{y}_r$, and ϕ in Figures 3.8 through 3.11, respectively, clearly show that the selected pier spacing parameter dominates the computed responses. Comparing these surfaces, it is seen that the maximum stress difference surface, $Z = \Delta\sigma_m/\sigma_r$ of Figure 3.9, overshadows the others in height, reaching a peak of 17.8 at $(X,Y) = (4,-4)$. Thus, the $\Delta\sigma_m/\sigma_r$ surface dominates the response behavior of the ϕ function of Figure 3.11. The $\bar{y}/\bar{y}_r$ surface, Figure 3.10, has the least effect on ϕ. It is recalled that $\phi = 4$ corresponds to the reference configuration. Figure 3.11 shows a minimum value of the

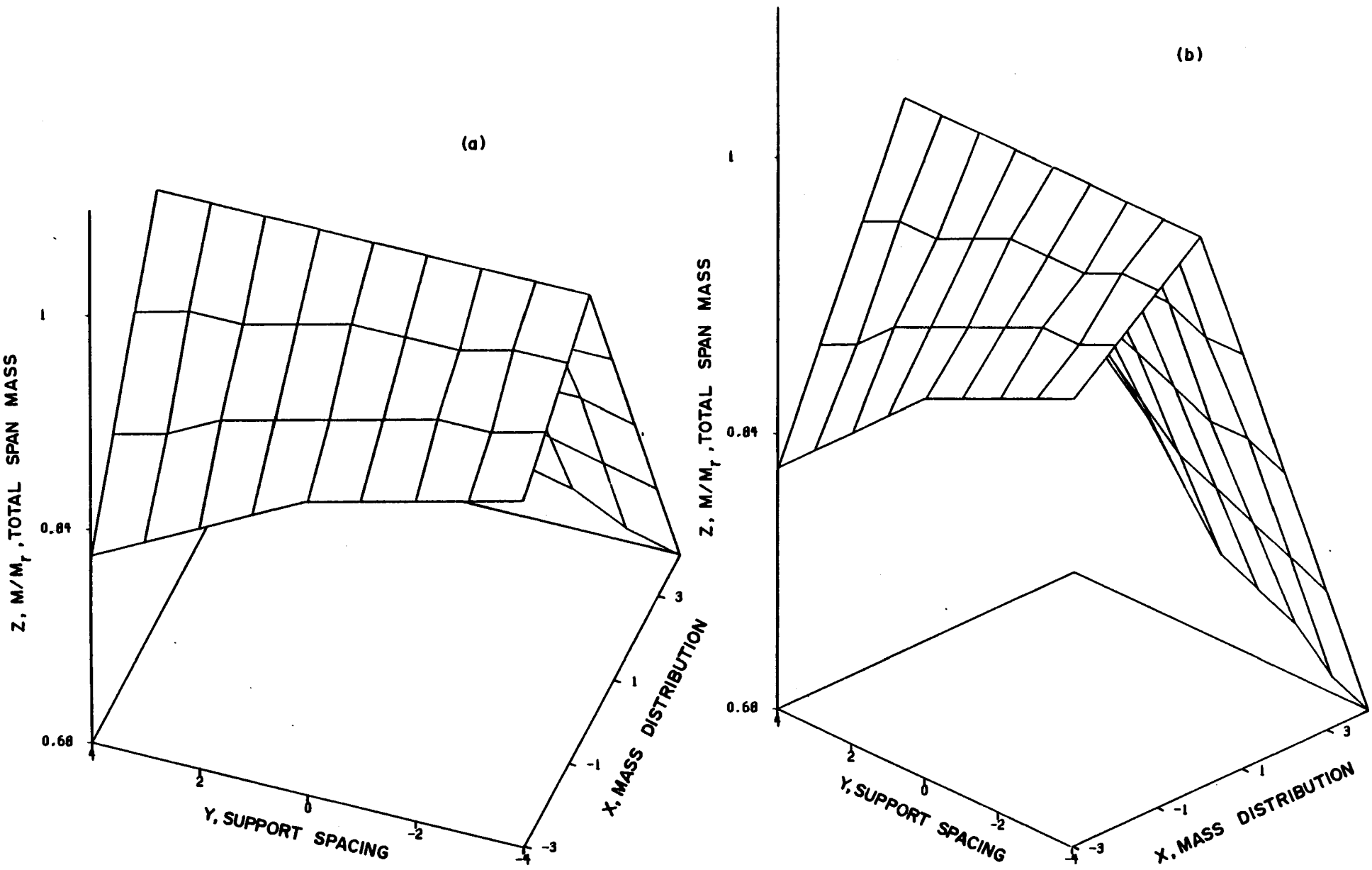

Figure 3.7 Surfaces for total span mass, Class A and C configurations

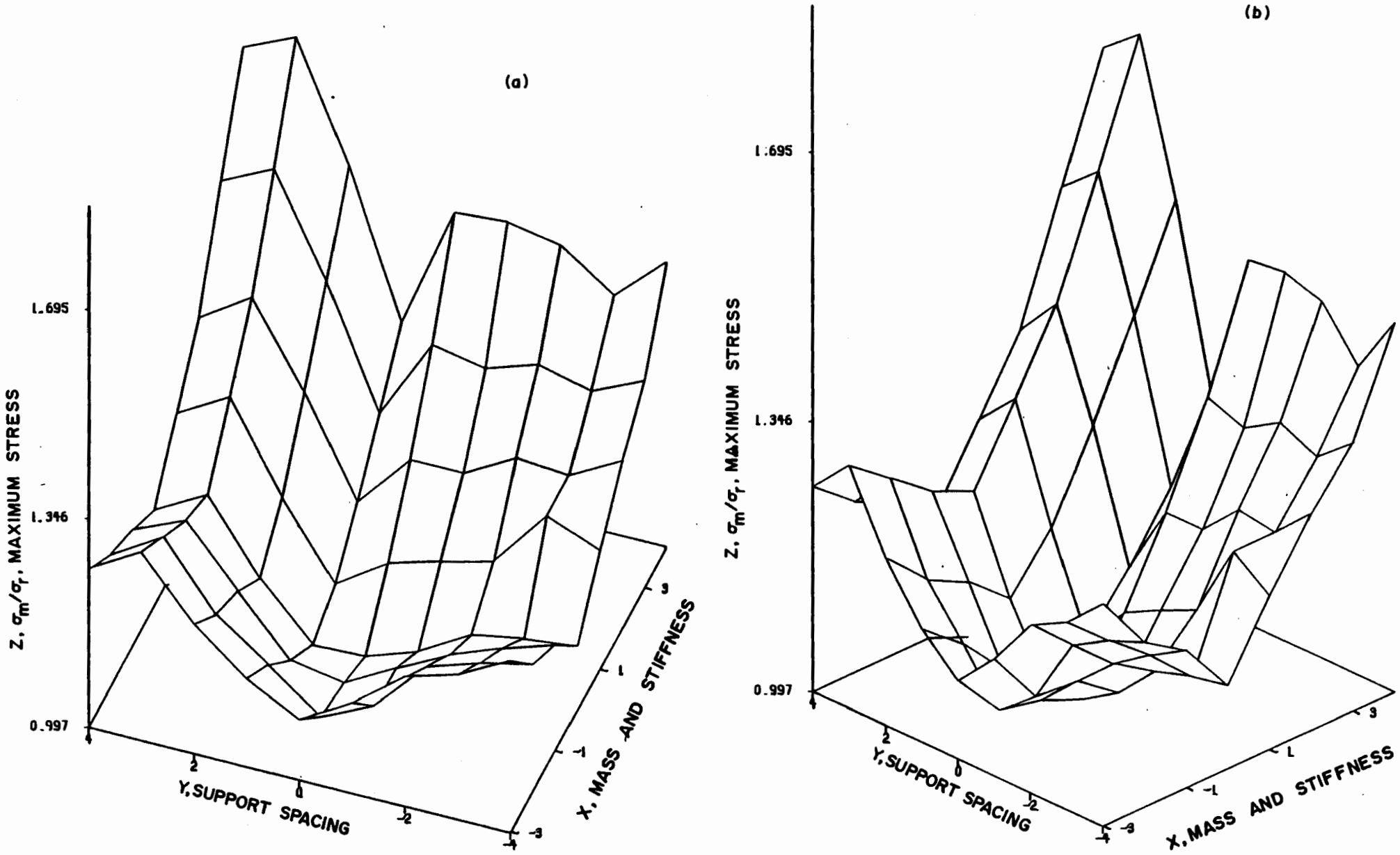

Figure 3.8 Maximum stress surfaces for Class A configurations, $\omega/p_r = 0.03$

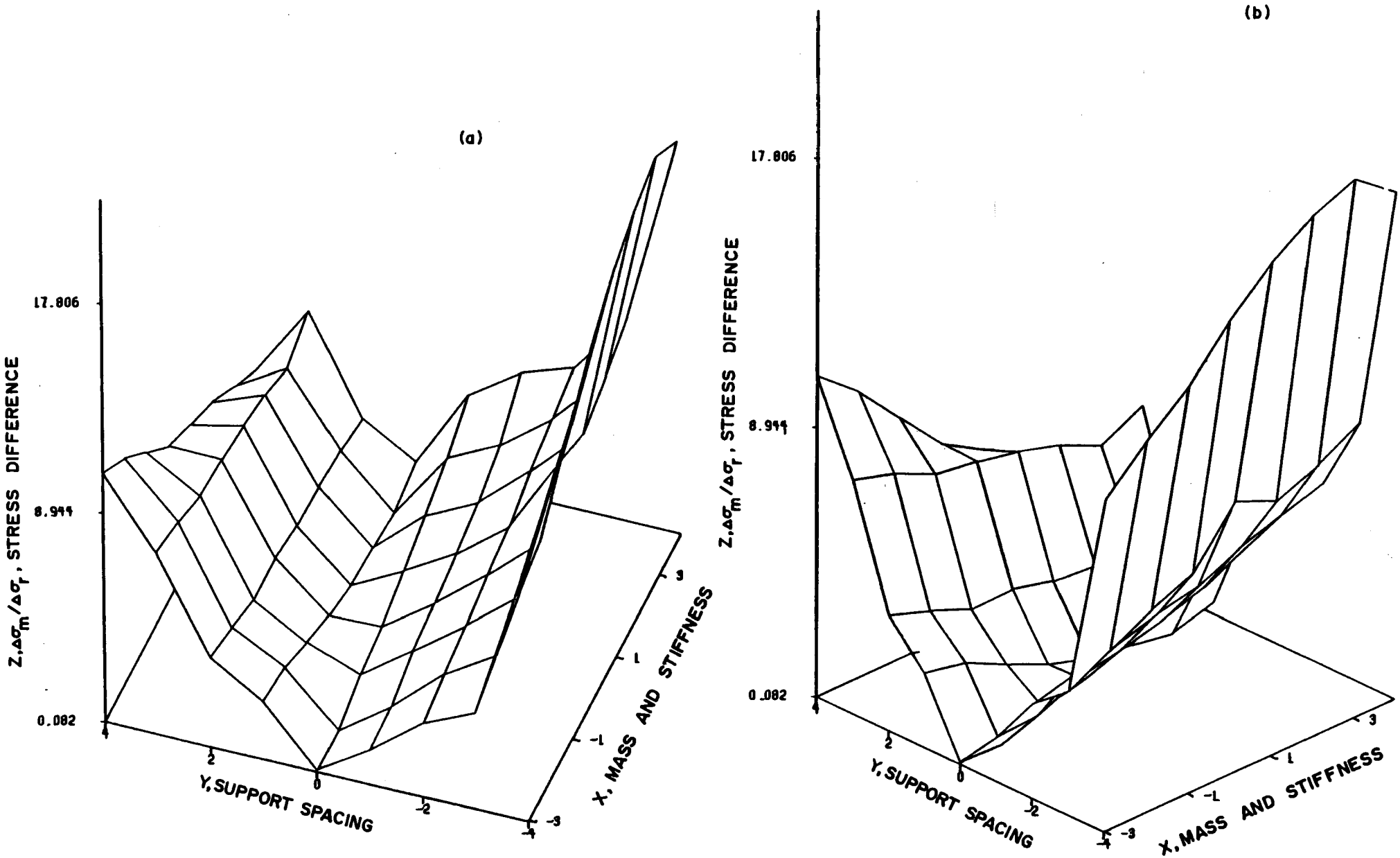

Figure 3.9 Maximum stress difference surfaces for Class A configurations. $\omega/p = 0.03$

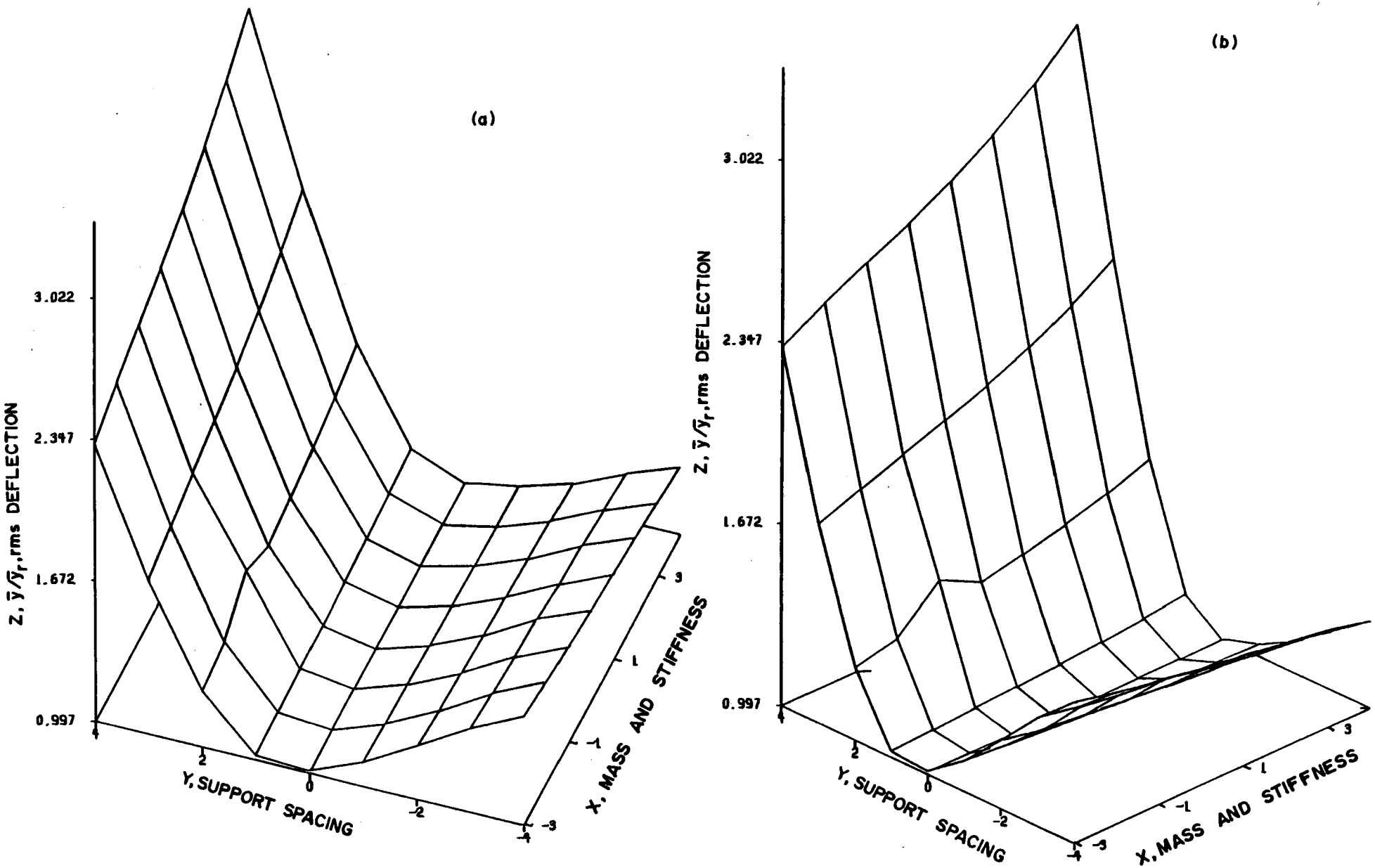

Figure 3.10 rms deflection surfaces for Class A configurations, $\omega/p_r = 0.03$

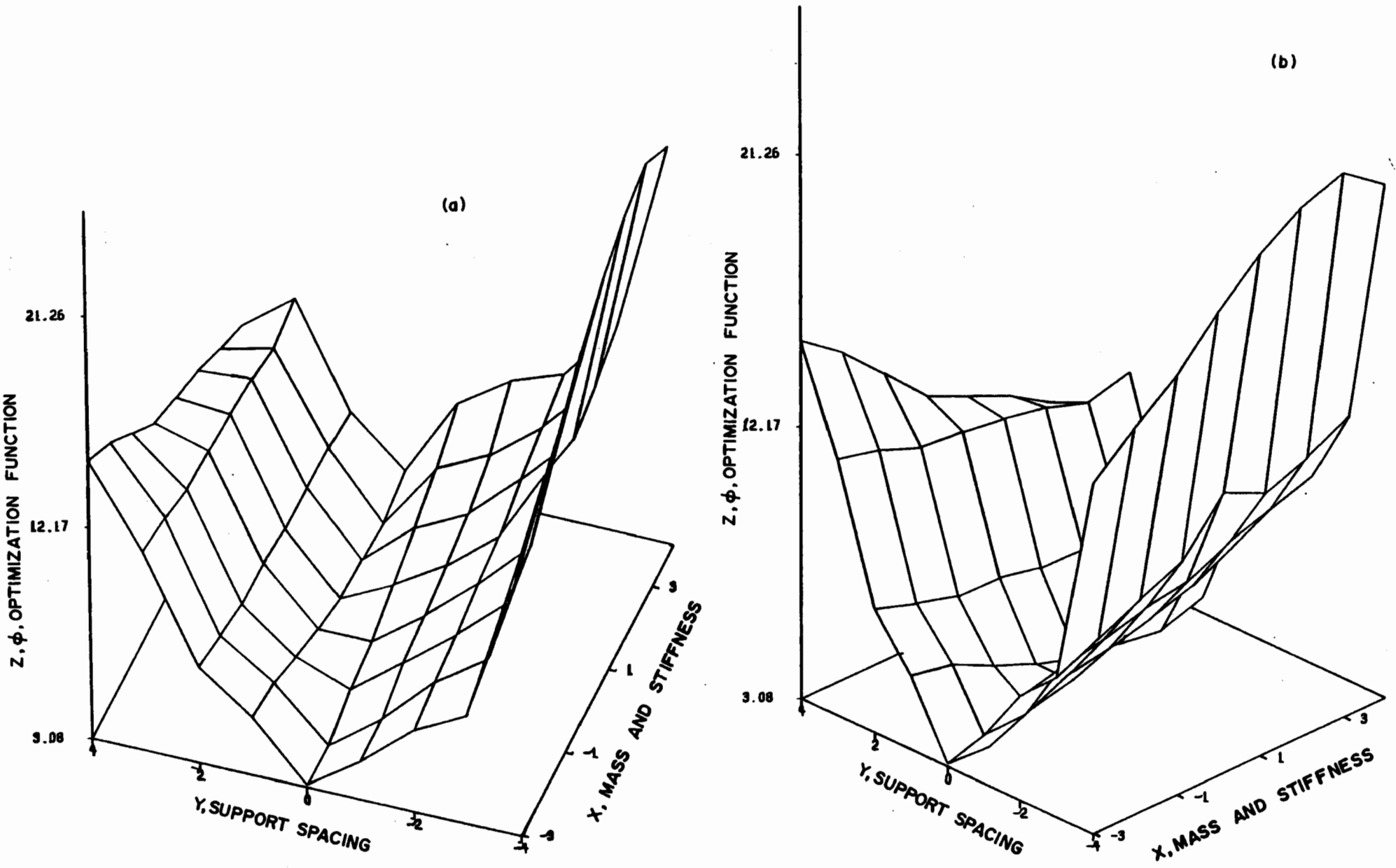

Figure 3.11 Optimization function surfaces for Class A configurations, $\omega/p_r = 0.03$

optimization function, where $\phi = 3.08$ at $(X,Y) = (-2,0)$. Thus, at least a 23 percent improvement in guideway efficiency over the reference configuration is possible. A "fine tuning" of the distributed parameters about these (X,Y) coordinates may improve this efficiency even further.

The calculated responses for Class B configurations ("I" beams of variable depth and constant flanges) are shown in Figures 3.12 through 3.15. Not shown is the uniform, total mass surface, which is a horizontal plane, or $Z = M/M_r = 1$. Inspection of these response surfaces representing σ_m/σ_r, $\Delta\sigma_m/\Delta\sigma_r$, $\bar{y}/\bar{y}_r$ and ϕ, respectively, reveals trends similar to the corresponding Class A surfaces. That is, the Y parameter has the largest influence on these responses; $\bar{y}/\bar{y}_r$ of Figure 3.14 has the least affect on ϕ and the high levels of the $\Delta\sigma_m/\Delta\sigma_r$ responses, Figure 3.13 dominate the ϕ function, Figure 3.15. Here, the minimum is $\phi = 3.13$ at $(X,Y) = (-3,0)$, indicating a 21.7 percent improvement in design efficiency for these parameter coordinates.

The calculated responses for Class C configurations (uniform stiffness, variable unit mass) are shown in Figures 3.16 through 3.19, corresponding to surfaces σ_m/σ_r, $\Delta\sigma_m/\Delta\sigma_r$, $\bar{y}/\bar{y}_r$ and ϕ. This total mass surface, the same as for Class A, is shown in Figure 3.7. As in the Class A and B studies, $\omega/p_r = 0.03$. There is one main difference between the four response surfaces here and the corresponding ones of Class A and B: the maximum stress surface, Figure 3.16 is much flatter for negative values of Y. From Figure 3.19, the minimum of the optimization function

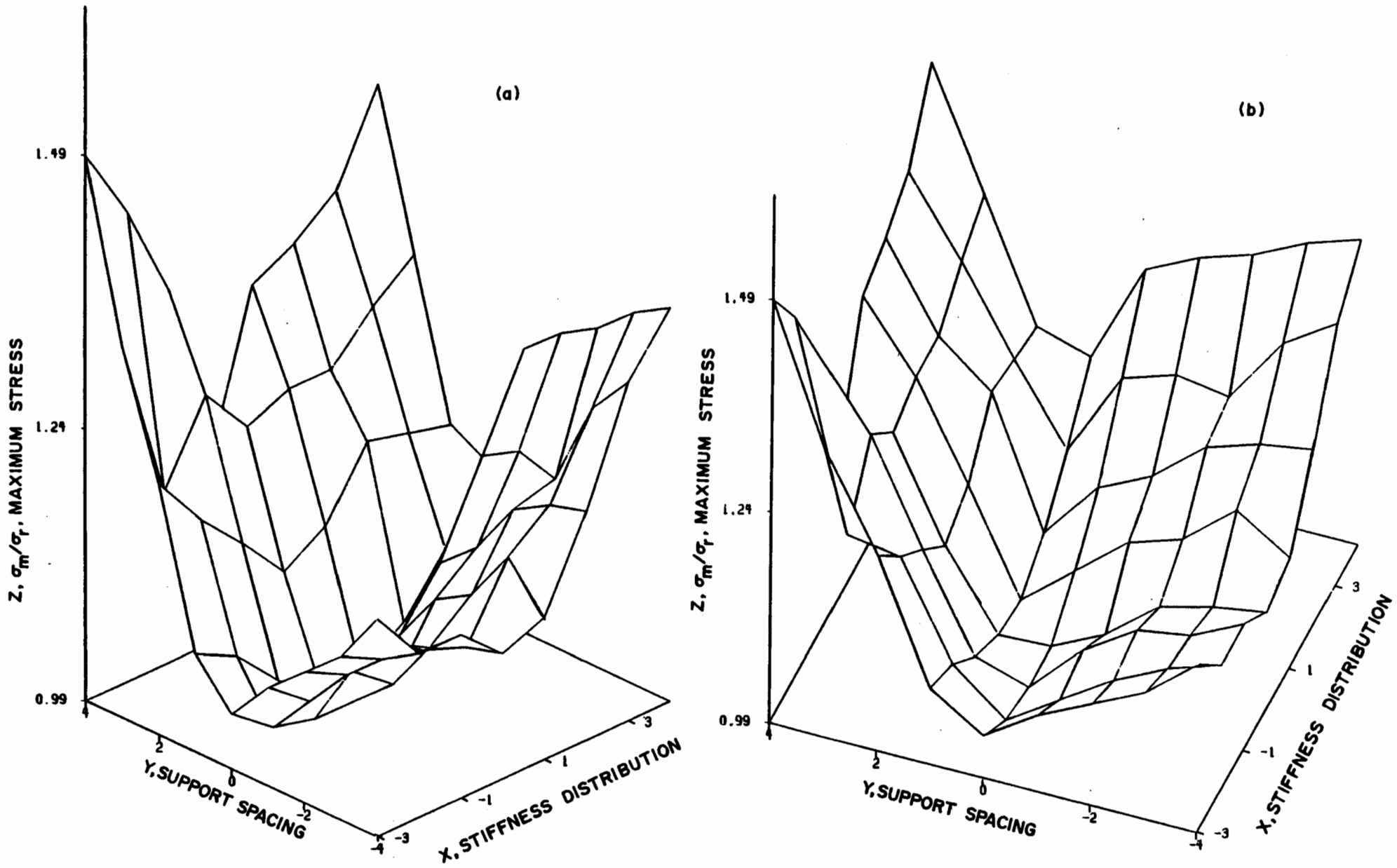

Figure 3.12 Maximum stress surfaces for Class B configurations, $\omega/p_r = 0.03$

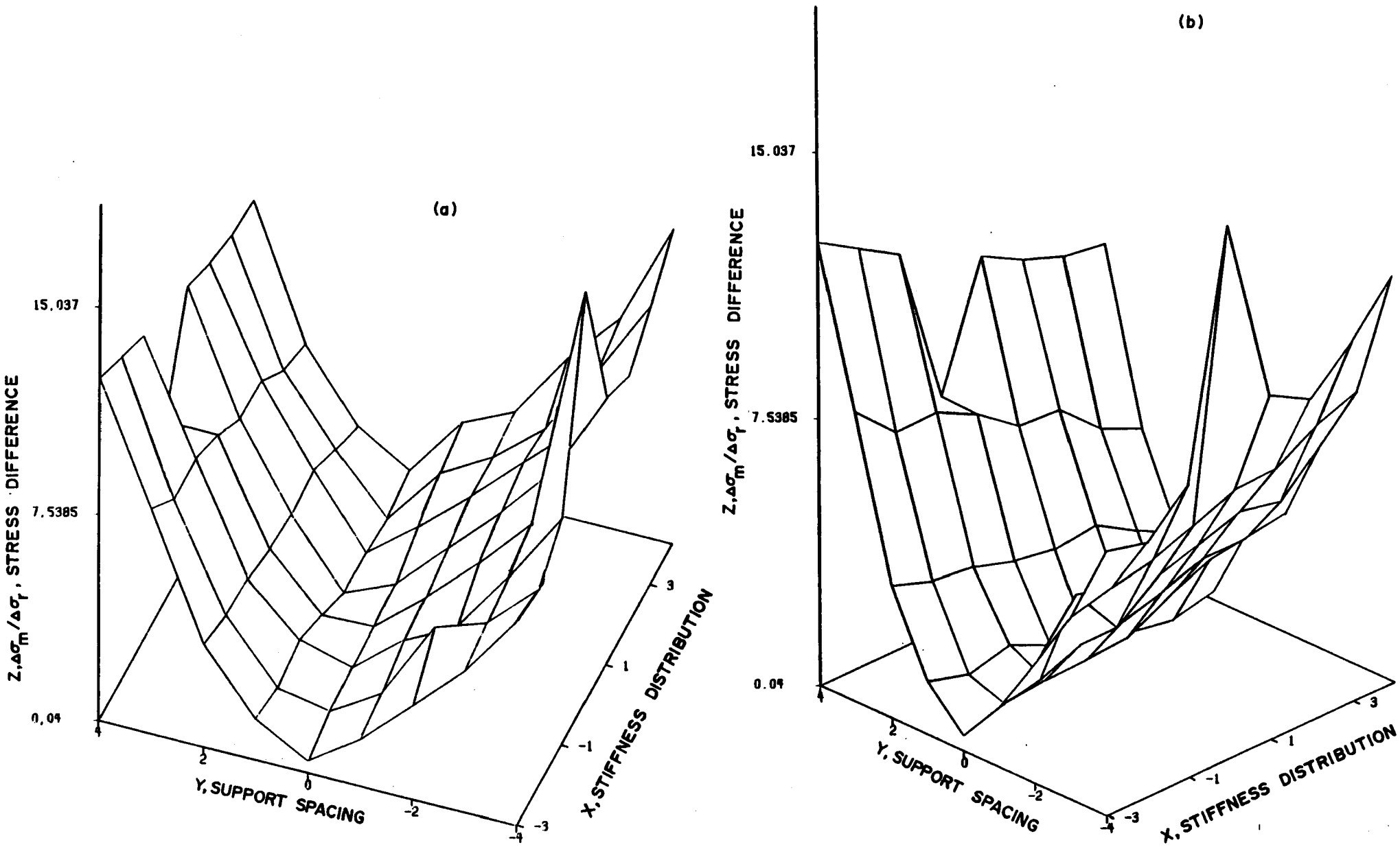

Figure 3.13 Maximum stress difference surfaces for Class B configurations, $\omega/p_r = 0.03$

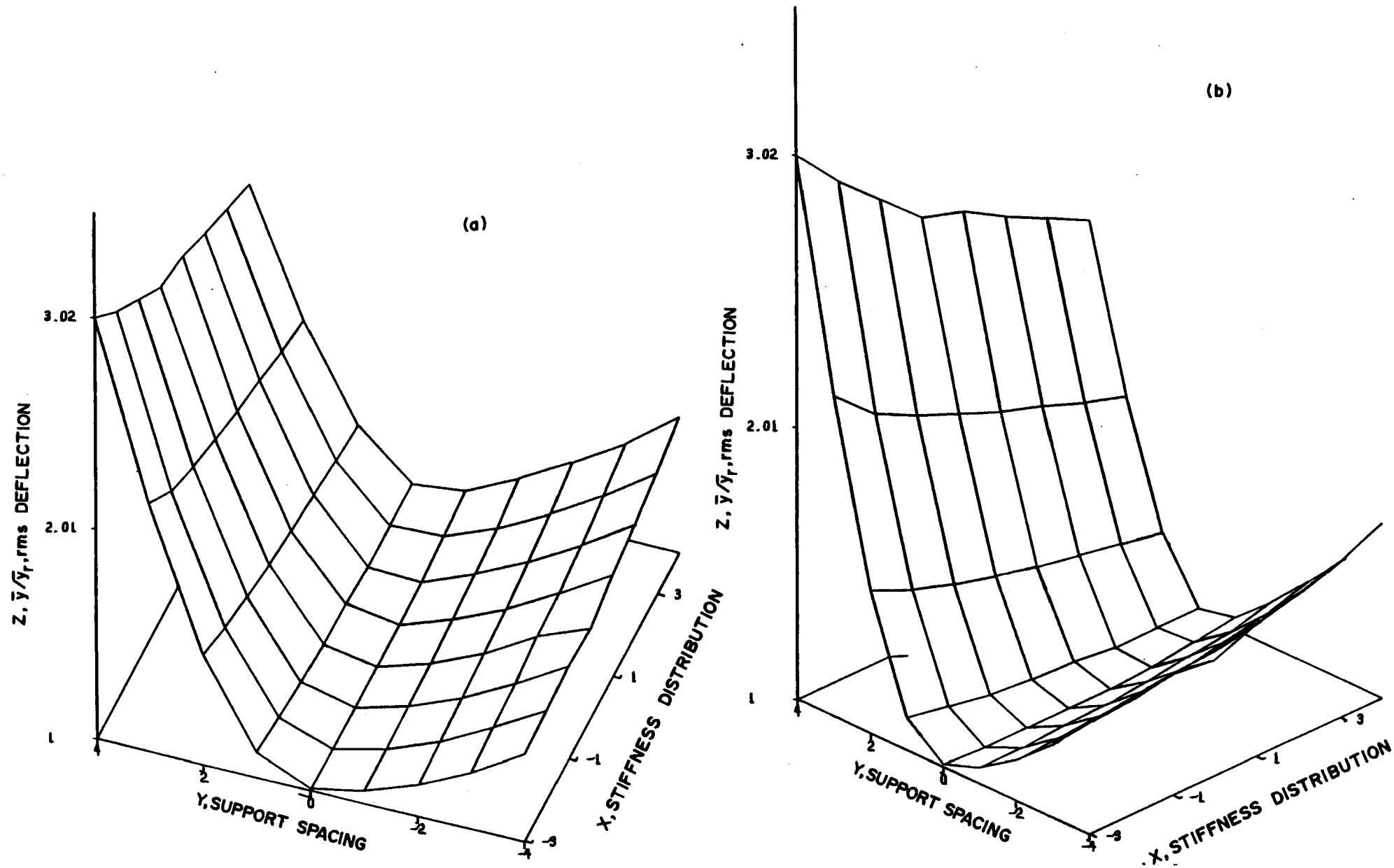

Figure 3.14 rms deflection surfaces for Class B configurations, $\omega/p_r = 0.03$

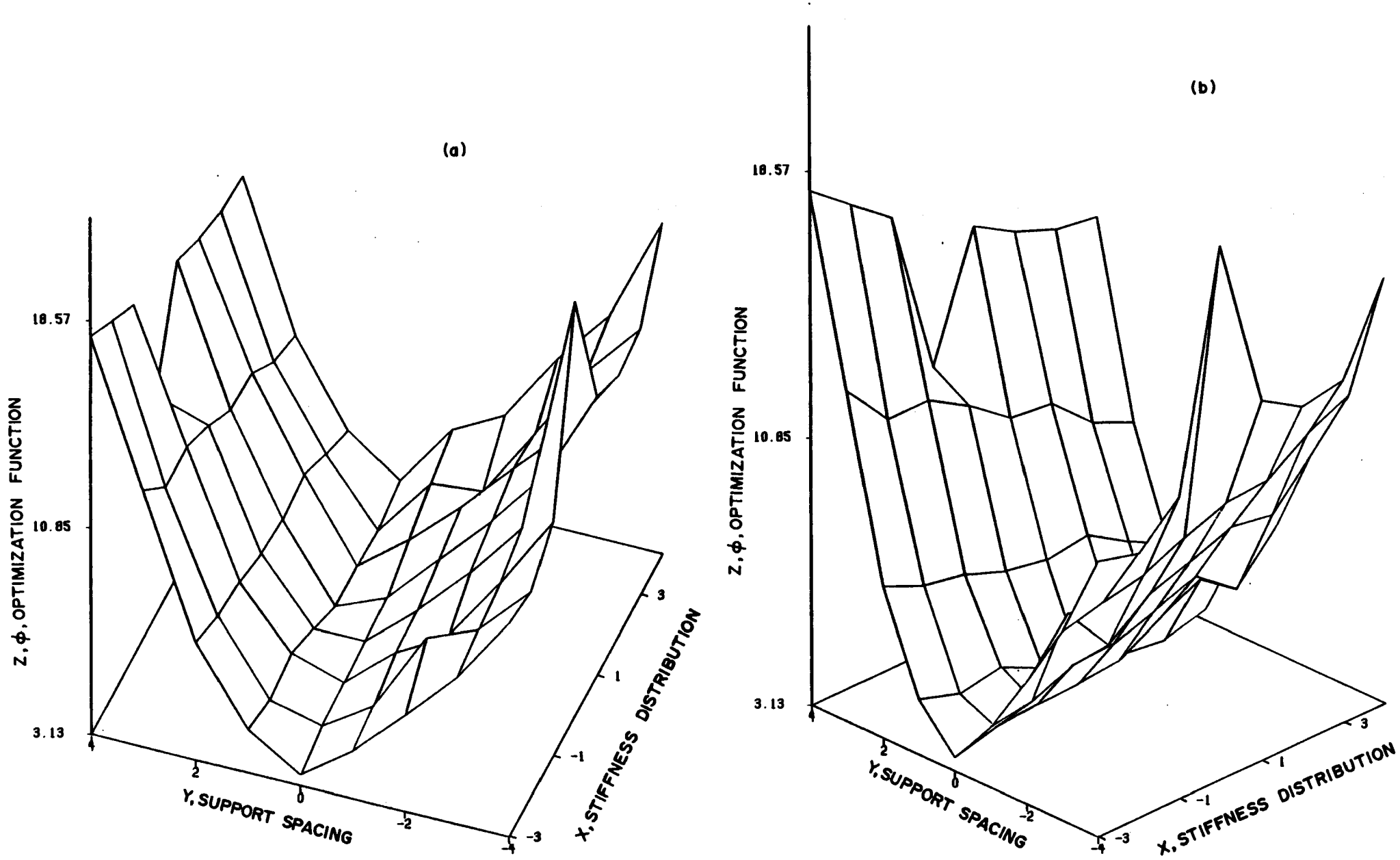

Figure 3.15 Optimization function surfaces for Class B configurations, $\omega/p_r = 0.03$

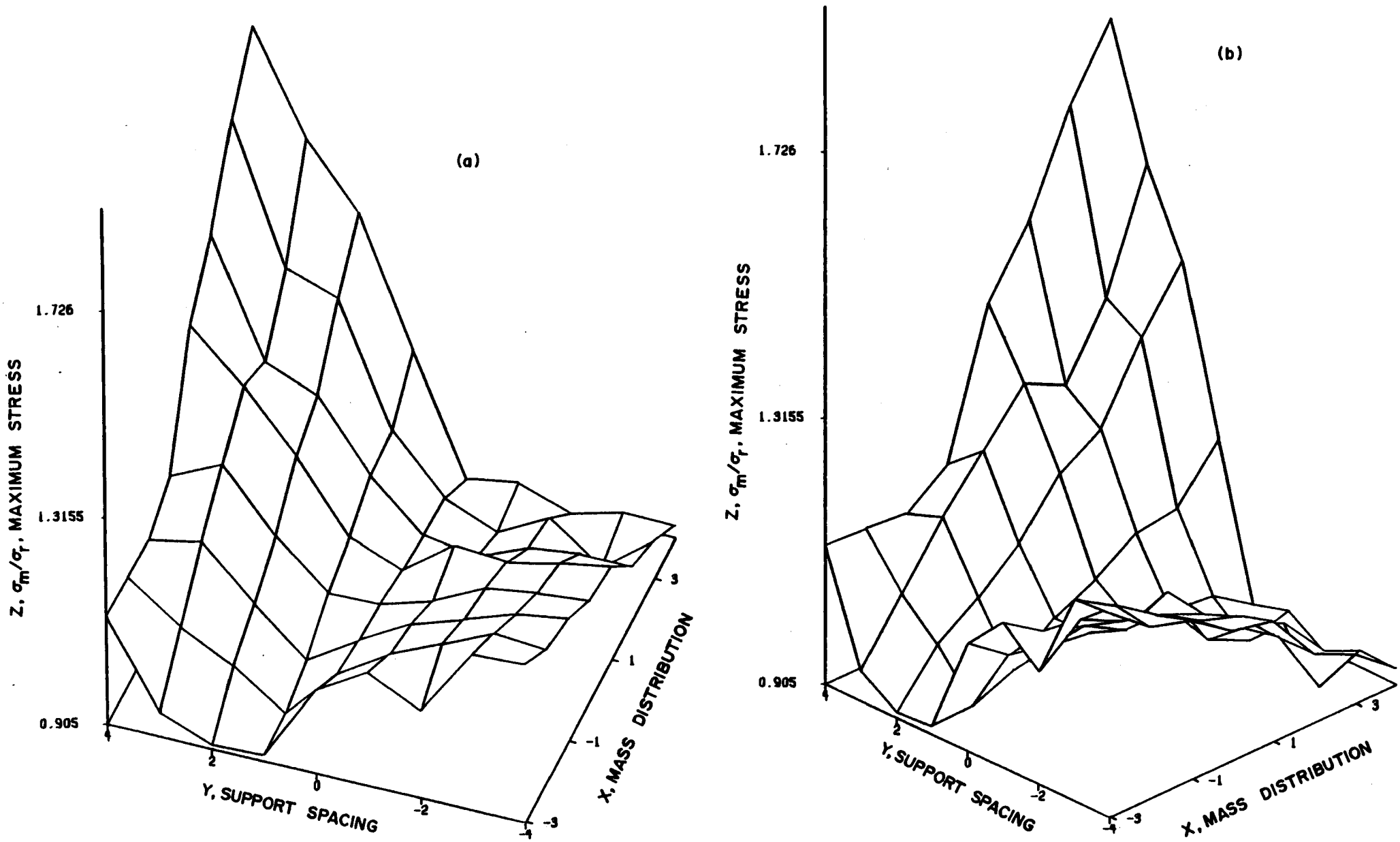

Figure 3.16 Maximum stress surfaces for Class C configurations, $\omega/p_r = 0.03$

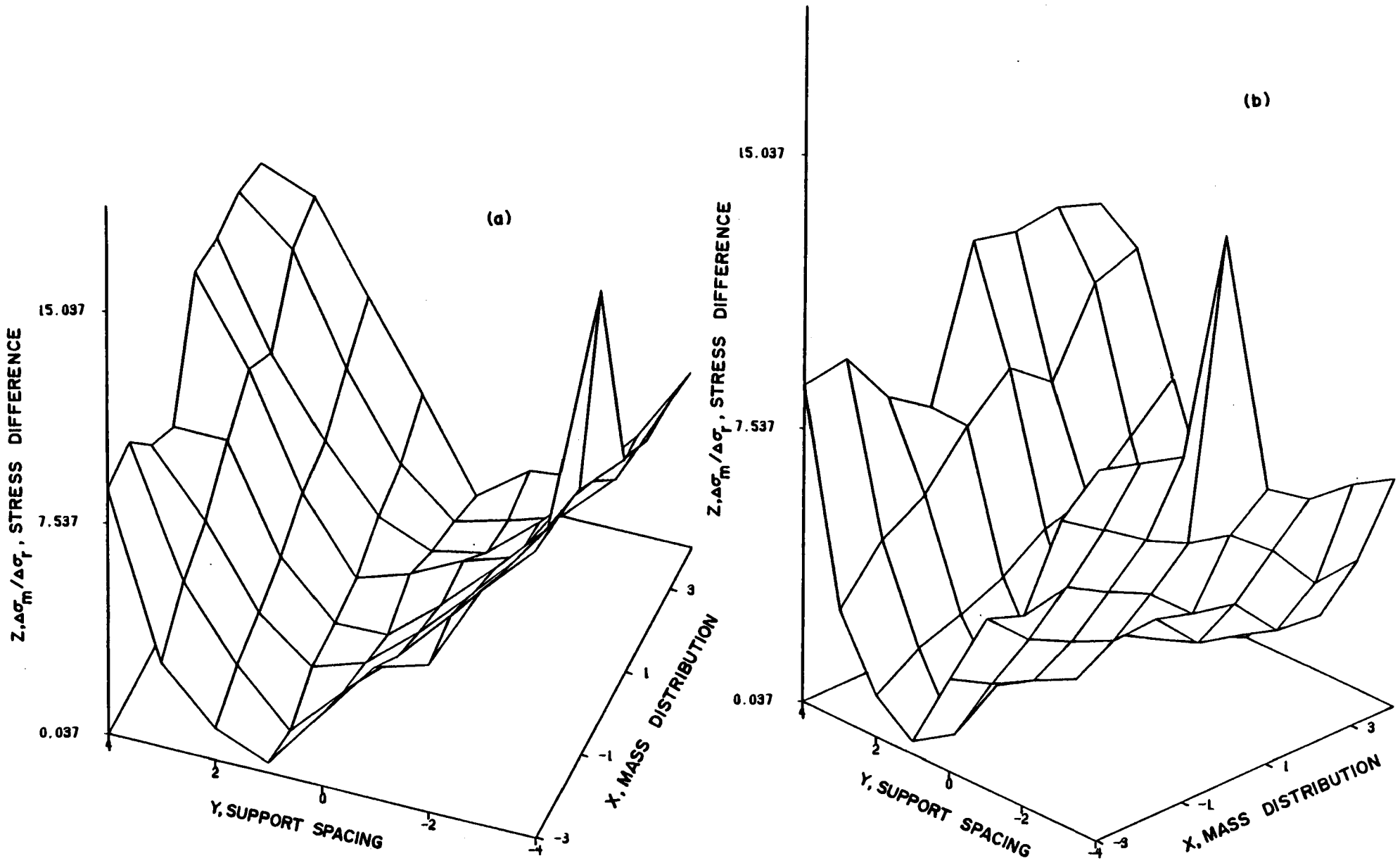

Figure 3.17 Maximum stress difference surfaces for Class C configurations, $\omega/p_r = 0.03$

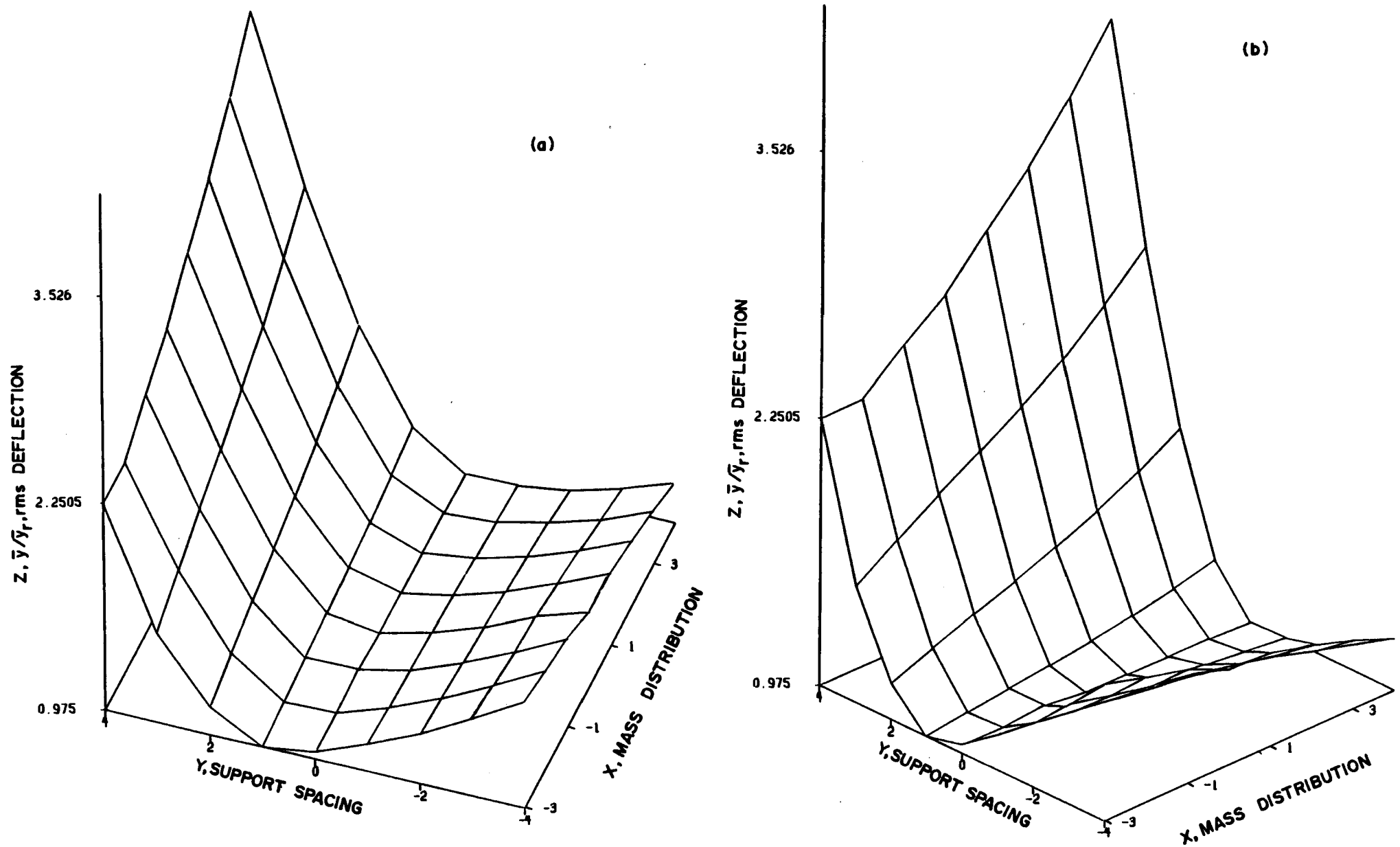

Figure 3.18 rms deflection surfaces for Class C configurations, $\omega/p_r = 0.03$

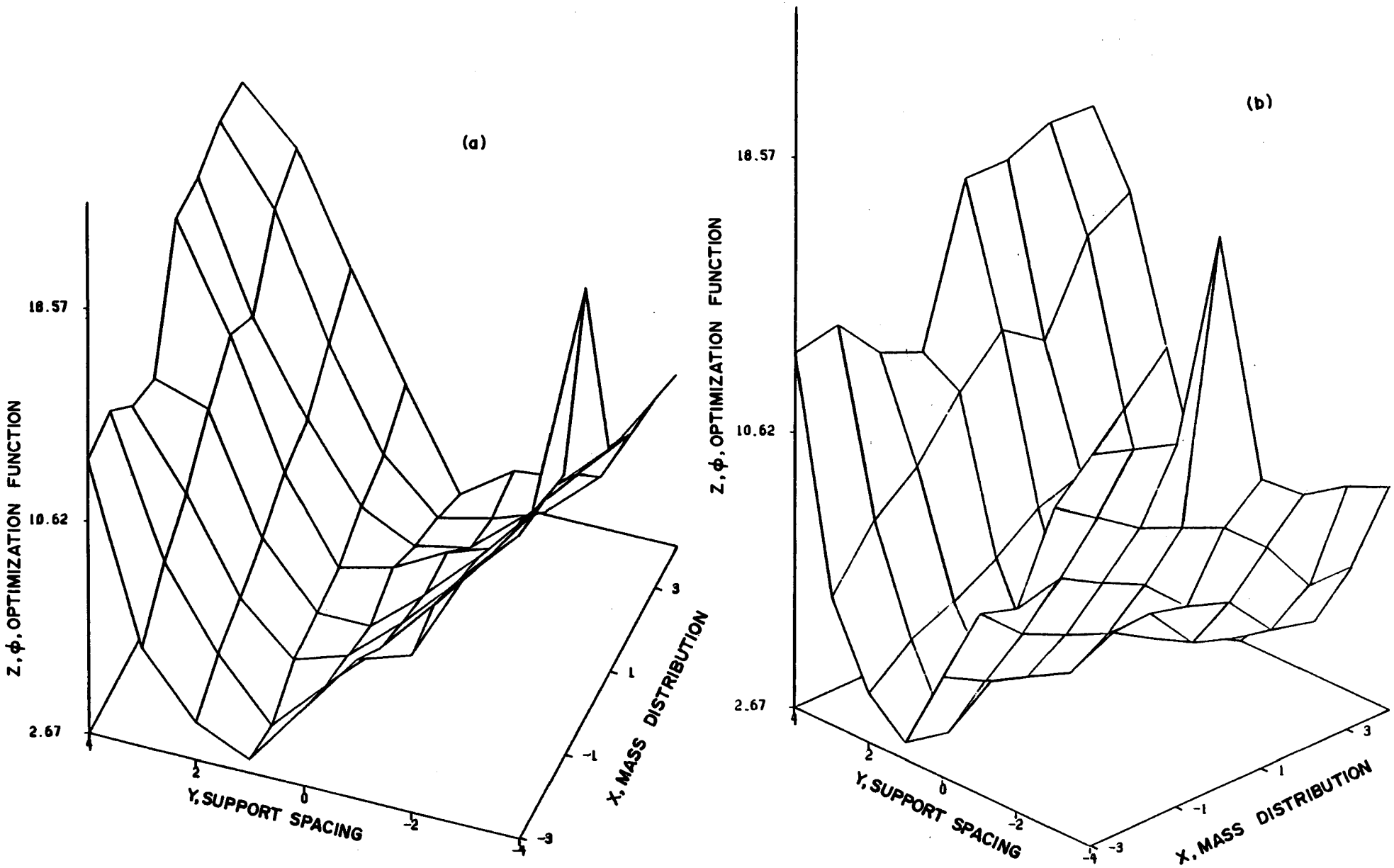

Figure 3.19 Optimization function surfaces for Class C configurations, $\omega/p_r = 0.03$

is $\phi = 2.67$ at $(X,Y) = (4,0)$, representing a 33.3 percent improvement over the reference configuration.

Considering all of the results presented in Figures 3.8 through 3.19, it is apparent the parameter coordinates for optimal configurations are well depicted by the minimums of the rms deflection surfaces. The numerical accuracy of these smooth surfaces is certain since the series for deflection are strongly convergent. It may be that some of the jagged peaks in the stress surfaces are artificial due to series which are less strongly convergent; or the peaks may be a true resonance phenomenon, unobliterated by the time averaging used to calculate $\bar{y}/\bar{y}_r$. At any rate it appears that the $\bar{y}/\bar{y}_r$ surfaces are logical indicators of optimal parameter coordinates. For this reason, these surfaces are used to demonstrate the effects of higher vehicle speeds or transit frequency ratios on optimal spans.

Each of the Figures 3.20 through 3.25 show the rms deflection surfaces for $\omega/p_r = 0.03$, 0.3 and 0.5. Figures 3.20 and 3.21, respectively, show two perspectives (a) and (b) of the same Class A configuration data; the counterpart views - for Class B are Figures 3.22 and 3.23; and for Class C are Figures 3.24, and 3.25. The most salient feature of all of these plots is the manner in which the edges where Y is a minimum curl up as ω/p_r increases. This indicates that relatively long end spans are much less desirable for higher vehicle speeds than for lower vehicle speeds. A comparison of Figures 3.20, 3.22 and 3.24 (or 3.21, 3.23 and 3.25) suggests that structural efficiency or $\bar{y}/\bar{y}_r$ is much more sensitive to changes in mass distribution than stiff-

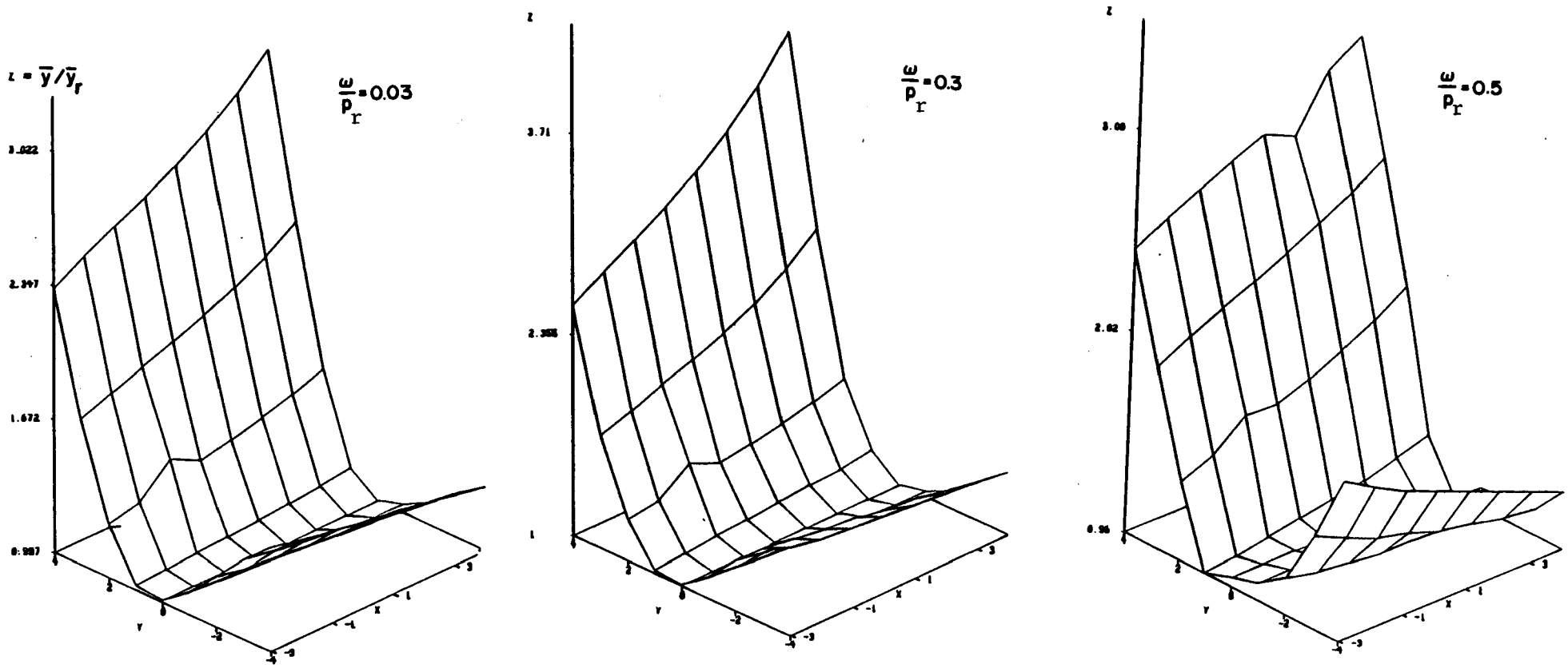

Figure 3.21 Class A rms deflection surfaces showing effects of transit speed, perspectives (a)

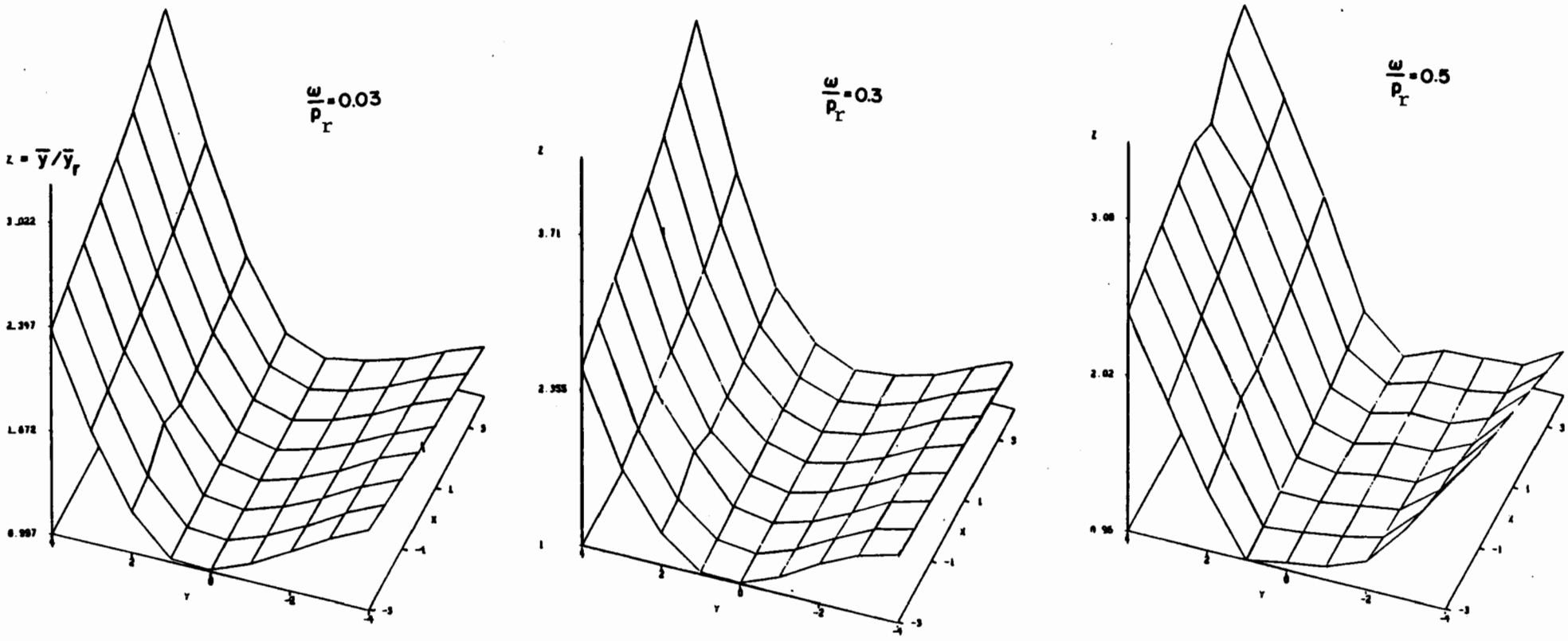

Figure 3.22 Class A rms deflection surfaces showing effects of transit speed, perspectives (b)

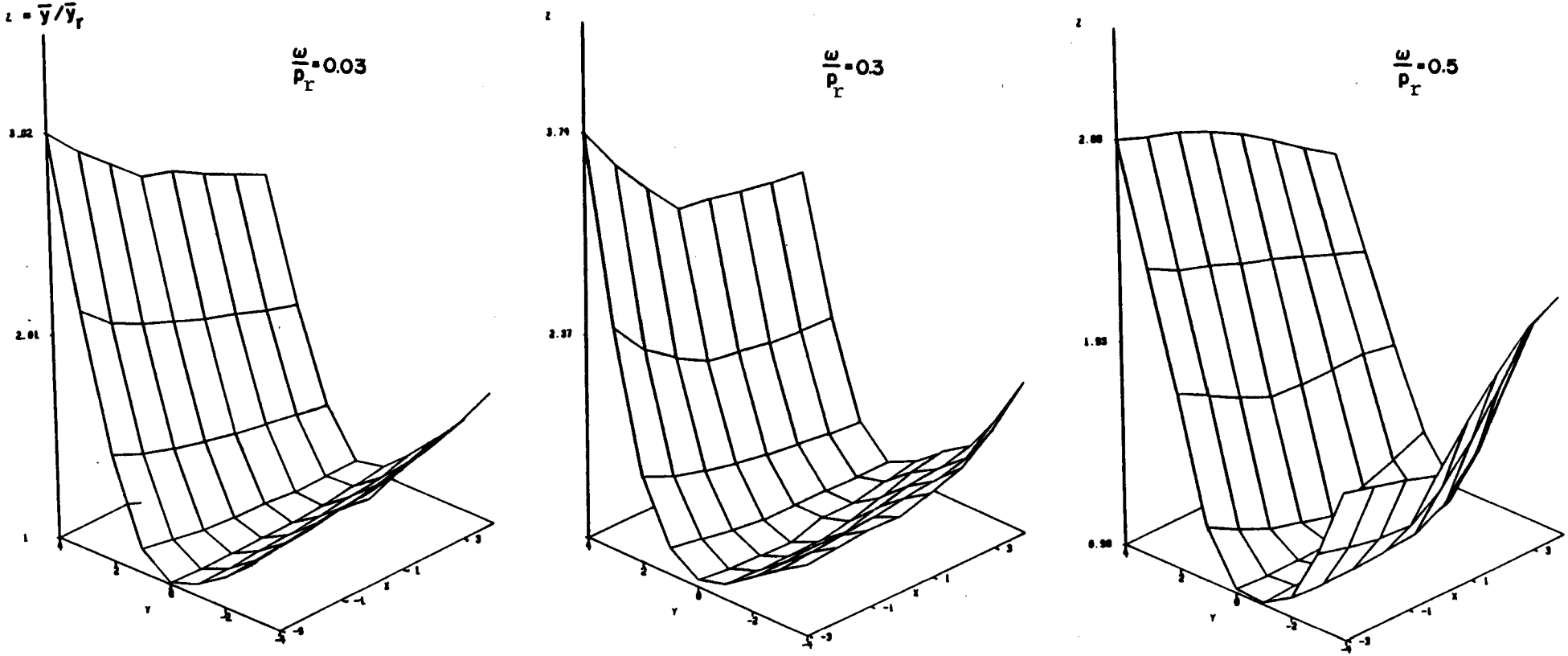

Figure 3.23 Class B rms deflection surfaces showing effects of transit speed, perspectives (a)

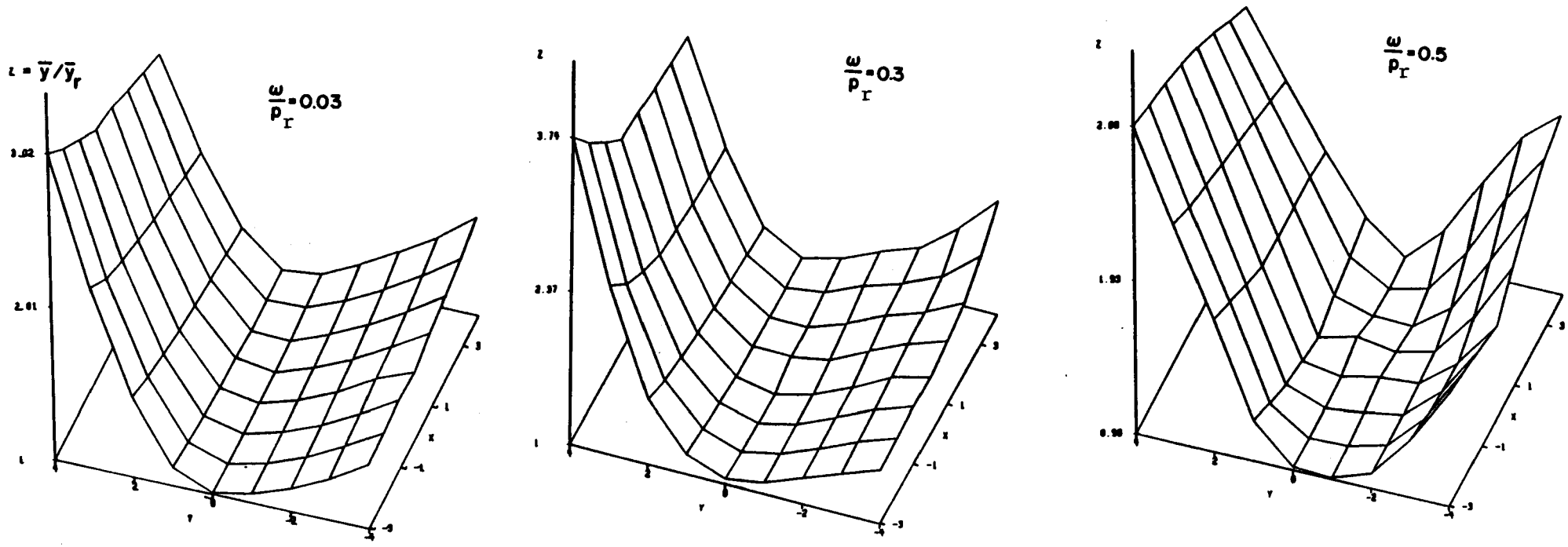

Figure 3.24 Class B rms deflection surfaces showing effects of transit speed, perspectives (b)

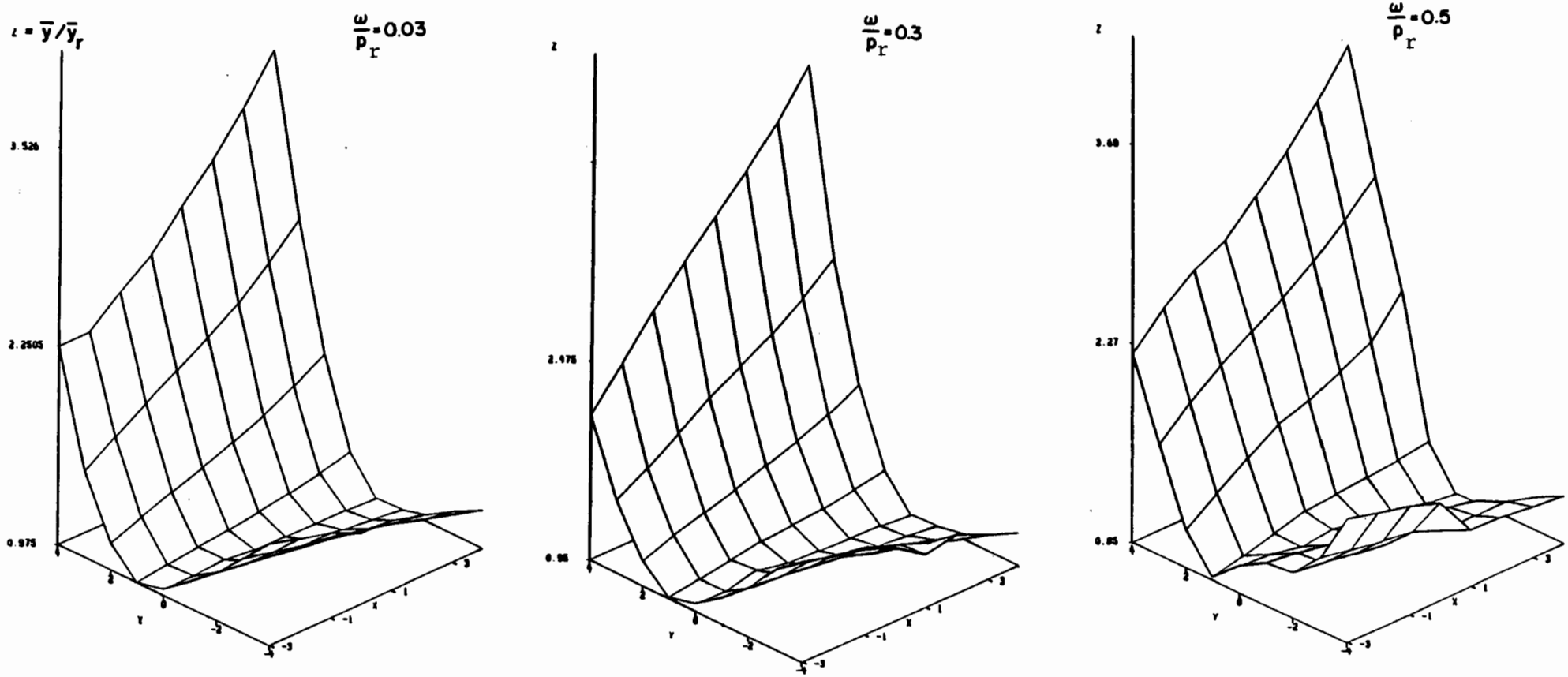

Figure 3.25 Class C rms deflection surfaces showing effects of transit speed, perspectives (a)

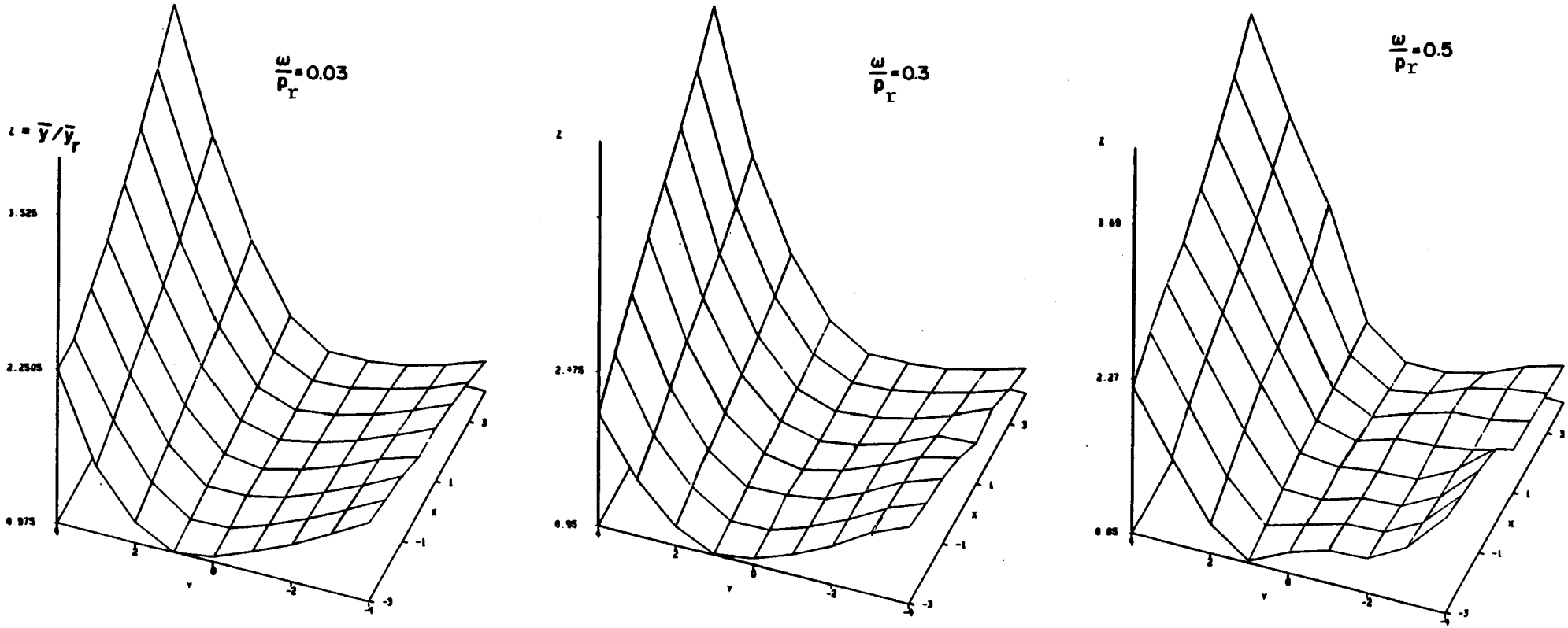

Figure 3.26 Class C rms deflection surfaces showing effects of transit speed, perspectives (b)

ness distribution. That is, the slopes of the surfaces are usually steeper along the mass direction, Figure 3.24, than along the stiffness direction, Figure 3.22. Finally, for all three transit vehicle speeds, the more efficient configurations are generally the ones with a greater unit mass on the extreme end spans than on the center one; and the pier spacings are such that the end spans are somewhat shorter than the center one. This is seen in Figures 3.24 and 3.25 for Class C configurations, for instance, where a minimum rms deflection has the parameter coordinates of $X = -2$ or -3 and $Y = 1$.

The main purpose in presenting the above results was to illustrate a methodology for optimal or efficient guideway design. In a strict sense, one should apply these data only to $N = 3$ configurations, based on the defined Classes A, B and C. An actual guideway composed only of several, parallel "I" beams could be close to Class B configurations; but if these beams were topped with a concrete bridge deck which added significant stiffness, then the above results for Class C could not be used. Such a new class of problems could readily be defined, however, and the methodology described could then lead to optimal configurations.

Reasonable estimates of efficient designs are often possible with a relatively crude mesh of the three design parameters. That is, interpolation of the rms deflection surfaces is a promising prospect. Viewing Figures 3.20, 3.22 and 3.24 as a group, it is seen that Class A surfaces are a crude "average" of those for Classes B and C. Thus it is possible for a structural designer, given a particular three-span beam, to estimate the effect of

varying either its cross sectional shape or its material, on its rms deflection. For example, assume that a three-span beam with a pier spacing equivalent to $Y = 1$ is to be designed for a vehicle speed in the range of the transit frequency ratio of $\omega/p = 0.3$. By studying Figures 3.22 and 3.24 (or Figures 3.23 and 3.25), one observes that an approximate minimum for the $\bar{y}/\bar{y}_r$ surface has the stiffness distribution (Class B configuration) of $X = X_B = 4$; and a unit mass distribution (Class C configuration) of $X = X_C = -3$. For a given preliminary guideway design, an absolute minimum of the $\bar{y}/\bar{y}_r$ surface would then be sought (for a fixed Y) by varying X_B about around 4 and X_C around -3, subject to all system constraints. It appears, in this case, that the stiffness of the center span segment, or X_B, would be increased somewhat; and the unit mass of the two end span segments would be higher than the center one, amounting to an increase in the X_C parameter.

It is concluded that these three-span parametric studies serve as a basis for the optimal dynamic design of higher order, continuous, beam guideways. The three key parameters governing the structural efficiency of higher N guideways are also the pier spacing, the beam stiffness distribution and the unit mass distribution. For $N = 3$, the structural efficiencies, which are increased in the range of 21 to 33 percent, are the most sensitive to pier spacing and the least sensitive to span stiffness distribution. This trend will probably carry over to higher N configurations as well. The computer program, described in the Appendix, can be used to verify these trends to quantify and

then "fine tune" the distributions of the three parameters needed for high efficiency guideways.

LIST OF SYMBOLS FOR CHAPTER 3

A - coefficient of mode shape equation

a - number of point forces

B - coefficient of mode shape equation

C - coefficient of mode shape equation

c - coefficient of optimization equation

D - coefficient of mode shape equation

E - normalizing factor

EI - bending stiffness

F - magnitude of point force

f - span length factor

G - transcendental factor

H - transcendental factor

h - depth of beam

I - moment of inertia

L - total structure length

ℓ - average span length

M - bending moment

m - mode number

$\bar{m}$ - mass per unit length

N - number of spans

n - individual span number

P - loading parameter

p - fundamental beam frequency

Q - modal amplitude

q - transverse load per unit length

r - subscript for reference values

S - section modulus

t - time

v - velocity

$\bar{v}$ - transverse displacement

X - plotting parameter

x - global space variable

Y - when subscripted: mode shape function

when unsubscripted: plotting parameter

y - global space variable

$\bar{y}$ - rms deflection under load

Z - plotting parameter

z - local space variable

α - cross section variation coefficient

β - cross section variation coefficient

γ - cross section variation coefficient

$\Delta\sigma$ - maximum stress difference

δ - Dirac delta

θ - transcendental factor

λ - frequency parameter

σ - maximum stress

ϕ - optimization function

ψ - transcendental factor

ω - vehicle crossing frequency

REFERENCES FOR CHAPTER 3

3.1 Fertis, D. G., Dynamics and Vibrations of Structures, John Wiley and Sons, N. Y., 1973, pp. 127-132.

3.2 Kolousek, V., Dynamics in Engineering Structures, Halsted Press, N. Y., 1973, pp. 132-135.

3.3 Wilson, J. F., "Dynamic Deflections of Multiple-Span Guideways Under High Speed Air Cushion Vehicles," Shock and Vibration Bulletin, 6, Dec. 1970, p. 47.

3.4 Wilson, J. F. and Barbas, S. T., "Dynamics of Near-Optimal Spans with Moving Loads" Preprint No. 80-654, ASCE Florida Convention, October, 1980.

3.5 Wilson, J. F., "Model Experiments for Span-Vehicle Dynamics," Journal of Engineering Mechanics Division, ASCE, Vol. 103, No. EM4, Proc. Paper 13160, August 1977, pp. 701-715.

3.6 Wilson, J. F., "Experiments in Guideway-Levitation Vehicle Interaction Dynamics," U. S. Dept. of Transportation Document No. PB 257941, Clearinghouse for Federal Scientific Information, Springfield, Va., July, 1976.

3.7 SAS/GRAPH Users Guide, SAS Institute, Inc., Cary, N. C., 1981.

4. ALTERNATIVE, HIGH EFFICIENCY DESIGNS FOR THE DUKE UNIVERSITY GUIDEWAYS

INTRODUCTION

The most efficient structures have the highest possible ratios of strength to weight, consistent with the system constraints. Investigated here are methodologies which can achieve highly efficient guideway designs for modern transit systems. Consideration is given to the practical constraints of material strength, dynamic loading, fabrication and erection. By way of illustration, precast, concrete, elevated guideways with "H"-shaped cross sections are proposed as practical alternatives to a successful state-of-the-art reference design, the transit system at Duke University. With some alternative configurations, 35 percent weight reductions are achieved, with an additional 8 percent reduction when rationally modified load factors are employed. In general, the most efficient designs use a minimum number of pier supports, properly spaced for continuous span configurations so that balanced stress is achieved. The implications of minimizing guideway costs through weight reduction are apparent.

The guideway structure typically represents as much as 35 percent of the total design life cost for urban mass transit systems, de Silva and Wormley, [4.2]. This proportional cost may be reduced for elevated guideway spans by employing highly efficient structural designs compatible with the loading of only one particular type of vehicle. Any such guideway designs,

whether of prestressed concrete, steel or a combination of these materials, also involve consideration of practical constraints such as the material strength, the building site, aesthetics, vibrations affecting ride comfort, the construction or erection procedure and the fabrication process. The highest efficiency designs are defined as those which, when subjected to such constraints, achieve the maximum possible ratios of span bending resistance to the total weight of all spans and their supporting piers. In high efficiency designs, the cross sectional area and the number of pier supports are both minimized while the fundamental bending frequency is maximized, Touma and Wilson, [4.5]. Continuous spans also promote high design efficiency, where up to 30 percent reduction in peak live load moment, compared to peak moments in end-to-end simple spans, can be achieved if optimal pier spacing is utilized, Wilson and Barbas, [4.7].

There is a broad class of elevated guideway systems for which guideway-vehicle dynamics, or inertial load interactions, are of secondary importance in the guideway design process. Two criteria are needed to define such a system to which static design procedures are applicable, Wilson, [4.6]. First, the mass m_v of all moving vehicles on any one span of length ℓ (the length between consecutive pier supports) must be less than 30 percent of that span mass, m_s; or $m_v/m_s<0.3$. Second, for a vehicle of constant speed v, the ratio of the vehicle passage frequency, $v/2\ell$, to the

fundamental guideway frequency p (hz) in transverse vibration, must be less than 20 percent, or $0.4\ell p > v$. Considered herein are several alternative, high efficiency concrete guideways which obey this static design criteria. Starting with an existing Automated Guideway Transit (AGT) system as the reference case, two methodologies leading to high structural efficiency are illustrated and some generalizations are deduced for use in future transit structure design.

REFERENCE DESIGN

About thirty rapid transit structural systems were implemented during the 1970's, De Leuw, [4.1]. Of these, the AGT elevated concrete section at the Duke University Medical Center (DUMC) was chosen as the reference design, Theumer, [4.4]. Figure 4.1 shows the cross section of this eight-span, continuous guideway with uniformly spaced pier supports. The shaded section is the precast, prestressed, double tee girder. The unshaded portions, including the horizontal levitation surface for the air cushion vehicle and the side guidance walls for the vehicle steerage wheels, are cast-in-place. The important design characteristics of the DUMC system are summarized.

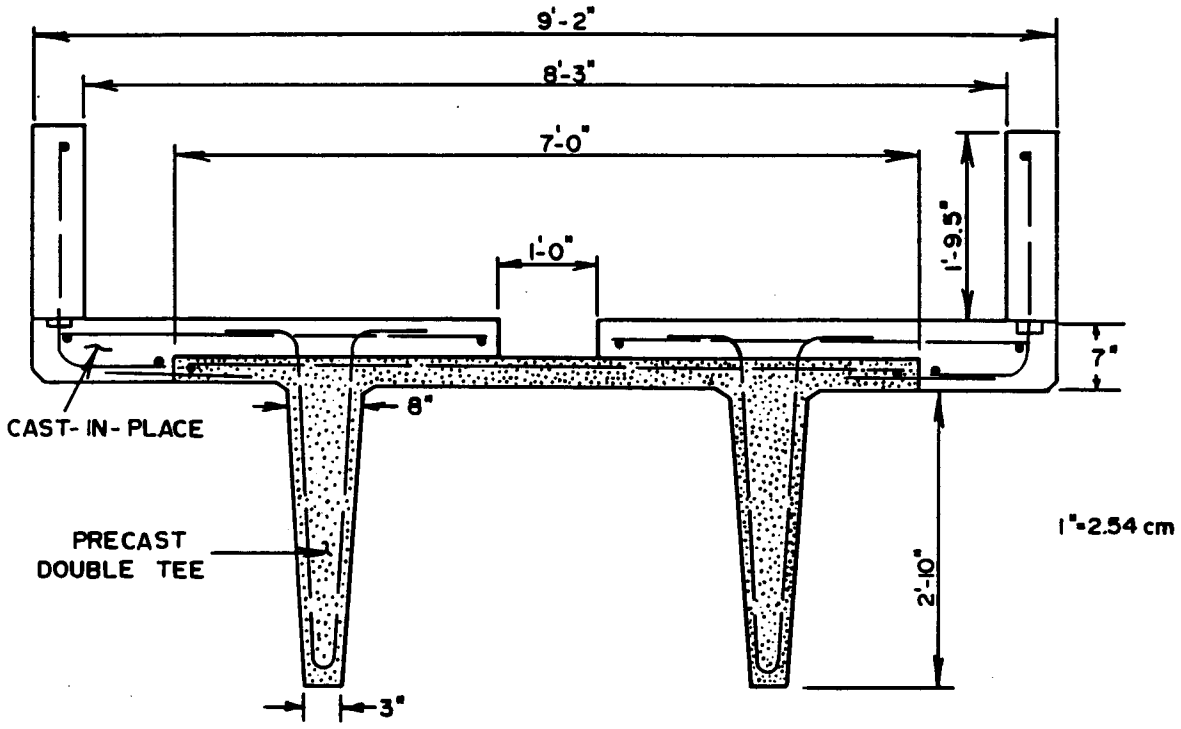

Figure 4.1 Cross section of the Duke University Medical Center elevated guideway

$EI = 4.98 \times 10^{11}$ lb-in^2 (1.43×10^9 N-m^2)	span bending stiffness
$\ell = 56$ ft (17.1 m)	pier spacing, on centers
$m_s = 222$ lb sec^2/in (3.89×10^4 kg)	span mass of length ℓ
$m_v = 39.9$ lb sec^2/in (6.99×10^3 kg)	single vehicle mass
$p = \frac{\pi}{2\ell^2} (\frac{EI\ell}{m_s})^{1/2} = 4.27$ hz	fundamental guideway frequency
$v = 25$ mph (40.2 km/hr)	vehicle design speed

From these data, $m_v/m_s = 0.18 < 0.3$; and $0.4\ell p = 65.2$ mph > 25 mph. Thus, for a single vehicle in transit, guideway-vehicle interaction dynamics are insignificant in the reference guideway design and the vehicle can be accurately represented by vertical loads of constant magnitude. In fact, the reference design was based on a uniform pressure of 880 lb/ft (1.28×10^4 N/m), the live loading L necessary to levitate a three vehicle train of mass $3m_v$ extending for 52.5 ft (16m) total length. This same three vehicle loading configuration was used in all of the alternative span design studies below.

PARAMETERS AND METHODOLOGIES IN EFFICIENT DESIGN

There are many possible parameters and approaches to consider in the design of efficient structures. One might consider alternative vehicle steerage-guideway interfaces to reduce or eliminate

the "outside-above" sidewall. Since such alternatives, shown in Figure 4.2, would mean a reference vehicle redesign, they are not considered here. The pier support columns (except for spacing) and foundation designs are also left unaltered. The three parameters which are accounted for herein are: material strength; vehicle loading factors; and construction or erection methodology, including alignment. Critical combinations of these parameters, tempered with practical considerations of fabrication, lead to cross sectional shapes and pier spacings with higher structural efficiency than the reference design.

To provide a wide range of alternatives to the reference guideway design, the following strategy is employed. First, designs are generated based on existing loadings as defined in AASHTO Bridge Design Specifications. From this point, the search for more efficient designs takes two paths: group I designs involving the search for minimum cross sectional areas, keeping the reference span lengths the same; and group II designs involving the search for the minimum number of pier supports while keeping both the total elevated length and the beam cross sectional area the same. After these studies are exhausted, the two paths are repeated with a revised and more realistic vehicle loading criteria. Finally, the effect of the construction methodology of shoring beams at midlength during erection is investigated. A matrix of this overall approach applied to the DUMC guideway is summarized in Table 4.1.

Certain assumptions and modifications are common to all four design regimes. The primary simplifying assumption is that the

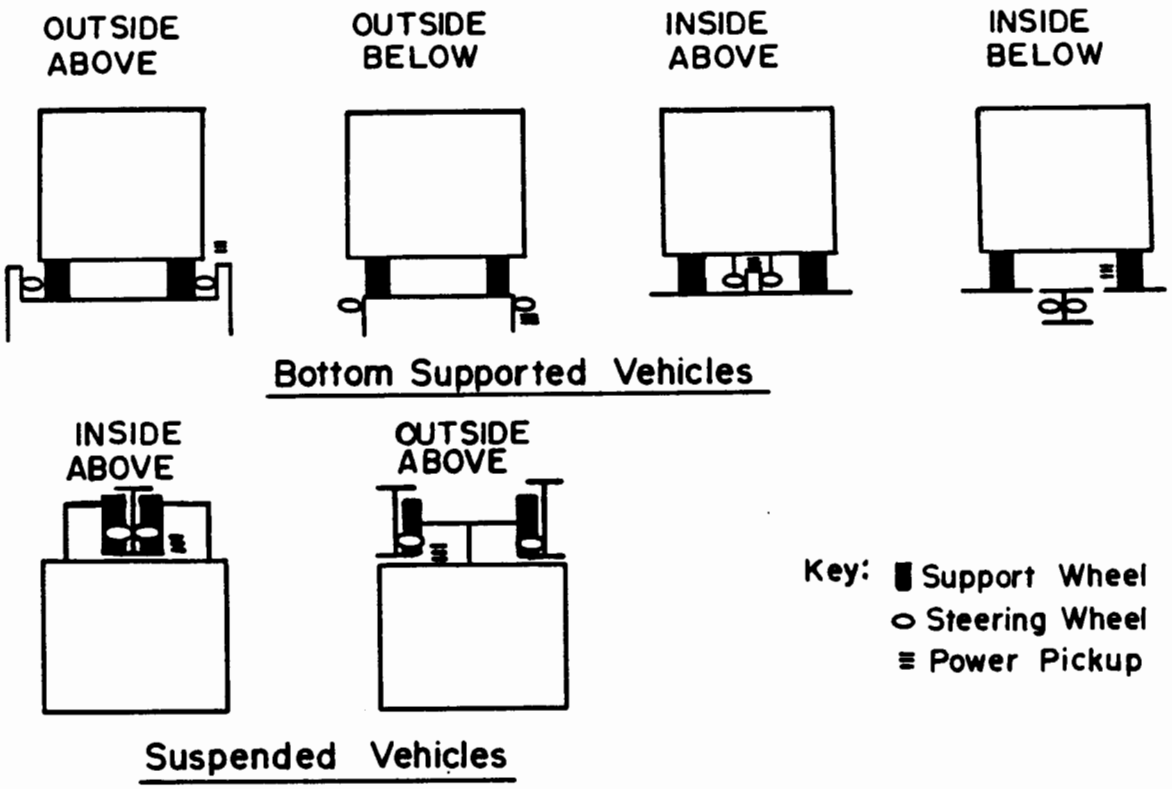

Figure 4.2 Alternative guideway/vehicle interface configurations

Table 4.1. Parameter matrix used for search of alternative, high efficiency designs.

	DESIGN GROUP	LOADING		MATERIAL			CONSTRUCTION METHOD	
				reinforced				
		AASHTO	modified AASHTO	normal strength	high strength	prestressed	simple support	shored
minimum weight span	Ia	●				●	●	
					●		●	
								●
				●			●	
								●
	Ib		●			●	●	
					●		●	
								●
				●			●	
								●
maximum span length	IIa	●					●	
							●	
							●	
	IIb		●				●	
							●	
							●	

elevated structure consists only of straight spans, although the reference structure includes one horizontal and one vertical curve. Designs produced under this assumption are applicable to the major portion of the structure. Modifications required to produce curved alignments are discussed presently. Another minor assumption concerning alignment is that the overall length of the structure is chosen as 450 ft (137 m) instead of 448 ft (136.5 m) when investigating the most efficient pier spacings. An important modification common to all alternative designs is that the cross section has the form of a precast "H" shaped beam, possibly with diaphrams in the lower half of the beam at spacings appropriate to restrain warping. See Figure 4.3. The new shape makes the sidewalls and ride surface integral with the rest of the cross section. In this way, the side walls no longer only provide lateral vehicle steerage control, but provide additional and significant bending resistance. Due to the nature of an air cushion suspension, probably no modification or addition to the precast ride surface would be required after erection of alternative designs. In all cases, advantage is taken of the high tolerances available in plant controlled precast concrete to help assure a comfortable ride.

With this overview of the basic assumptions and the design strategy, a further look at the three basic design parameters is in order.

Material parameter. Materials investigated for minimal weight structures are limited to those required to produce normally reinforced or prestressed concrete. Thus, valid comparsons can be made to the reference design of similar materials.

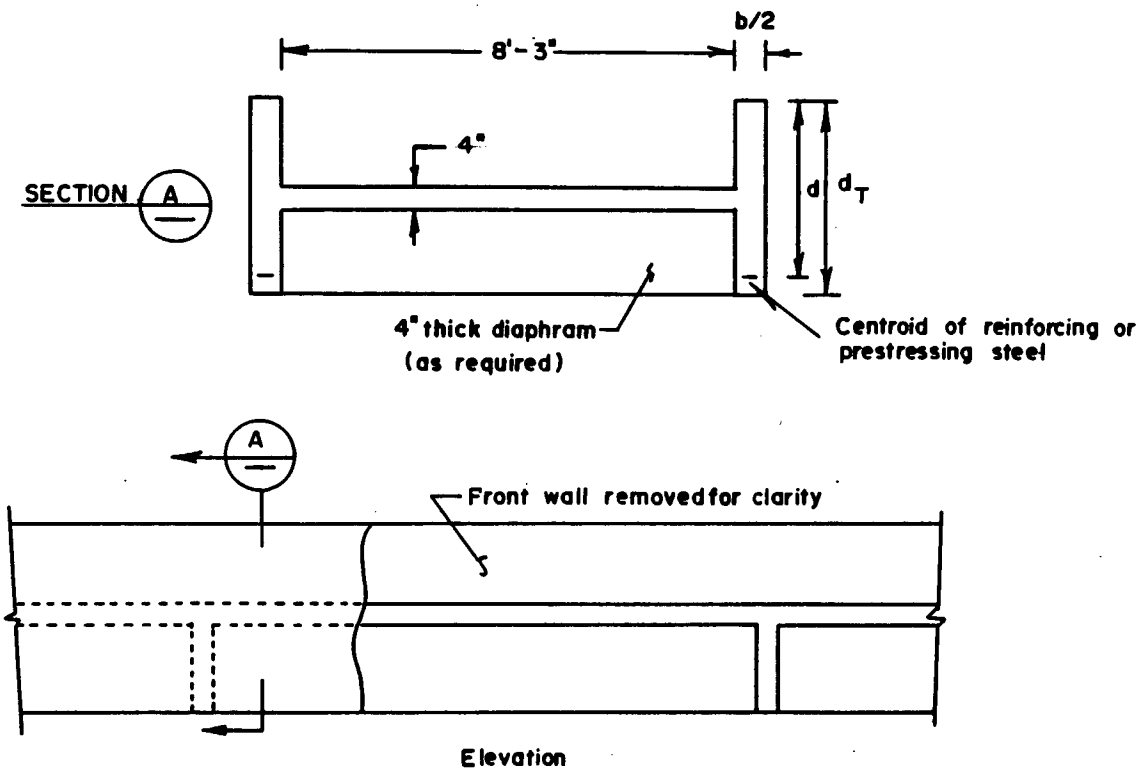

Figure 4.3 Proposed "H" shaped guideway cross section

Within this framework, three options are investigated: "normal" strength reinforced concrete; "high" strength reinforced concrete; and prestressed concrete. The normal strength design will use a twenty-eight day concrete strength of 4000 psi (12×10^6 N/m^2) and steel yield strength of 60 ksi (414×10^6 N/m^2). A 6000 psi (18×10^6 N/m^2) concrete and 80 ksi (552×10^6 N/m^2) steel will be assumed for the high strength design. The prestressed design will employ 5000 psi (15×10^6 N/m^2) concrete and 270 ksi (1862×10^6 N/m^2) ultimate prestressing steel. These are the same parameters used to design the double tee beams of the reference design. Use of high strength materials in a concrete design is a desirable feature. The dead load of a concrete structure is usually a significant portion of the final loading condition. High strength concrete allows the designer to produce a cross section capable of resisting the same loads as a normal strength design but at an appreciable saving in dead load. This weight savings will result in a reduction in load on the high strength design, thus implying even further savings. Use of prestressed concrete is most desirable when live load deflections control the design. A properly conceived prestressed beam will not crack under service loads. This allows the moment of inertia of the full concrete section to resist deflection.

Load factor parameter. Initially, designs are based on the same load definitions as the reference design, a design which employed the 1973 AASHTO Bridge Design Specification as well as the 1974 and 1975 Interim Specifications. The controlling equation in this case is:

$$\text{Ultimate Load} = 1.3(D+1.25(L+I))$$

D = dead load

L = live load

I = impact = .25L

Here, the live load is multiplied by a factor of 1.25 squared. One of these 1.25's is to account for "impact." Impact may consist of load increases due to dynamic interaction between a relatively massive, rapidly moving load and a relatively light-weight and flexible supporting structure; or dynamics associated with braking; or even the dynamic effect of a large truck driving into a pot hole in the bridge deck. The other 1.25 factor accounts for a variety of uncertainties in highway bridge live loadings such as temporary "overloads" due to unusual vehicles and eccentricity of lane loading. The reason for eliminating the first dynamic factor of 1.25 to account for guideway-vehicle interactions has already been justified for the reference design and will be assumed for minimal weight alternative designs. Since the guideway is designed for a single vehicle type, and those vehicles are levitated by cushions of air, the need for the second AASHTO dynamic impact factor of 1.25 is also questionable. However, since braking loads through the use of skids may afford some impact, the extent of which still needs experimental verification, the following equation probably represents a reasonable lower bound for alternative DUMC guideway designs. The 1.3 safety factor on ultimate or collapse load is maintained throughout.

$$\text{Ultimate Load} = 1.3(D+1.1L)$$

Construction or erection methodology. Construction of the reference guideway is first summarized. The precast double tee beams were placed end-to-end on the piers, each forming a simple span. A block of concrete was then cast at the interior supports (see Figure 4.4) to produce the continuous, eight-span configuration. Then the levitation surface and side walls were cast. This method of construction effectively freezes the simple beam bending moment of the double tee dead load into the final structure. Figure 4.5 illustrates the breakdown of the existing dead load moment. Note that the double tee simple beam moment has a significant if not controlling effect on the final girder design.

Now consider an alternative: temporary shoring during construction. A temporary support at midspan can reduce the "frozen in" maximum positive moment due to dead load by approximately one half. Use of shoring, however, is a very site-dependent proposition. For example, should the location of a temporary support be in the middle of a busy street this type of construction would not be viable. At the site of the reference design, however, there are no such objections to shoring. Thus, an attractive reduction in dead load moments is possible. Note, however, that a central temporary support produces negative midspan moments. This is not necessarily consistent with the philosophy of the reference design. Prestressed girders generally are proportioned so that the stress on the top fiber of the beam is nearly zero under dead load. Therefore a negative midspan moment would result in relatively high concrete tensile stresses, a very undesirable situation. This condition could be alleviated by using normal

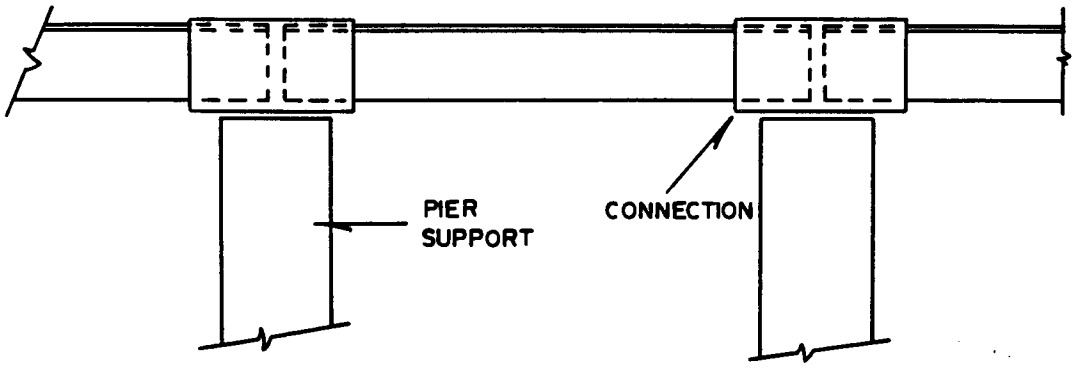

Figure 4.4 Connection of simple spans to form continuous elevated guideways

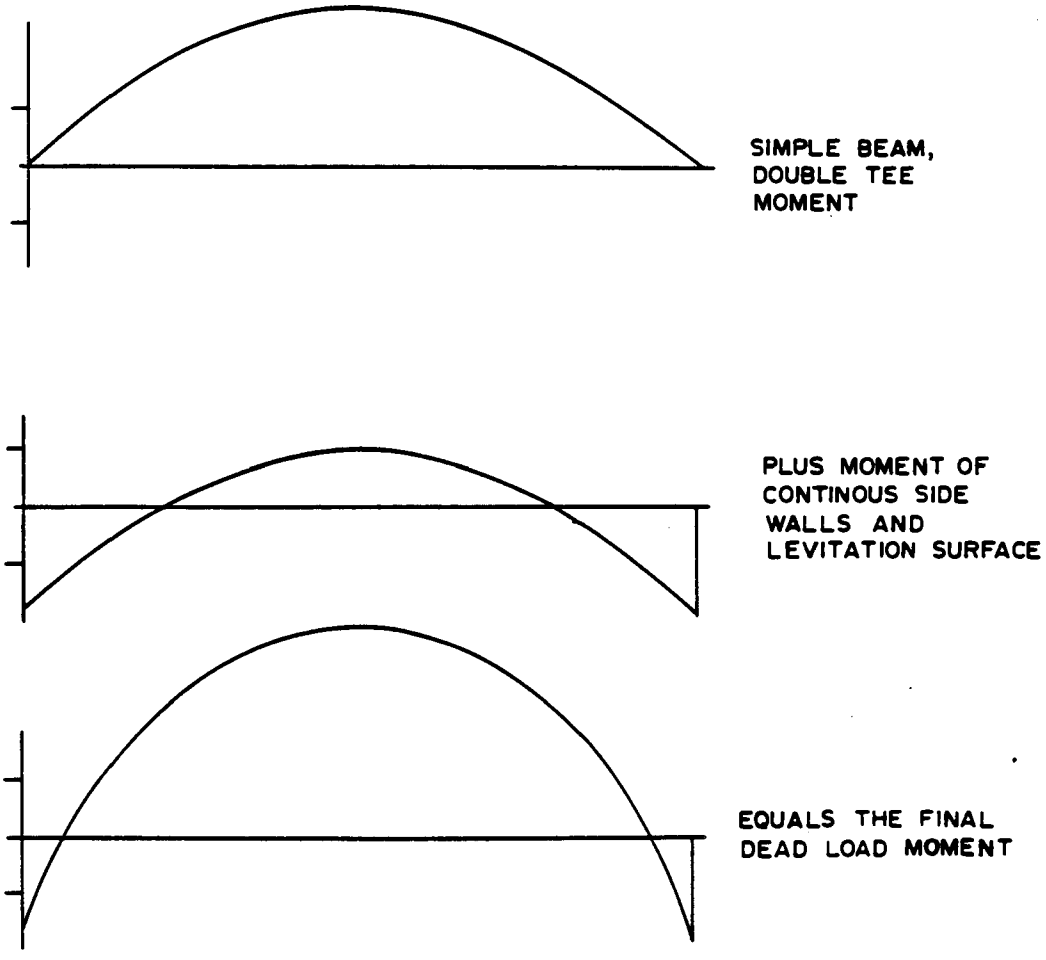

Figure 4.5 Dead load moment distribution in the reference guideway

reinforcing in the top fiber to take the construction related tensile load. Concrete cracking would still have to take place in order to mobilize the strength of the added top steel. Possible detremental effects of this cracking on prestressing steel must be considered. At any rate, temporary shoring at midspan reduces the construction moments to those associated with a two-span continuous beam with span lengths one half that of the simple beam. This reduces the maximum construction moment to one forth the unshored case. It is noted that the maximum construction moment is now negative and the maximum positive moment due to construction is now less than 15 percent of the simple beam moment.

Now one is faced with the problem of determining the built-in moments related to shored construction. In this procedure, instead of freezing moments into the final structure, one is effectively building in the end rotations of the beams. Therefore, the built-in moments can be found by superimposing the dead load moment of the continuous beam with that of a beam subjected to a fixed end rotation. Fixed end rotations result in a beam subjected to pure bending. The magnitude of this bending moment is easily calculated from the classical relation between moment, bending stiffness and radius of curvature. Figure 4.6 reflects these concepts. The amount of end rotation can be controlled to achieve minimum built in stresses by an upward displacement of the beam at its central shore. This displacement can be easily controlled by the proper use of hydraulic jacks. A doubly reinforced "H" is easily adapted to the above type of construction. The horizontal

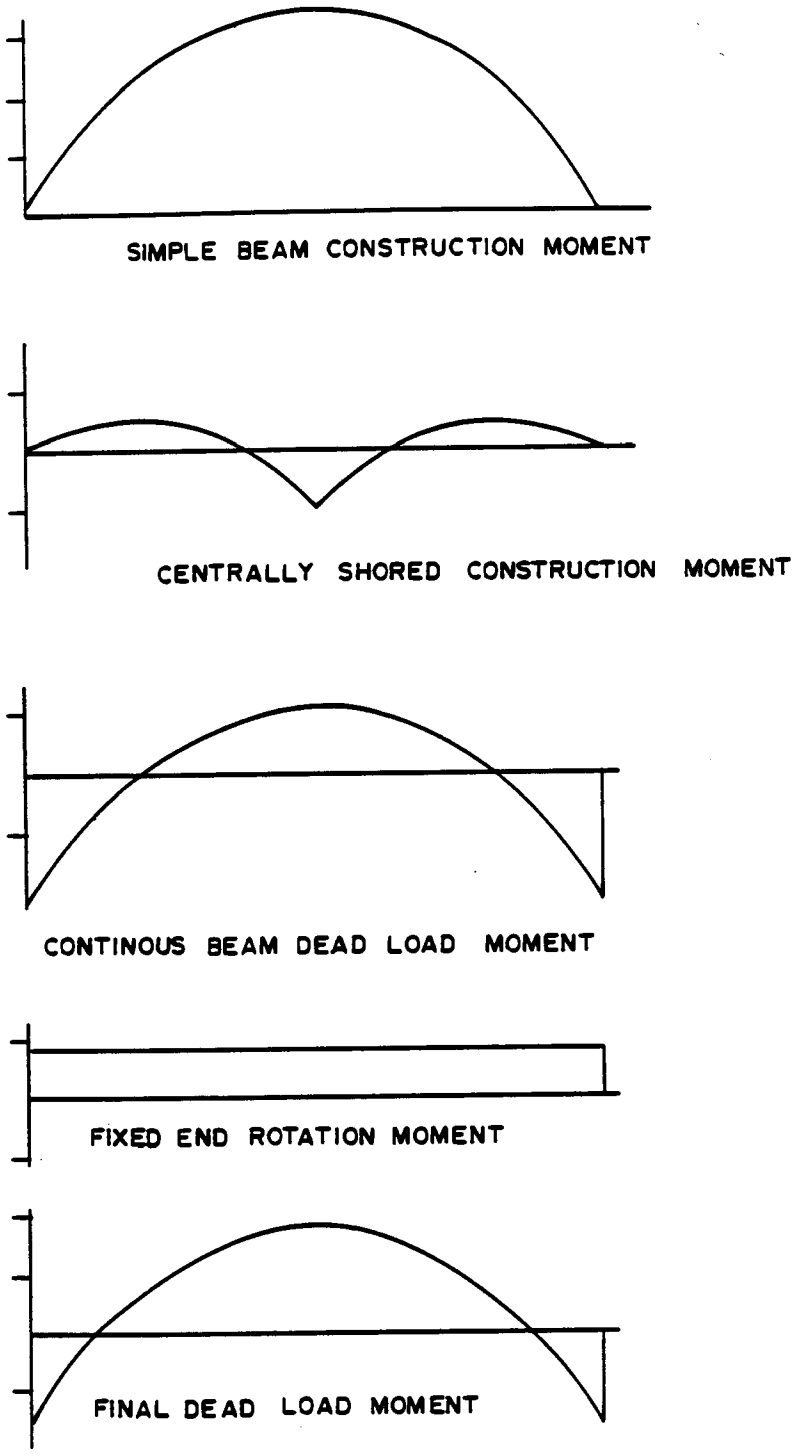

Figure 4.6 Effect of shoring on dead load guideway moment

symmetry of the "H" allows it to resist positive and negative moments equally.

Now examine the bending moments at the interior supports that come about from temporary shoring, and their overall effect on the final structure. Simply supported construction will theoretically result in no moment whatsoever at interior supports. It is obvious that temporary central supports will result in negative dead load moments at these support locations, of the same magnitude as the maximum positive dead load moments produced. Proper detailing of beam to beam connections can easily cope with this situation. A detail similar to that of Figure 4.4 essentially constitutes a radical increase in the compression flange of the cross section. All that remains is to insure a proper joining of tension steel in order to resist relatively large negative moments. This can be accomplished by using a mechanical coupling, welding (not the preferred choice), or lap splicing. See Figure 4.7

As a final comment on construction of the proposed precast "H" consider the problems associated with lifting the beams. Since the side walls and riding surface are now integral parts of the beam, the weight of precast "H" that must be lifted may be greater than lifts associated with the reference design, for the same span length. However, when the final inplace weights of the two structures are compared, the "H" is significantly lighter. If central shoring is used as a means of construction, pick-up points for the beam must be located with care. Lifting the beam by its ends would result in subjecting the girder to simple beam bending thus defeating the purpose of central shoring. The diaphrams in

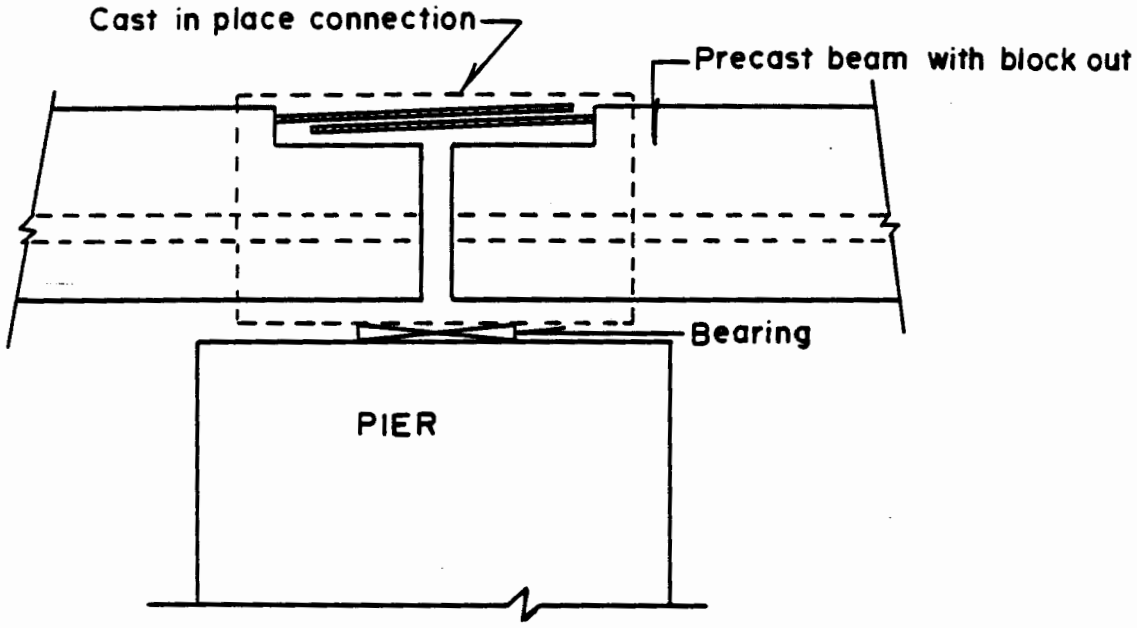

Figure 4.7 Lap splice for guideway continuity

the lower half of the "H" present attractive pick-up locations.

FABRICATION

Fabrication of an "H" may be somewhat more complex than fabricating a double tee. Both are relatively simple open shapes. It may be economically desirable for the diaphrams in the lower half of the "H" to be deleted in favor of increased torsional capacity in the sides of the "H" and/or increased bending capacity of the "H's" horizontal slab. This would result in increased material cost; but by simplifying the form work, the price of fabrication is reduced. For certain sections of guideway, the "beefed up" simple "H," without diaphrams, may prove to be the most economical choice. Note that if the diaphrams are removed, pick-up points on the beams must be carefully selected and stability during lifting must be given further consideration. Probably the tradeoffs in cost will be such that relatively straight, precast sections would be more economical to fabricate without diaphrams.

Forming of curved section of "H" shaped guideway may take many approaches depending on the nature of the curves involved. The choice of a specific forming system will be determined by the economics of the individual construction situation. As an example, consider a guideway system layed out using a restricted number of specific curves. Then only a few separate sets of forms or perhaps even one form based on the "modular tooling" concept may prove to be most desirable for precasting all elevated sections of the system, De Leuw, et al, [4.1]. Modular tooling uses one large

form that contains all phases of the typical geometric alignment employed in the guideway layout. See Figure 4.8. Beams are then cast in the appropriate section of the form that corresponds to the curvature of guideway desired. Guideway layouts of limited horizontal curvature may also provide vehicle designers with information beneficial to the tuning of lateral vehicle suspensions for increased ride comfort.

If a sufficiently large section of elevated guideway with varying alignment is required, then precasting the beams with adjustable forms may prove the most economical means of fabrication. For instance, the monorail beams for the Walt Disney World people mover were cast using adjustable forms to produce varying horizontal and vertical curves as well as various superelevations (Most, 1972). Adjustable forms were also used to fabricate the Dallas Fort Worth airport and Dearborn, Michigan's Fairlane guideways. For a system with only a few curves or for unique alignments, a fully cast-in-place or a combination of precast and cast-in-place construction may prove the most cost-effective means of fabrication. A fully cast-in-place system may take advantage of the diaphrams in the "H" by using a pan type forming system. Curvature would be produced by proper angling of pans and then adding the upper side walls. See Figure 4.9.

RESULTS: PARTICULAR ALTERNATIVE DESIGNS

Since the "H" shaped guideway cross section appears practical both from the fabrication and construction viewpoints, it is employed as the basis for the alternative designs.

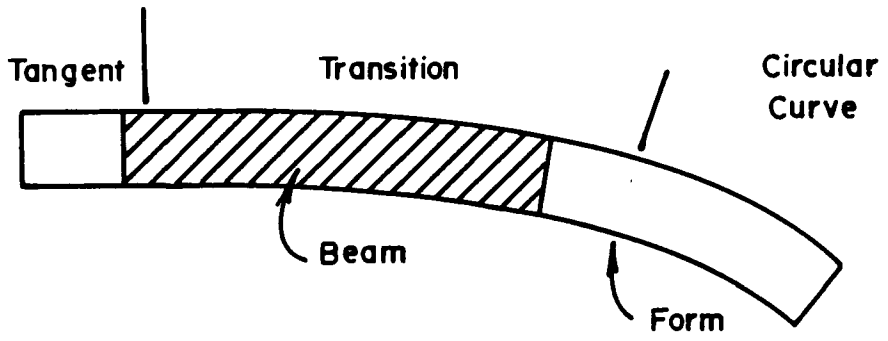

Figure 4.8 Modular tooling in guideway construction

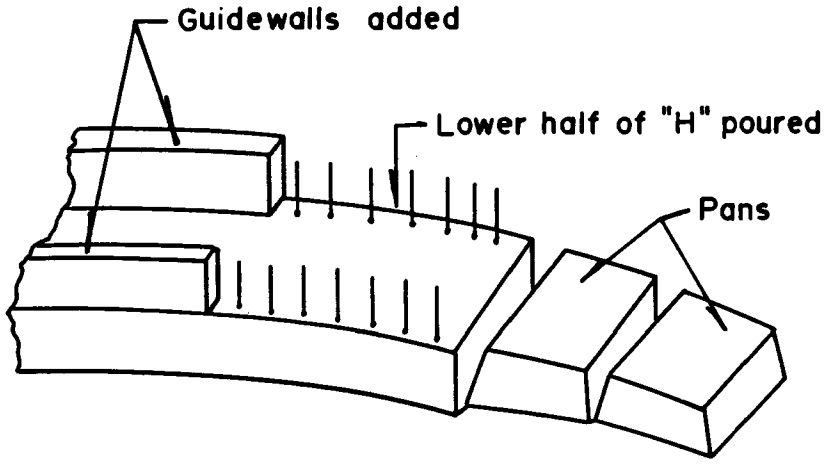

Figure 4.9 Pan construction of a curved guideway

The bending calculations for normally reinforced beams are based on ACI publication SP-17(73). The formulas used are summarized. The ultimate moment capacity is given by

$$M_u = FK_u \tag{4.1}$$

where

$$F = bd^2/12000 \tag{4.2}$$

and

$$K_u = \phi f'_c \omega (1 - .59\omega) \tag{4.3}$$

and

$$\omega = \frac{A_s f_y}{bd f'_c}; \ \phi = 0.9. \tag{4.4}$$

The units used are; b, d in inches, f'_c, f_y in pound per square inch, A_s in square inches and M_u in kip-feet (10^3lb-ft).

The bending calculations for prestressed beams are based on the Portland Cement Association's publication Notes on ACI 318-77. The formulas used are summarized. The ultimate moment capacity is given by

$$M_n = A_{ps} f_{ps} \left(d - .059 \frac{A_{ps} f_{ps}}{b f'_c}\right) \tag{4.5}$$

where

$$f_{ps} = f_{pu}(1 - 0.5\omega_{pu}) \tag{4.6}$$

and

$$\omega_{pu} = \frac{A_{ps} f_{pu}}{bdf'_c} \tag{4.7}$$

Units should be in a consistent system, i.e., inches and pounds.

Table 4.2 summarizes the numerical results for the group I designs defined in Table 4.1. Formulas on which all calculations are based are Eqs.(4.1)-(4.7) above. The greatest weight savings for the two different loading conditions considered were for the prestressed design placed as simply supported beams; and for the high strength, normally reinforced beam using central shoring during construction. Note that two different prestressed senarios were considered under group Ia. First a beam that did not require any additional reinforcement to accommodate stresses at transfer, was sized. A prestressed beam based on absolute minimum weight was then generated assuming that sufficient rebar for transfer stresses could be provided. These two designs provide upper and lower weight bounds for an actual prestressed girder. Therefore, a possible increase in weight by five to fifteen percent of the value given in group Ib (prestressed) of Table 4.2 would be indicative of a more realistic beam.

The normally reinforced girders were assumed to be singly reinforced. All designs were based only on bending resistance. Should deflections control the design of these beams, an appropriate increase in weight should be considered. The following procedure was used to obtain the parameters listed in Table 2. First, a thickness of four inches was assumed for the horizontal slab portion of the "H" section. Values of b/2, the desired side wall thickness, and d_T, the total section depth, were chosen. With these parameters fixed, a total dead load was calculated. This dead load and the known live load were combined by the

Table 4.2. Weight changes for group I alternative "H" guideways, compared to the reference case

Design			WT. 10^3lb	WT. 10^3N	b in	b cm	d in	d cm	A_{s_2} or A_{ps} in^2	A_{s_2} or A_{ps} cm^2	TOTAL WT. CHANGE percent	LIFT WT. CHANGE percent
Ia AASHTO load	Normal Strength	simple support	57.7	257	12	30.5	39	99.1	7.16	46.2	-30.1	42.5
		shored	53.2	237	12	30.5	33	83.8	6.34	40.9	-35.6	31.4
	High Strength	simple support	53.2	237	12	30.5	33	83.8	5.70	36.8	-35.6	31.4
		shored	50.9	226	12	30.5	30	76.2	4.75	30.6	-38.4	25.7
	Prestressed (both simple supports)	no transfer rebar	59.5	265	10	25.4	39	99.1	1.84	11.9	-28.0	46.9
		transfer rebar	51.6	230	10	25.4	39	99.1	1.84	11.9	-37.5	27.4
Ib modified load	Normal Strength	simple support	55.4	246	12	30.5	36	91.4	6.39	41.2	-32.9	36.8
		shored	49.0	218	10	25.4	33	83.8	4.85	31.3	-40.7	21.0
	High Strength	simple support	49.0	218	10	25.4	33	83.8	4.79	30.9	-40.7	21.0
		shored	47.3	210	10	25.4	30	76.2	3.81	24.6	-42.7	16.8
	Prestressed	simple support	47.4	211	8	20.3	36	91.4	1.53	9.9	-42.3	17.8

appropriate loading equation to obtain the maximum ultimate mid-span moment in the beam. To determine the bending capacity of the girder, the cross sectional area of steel (A_s for nonprestressed or A_{ps} for prestressed) and an appropriate distance from extreme fiber to steel centroid, d, were selected. Finally the bending resistance and ultimate moment were compared to check the adequacy of the design for stress.

Investigation of a maximum span length approach to efficient designs in group II did not yield results as varied as the least weight spans in group I. Essentially only one more efficient configuration resulted from all the possible design parameters. This was a four span structure with two end spans of 100 ft (30.5 m) each and two central spans of 125 ft (38.1 m). Here end spans 20 percent shorter than main spans were employed in an attempt to balance maximum positive dead load moments. There are two reasons for the lack of variety in these latter results. First is the overriding effect of dead load moments as span length increases. This had a neutralizing effect on the reduced live load moments. Under the assumption that the end spans were eighty percent of main spans, where the total guideway length was 450 ft (137 m), the next longer span possible after the 125 ft (38.1 m) maximum already considered was 173 ft (52.7 m). This latter length results in a dead load moment which is not practical. The second factor controlling the efficient choice of the number of long span designs was that no consideration was given to shored construction. For spans of 100 ft (30.5 m) and longer, use of more than one temporary support may improve structural efficiency. Since

investigation of multiple shoring locations and ever increasing span lengths would only serve to cloud the comparison with the reference structure, only simply supported construction of long spans in group II was considered.

For the 125 ft (38.1 m) length, many designs using the reference design weight per unit beam length are possible. However, one should realize that fabrication, transportation and erection of such a girder would be extremely difficult. On the other hand the use of the 56 ft (17.1 m) span length involves an unnecessary amount of foundation work. Thus, the most efficient alternative design would be both lighter in weight and longer in span. The possibility of "fine-tuning" such structural designs is clearly indicated by these results.

The results of the maximum span and minimum weight calculation were checked to determine if vehicle-guideway dynamic interaction was as insignificant as assumed. The minimum weight designs all had frequencies on the order of 4 hz, thus bearing out the assumption of minimal interaction as discussed in the Introduction. Although the maximum span designs resulted in fundamental guideway frequencies approximately one half that of the reference design, the critical vehicle speed above which dynamic interactions become significant was again well above the 25 mph (40.2 km/hr) reference design limit. In both cases also, m_v/m_s remained below the 0.3 value, thus justifying the static design procedures used for the alternative designs.

Finally, the authors wish to emphasize that these hypothetical studies were made purely for the purpose of illustrating a design

methodology. Such studies should not at all detract from the excellent state-of-the-art DUMC facility used as a reference case.

CONCLUSIONS

In order to improve the structural efficiency of a concrete guideway which employs an outside-above vehicle interface, consideration should be given to the bending resistance offered by the guide walls. The way to mobilize this added resistance is to cast the guide walls as an integral part of the guideway cross section. Combining a modified "H" cross section with a proper choice of construction method results in a 30 to 35 percent weight savings in the superstructure over the reference design. With a rational reduction in load factors, an additional eight to ten percent weight reduction is achieved. Efficiency of a guideway can also be improved by decreasing the number of pier supports required. For instance, with the modified "H" cross section which has the same total weight as the reference superstructure, span lengths twice that of the reference design are practical. In general, the proper balancing of weight and span length is up to the individual designer whose judgement must be tempered by the specific and sometimes subtle constraints. The important point is that the percent of total guideway weight reduction is a common measure of cost reduction used in construction cost estimating. Thus, if fabrication and erection costs remain constant, the minimum weight design implies the minimum cost design.

LIST OF SYMBOLS FOR CHAPTER 4

A_{ps} - Area of prestressing steel

A_s - Area of nonprestressed reinforcing steel

b - Width of compression flange

D - Dead load

d - Depth of reinforcing steel centroid from extreme fiber

d_T - Total depth of beam

EI - Bending stiffness

F - A flexural coefficient

f'_c - 28 day concrete compressive strength

f_{ps} - Prestressing force

f_{pu} - Ultimate strength of prestressing steel

f_y - Yield strength of nonprestressed reinforcing steel

I - Impact load

K_u - A strength coefficient

L - Live load

ℓ - Span length

M_n - Ultimate bending resistance of prestressed beam

m_s - Span mass

M_u - Ultimate bending resistance of nonprestressed beam

m_v - Vehicle mass

p - Guideway frequency (hz)

v - Vehicle speed

ϕ - Capacity reduction factor

ω - Ratio of tensile and compressive stress for nonprestressed beams

ω_{pu} - Ratio of tensile and compressive stress for prestressed beams

REFERENCES FOR CHAPTER 4

4.1 De Leuw, Cather and Company (1979), AGT Guideway and Station Technology Vol. 7, UMTA Report IT-06-0152-79-6.

4.2 De Silva, C. W. and Wormley, D. N. (1979), Material Optimization in a Torsional Guideway Transit System, Journal of Advanced Transportation, Vol. 13, No. 3, 41-60.

4.3 Most, R. F. and Dolan, C. W. (1972), Walt Disney World Monorail Designed for Smooth Riding, Civil Engineering.

4.4 Theumer, N. D. (1980), Automated Guideway Transit: The Duke University Automated People/Cargo Transportation System, Journal of Advanced Transportation, Vol. 14, No. 2, 161-176.

4.5 Touma, A. and Wilson, J. F. (1973), Design Optimization of Prestressed Concrete Spans for High Speed Ground Transportation, Computers and Structures, Vol. 3, 265-279.

4.6 Wilson, J. F. (1977), Model Experiments for Span-Vehicle Dynamics, Journal of the Engineering Mechanics Division, ASCE, Vol. 103, No. EM4, 701-715.

4.7 Wilson, J. F. and Barbas, S. T. (1980), Dynamics of Near-Optimal Spans with Moving Loads, ASCE Proc. Paper No. 80-654.

APPENDIX - DESCRIPTION OF COMPUTER PROGRAMS

A listing of each of the following computer programs, written in Fortran IV, can be obtained from the Principal Investigator, James F. Wilson, Structural Dynamics Laboratory, Department of Civil Engineering, Duke University, Durham, N. C. 27706.

1. PROGRAM I. This program calculates the dynamic responses of continuous, uniform spans of up to N = 6 using the normal mode method. The supports are evenly spaced. The loading is a single, vertical point force of constant intensity, traveling at constant speed. Span inertia is included.

2. PROGRAM II. This program calculates the dynamic responses of continuous, uniform spans of up to N = 10 using the normal mode method. The supports are evenly spaced. The loading can be from two to ten vertical point forces, all of equal magnitude and constant intensity, at arbitrary, fixed spacings, and at constant speed. Span inertia is included.

3. PROGRAM III. This program is identical to PROGRAM I, with a single exception: the pier support spacing is arbitrary.

4. PROGRAM III-N. This program is identical to PROGRAM II, with a single exception: the pier support spacing is arbitrary.

5. PROGRAM IV. This program calculates the dynamic responses of continuous spans up to N = 10 using the normal method. The supports are unevenly spaced; and both the stiffness EI and mass per unit length $\bar{m}$ can be different, segment to segment. The loading can be from two to 10 vertical point forces, all of equal

magnitude and of constant intensity, at arbitrary, fixed spacings and at constant speed. Span inertia is included.

6. MASS. This program calculates the dynamic deflection and moment under a single moving mass load. The vertical inertia effects of the moving mass are included; but the span inertia effects are neglected. The program EPISODE, Reference [2.4], is used to solve the differential equation.